UNIVERSITY OF CALIFORNIA
RIVERSIDE

The Complex Dimensions of Space-Filling Curves

A Dissertation submitted in partial satisfaction
of the requirements for the degree of

Doctor of Philosophy

in

Mathematics

by

Adam Doren Richardson

June 2022

Dissertation Committee:

Distinguished Professor Michel L. Lapidus, Chairperson
Professor Bun Wong
Professor Yat Tin Chow

The Dissertation of Adam Doren Richardson is approved:

Committee Chairperson

University of California, Riverside

Acknowledgements

This achievement would not be possible without the multiple families of support I have had over many years of my life and my math education. First and foremost, I would like to thank my advisor Professor Michel L. Lapidus for introducing me to his profoundly beautiful theory, and for always inspiring and encouraging me. I fell in love immediately with the theory of complex dimensions, and I know it is something I will continue to study as long as I live. The privilege of knowing that you will have enough fascinating mathematics to explore for a lifetime is one that I wish upon every math graduate student. I also want to thank him for facilitating a warm and welcoming research group in which to explore these ideas, another privilege I hope every graduate student gets to experience.

Thank you to Professor Bun Wong and Professor Yat Tin Chow for being kind advisors and helping me along my path at UCR. Thank you to Margarita Roman for always encouraging me and always staying on top of the mountain of details that need to be managed in order to help all of us math graduate students succeed.

Thank you to Dr. Therese-Marie Landry for always being strong and understanding, helpful and conscientious. Thank you to Will Hoffer for being an exemplary mathematician to look up to. Thank you to Dr. Edward Voskanian and Dr. Michael Maroun for all of your advice and encouragement, it always gives me clarity and hope. Thank you to Raymond Matson for making me feel welcome and keeping me in the loop.

Thank you to Dr. Joseph Bennish for first introducing me to space-filling curves, and being an inspirational mentor in my early career who always seemed to know what I would find interesting. Thank you to Dr. David Gau for giving me Gerald A. Edgar's book [Edg90] to enjoy, setting me off on my studies of fractal geometry. Thank you to Dr. Tangan Gao and Dr. Will Murray for being incredibly accommodating department chairs and continually helping me manage all of my endeavors. Thank you to Dr. John Brevik for accepting me into the CSULB graduate program and requiring us budding mathematicians to be careful and rigorous in our work. Thank you to Dr. Josh Chesler for seeing me, and for the incredible amount of help, encouragement, and support over the years, I really cannot thank

you enough. Thank you to Dr. Sheldon Axler for showing me back in precalculus that math is designed to make sense and that anyone can do it. Thank you to Rich Weber for starting me on this journey so many years ago in intermediate algebra by showing me what exponent notation really means.

Next, I must apologize to the friends, family, and colleagues that I have not been able see or keep in contact with over the past few years while on this journey; please know you have always been in my thoughts and I'm sorry I could not be there, especially during such tumultuous times.

Thank you to The Doctor for helping me understand time and space. Thank you to my mom, my dad, and my sisters for being perfect people. Finally, I would like to thank my wife, Robyn, for being strong and supportive for so many years, and our little girls, Verity and Luna, the truth and the light in the night. I love all three of you so much, and this really would not be possible without you.

This dissertation is dedicated to all of the undergraduate students currently learning intermediate algebra; remember that you absolutely *can* do math, and if something in mathematics doesn't make sense, it's usually because it's not being explained well enough.

ABSTRACT OF THE DISSERTATION

The Complex Dimensions of Space-Filling Curves

by

Adam Doren Richardson

Doctor of Philosophy, Graduate Program in Mathematics
University of California, Riverside, June 2022
Distinguished Professor Michel L. Lapidus, Chairperson

Space-filling curves have been colloquially referred to as "fractals" since the term was coined and defined by Benoit Mandelbröt in the late 1970s. However, space-filling curves themselves do not satisfy Mandelbröt's definition, and other definitions of fractality also neglect to properly classify space-filling curves as fractals. This is due to the fact that, as sets, they are topologically simple because they fill N-dimensional space and, thus, coincide with N-dimensional space. In the 1990s through the present, Distinguished Professor Michel L. Lapidus and various collaborators have developed a more accurate definition of fractality based on a larger theory of *complex dimensions* of fractal sets. These complex dimensions correspond to the existence of singularities of certain complex-valued zeta functions associated with fractal sets. These singularities are termed *complex dimensions* due to their connection with "fractal dimensions" such as the Minkowski dimension, and the complex-valued zeta functions used in analytic number theory. The theory has been incredibly fruitful over the years, even allowing for the Riemann hypothesis to be recast in terms of the complex dimensions of the geometric zeta function of an appropriate fractal string. Today, it has allowed the present author to prove that a class of space-filling curves are, indeed, fractals, and to provide insight into the oscillatory properties of these curves via their complex dimensions.

In this dissertation, Chapter 1 provides the motivating background for the study of complex dimensions of fractal sets. Chapter 2 introduces the theory of fractal strings in $\mathbb{R}$ and the complex dimensions of fractal strings. Chapter 3 generalizes the theory to dimensions greater than 1. Chapter 4 provides all the necessary background in the theory space-filling curves required to make sense of the results of this dissertation. Chapter 5 details the construction of a class of relative fractal drums (RFDs) associated to a class of plane-filling curves. This construction allows us to detect the complex dimensions of such curves for the first time, and thereby properly classify them as fractals in a rigorous way. Chapter 6 details how this class of RFDs also allows us to investigate the oscillatory properties of these curves, in particular in the points and the volume of the tubular ε-neighborhood of the curves. Chapter 7 concludes the dissertation with some conjectures about future results involving different classes of space-filling curves.

Contents

List of Figures

Chapter 1

Introduction

The mathematical concept of *dimension* has been seriously studied since the 19th century, and it emerged initially to give sufficient generalized meaning to intuitive concepts like a line, a curve, and a surface, as well as higher dimensional objects. Until the 20th century, the notion of dimension was exclusively a nonnegative integer. In [Edg90], Gerald A. Edgar quotes Hermann Weyl on the notion of dimension: "We say that space is 3-dimensional because the walls of a prison are 2-dimensional." This intuition is codified in the topological notions of dimension called the *small* and *large inductive dimensions*. In the 1920s the theory of *fractal dimensions* was detailed by Minkowski, Hausdorff, Besicovich, and Bouligand, extending the notion to nonnegative real numbers in order to explore geometric properties of "rough" arbitrary sets in Euclidean space. This gave rise to the *Hausdorff dimension* and *Minkowski-Bouligand dimension* (also known as the *box dimension*) which are fundamental tools of fractal analysis. In the 1990s Michel L. Lapidus proposed the idea of *complex dimensions* of bounded fractal strings based on collaborative work in, for example, [LvF13]. The notion of complex dimensions gives us the most accurate way of defining *fractality* to date.

In the late 1970s, Benoit Mandelbröt coined the term *fractal* and gave the following intuitive description of a fractal in his book *The Fractal Geometry of Nature* [Man82]: "a rough or fragmented geometric shape that can be split into parts, each of which is (at

least approximately) a reduced-size copy of the whole." In an attempt to make this notion mathematically rigorous, he initially settled on the following definition.

Definition 1.0.1 ([Man82])**.** A *fractal* is by definition a set for which the Hausdorff-Besicovitch dimension strictly exceeds the topological dimension.

However, in the late 1980s after another decade of research involving "fractals" and "fractal-like" constructions and behaviors, Mandelbröt admitted in Peitgen and Richter's book, *The Beauty of Fractals* [PR86], that "[The definition's] generality was to prove excessive: not only awkward but genuinely inappropriate. [...] This definition left out many 'borderline fractals', yet it took care, more or less, of the frontier 'against' Euclid. But the frontier 'against' true geometric chaos was left wide open! I know definitions matter little, but this one can still be improved upon."

These "borderline fractals" are not as borderline as one might imagine (and as we will see in detail, shortly) and their exclusion by this definition is, indeed, apparently and evidently inappropriate. The existence of mathematical objects that exhibit the heuristic qualities of what mathematicians would like to label as "fractal" that fail to fulfill the hypotheses of Definition 1.0.1 naturally led to other attempts at developing a more accurate formal definition. Kenneth Falconer writes in his book *Fractal Geometry: Mathematical Foundations and Applications* [Fal90], "My personal feeling is that the definition of a 'fractal' should be regarded in the same way as a biologist regards the definition of 'life'. There is no hard and fast definition, but just a list of properties characteristic of a living thing, such as the ability to reproduce or to move or to exist to some extent independently of the environment. Most living things have most of the characteristics on the list, though there are living objects that are exceptions to each of them. In the same way, it seems best to regard a fractal as a set that has properties such as those [in Definition 1.0.2 below], rather than to look for a precise definition which will almost certainly exclude some interesting cases." We list the properties he suggested in Definition 1.0.2, here.

Definition 1.0.2 ([Fal90])**.** When we refer to a set F as a *fractal* we will typically have the following [properties] in mind.

(i) F has a fine structure, i.e. detail on arbitrarily small scales.

(ii) F is too irregular to be described in traditional geometrical language, both locally and globally.

(iii) Often F has some form of self-similarity, perhaps approximate or statistical.

(iv) Usually, the "fractal dimension" of F (defined in some way) is greater than its topological dimension.

(v) In most cases of interest F is defined in a very simple way, perhaps recursively.

The definition of a "fractal dimension" as mentioned in Property (iv) varies, but common dimensions used are the *Minkowski-Bouligand dimension* or *box dimension* (see Definition 2.1.9 in Chapter 2), and the Hausdorff dimension. Some authors will also include the property of nowhere differentiability as characteristic of fractality.

The present author has not been satisfied with the various definitions and purported properties of fractals specifically because there are often many "fractal" counterexamples. This does not mean that we, as mathematicians, should cast aside the search and need for a proper formal definition, nor does it mean that we should settle for ambiguity to avoid exclusion, but more likely that our understanding of this idea we call "fractality" is still inchoate and we have simply been unable to properly characterize the phenomenon. At least until the work of the present author's Ph.D. advisor, Distinguished Professor Michel L. Lapidus. Professor Lapidus once said: "One cannot think of a fractal as only a set, sometimes it is a structure, sometimes it is a process." Detecting that structure requires the theory of *complex dimensions* (see Chapters 2 and 3). We proceed now to offer up some counterexamples to Definitions 1.0.1 and 1.0.2 which illustrate why a more appropriate definition is necessary.

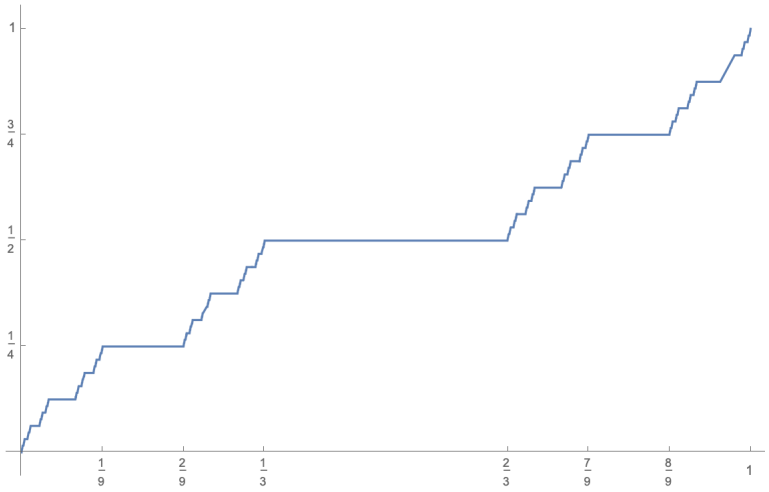

Figure 1.0.1: The Cantor-Lebesgue function, or "The Devil's Staircase".

Counterexample 1.0.1 (The Cantor-Lebesgue Function, or "The Devil's Staircase")**.** Every math graduate student who has taken a course in real analysis is intimately familiar with this function, and it serves as an example of a fractal that fails the requirements of Definition 1.0.1, and/or Property (iv) in Definition 1.0.2). To show this, let f be the Cantor-Lebesgue function (see Figure 1.0.1), and recall the construction of f (see, for example, [Fol99] Chapter 1, Proposition 1.22): let $\mathcal{C}$ be the usual middle-third Cantor set in $[0,1] \subset \mathbb{R}$. Recall that any point in $\mathcal{C}$ can be described in a ternary form where each ternary digit is a 0 or a 2, i.e. $x = \sum_{n=1}^{\infty} \frac{a_n}{3^n}$ where $a_n \in \{0, 2\}$. Define f as

$$f(x) = \begin{cases} \displaystyle\sum_{n=1}^{\infty} \frac{b_n}{2^n} & \text{where } b_n = \frac{a_n}{2} \text{ and } x \in \mathcal{C} \\ \displaystyle\sup_{\substack{y \leq x \\ x \in \mathcal{C}}} f(x) & \text{if } x \in [0,1] \setminus \mathcal{C}. \end{cases} \tag{1.0.1}$$

In other words, f is constant off of $\mathcal{C}$. By inspection, in particular by examining Figure 1.0.1), this function has characteristics that most mathematicians would describe as fractal. However, it is also rectifiable (it has length 2, in fact, a curious property) so this means that its Hausdorff dimension coincides with its topological dimension, 1, so it is not a fractal by Mandelbröt's original definition. Note also that, since the 0-dimensional Lebesgue measure

of $\mathcal{C}$ is 0, f is almost everywhere differentiable on $[0,1]$, so the nondifferentiability criterion some choose to cite as characteristic of fractals is also not satisfied.

Counterexample 1.0.2 (The a-string)**.** This quintessential example can be found in the paper *Fractal Drums, Inverse Spectral Problems for Elliptic Operators and a Partial Resolution of the Weyl-Berry Conjecture* [Lap91] written by Professor Michel L. Lapidus as well as the book *Fractal Geometry, Complex Dimensions and Zeta Functions* [LvF13] by Professor Lapidus and Dr. Machiel van Frankenhuijsen. The a string is a simple construction. Let $a > 0$ and consider the collection of lengths $\mathcal{L}_a = \{l_j\}_{j=1}^{\infty}$ where

$$l_j = \frac{1}{j^a} - \frac{1}{(j+1)^a} \quad \text{for } j \in \mathbb{Z}^+.^{1} \tag{1.0.2}$$

This collection is known as the a-string, and it can be realized as a countable union of intervals formed by removing the points $\frac{1}{j^a}$ from the interval $(0,1)$:

$$\Omega_a = \bigcup_{j=1}^{\infty} \left(\frac{1}{(j+1)^a}, \frac{1}{j^a} \right). \tag{1.0.3}$$

The boundary of this set is

$$\partial\Omega_a = \left\{ \frac{1}{j^a} : j \in \mathbb{Z}^+ \right\} \cup \{0\}. \tag{1.0.4}$$

As shown in [Lap91], Appendix C, $\partial\Omega_a$ has Minkowski dimension $D = \frac{1}{1+a}$ for any $a > 0$. Let's take $a = 1$ for a moment, for clarity. If $a = 1$, then the 1-string is just the *harmonic string*, and the boundary of the 1-string is simply the *harmonic sequence* and its limit point 0: $\left\{0, 1, \frac{1}{2}, \frac{1}{3}, \frac{1}{4}, \ldots\right\}$. This set has Minkowski dimension $D = \frac{1}{1+1} = \frac{1}{2} > 0$, thus, we have a set that satisfies Properties (i), (iii), (iv), and (v) of Definition 1.0.2, yet it is clearly not a fractal.

Counterexample 1.0.3. As a final counterexample, we have *space-filling curves*. The theory of space-filling curves is laid out in detail in Chapter 4, but for now, we can take the

[1] The symbol $\mathbb{Z}^+$ denotes the set positive integers: $\mathbb{Z}^+ = \{1, 2, 3, \ldots\}$.

Hilbert curve (see Section 4.2) as a counterexample. The Hilbert curve is the image of a continuous surjective mapping from the unit interval $[0, 1]$ to the unit square $[0, 1] \times [0, 1]$. More directly, its image is the unit square itself. The unit square satisfies none of the properties in Definition 1.0.2, and no one would describe it as fractal, yet the Hilbert curve is often labeled as a fractal, not because of its image, but because of its *process of generation*. One might also note how the Hilbert curve is nowhere differentiable (see [Sag94], Section 2.5) as evidence of its fractality, but there are space-filling curves which are almost everywhere differentiable, e.g. Lebesgue's space-filling curve (see [Sag94] again, Chapter 5, Theorem 5.42).

We will revisit each of these examples, but space-filling curves offer a perfect example of how fractality is a subtle phenomenon, and, at least until this dissertation, the label of "fractal" bestowed upon them has been strictly colloquial and convenient. To make sense of the fractal nature of space-filling curves, we first need the theory and machinery of *complex dimensions*, to which we now turn.

Chapter 2

The Theory of Complex Dimensions in $\mathbb{R}$

2.1 Preliminaries

Presently, we restrict ourselves to the case when the ambient space in which we are working is $\mathbb{R}$, i.e. $\mathbb{R}^N$ where $N = 1$. The next chapter will detail the generalization of this 1-dimensional theory to higher dimensions. A similar exposition can be found in the the book *Fractal Geometry, Complex Dimensions and Zeta Functions* by Michel L. Lapidus and Machiel van Frankenhuijsen [LvF13], and this author encourages the interested reader to pick up a copy and dive into the fascinating details discussed there. To begin, we define a *fractal string*.

Definition 2.1.1. An *ordinary fractal string* $\mathcal{L}$ is a bounded open subset Ω of $\mathbb{R}$. Such a set can be decomposed into a countable union of disjoint open intervals (see, for example, [Fol99]) of length l_j, and we can write $\mathcal{L} \coloneqq \{l_j\}_{j\geq 1}$. We can assume without loss of generality that $l_1 \geq l_2 \geq l_3 \geq \cdots \geq 0$ where each length is counted according to multiplicity. The *boundary* of $\mathcal{L}$ is denoted by $\partial\mathcal{L}$ and is defined as the boundary, $\partial\Omega$, of Ω.

Note that $\sum_{j\geq 1} l_j < \infty$ since Ω is bounded, and, indeed, this sum is equal to the 1-dimensional Lebesgue measure of Ω. Note also that the number of lengths of an ordinary

fractal string could be finite, but the more interesting examples have an infinite number of lengths. Moreover, this definition is made intentionally general so that the theory can be applied to other related mathematical constructs, and we will formalize the definition of *fractality* below (see Definition 2.3.5) to differentiate fractal objects from non-fractal objects.

Another important interpretation of an ordinary fractal string is that of a 1-dimensional *drum* with fractal boundary. If we consider a single interval for a moment, it can be viewed as a string that, when plucked, produces a sound. A fractal string is a union of these strings. In higher dimensions, the appropriateness of the term "drum" may be easier to see if one imagines, say, a timpani drum. We also use the term *ordinary* here since this definition can be generalized to strings whose lengths have non-integer multiplicity, but since our applications do not, at least at present, require non-integer multiplicities, we will omit that part of the theory. Again, we encourage the interested reader to explore [LvF13] because there is a fountain of fascinating related ideas there.

Definition 2.1.2. The *geometric counting function of* $\mathcal{L}$ is the counting function of the reciprocal lengths that comprise $\mathcal{L}$:

$$N_{\mathcal{L}}(x) \coloneqq \#\left(\{j \geq 1 : l_j^{-1} \leq x\}\right) = \sum_{j:\, l_j^{-1} \leq x} 1 \tag{2.1.1}$$

where $\#(\cdot)$ is the counting measure.

Next we need some basic definitions that will be used throughout this text.

Definition 2.1.3. For any $x \in \mathbb{R}$, the *floor* of x is defined as the largest integer less than or equal to x and is denoted $\lfloor x \rfloor$. Sometimes this is simply called the *integer part* of x. The *ceiling* of x is defined as the smallest integer greater than or equal to x and is denoted $\lceil x \rceil$. The *fractional part* of x is defined as the noninteger part of x and is denoted $\{x\}$. In particular, this notation allows us to write $x = \lfloor x \rfloor + \{x\}$ and $x = \lceil x \rceil + \{x\} - 1$.

Definition 2.1.4. For a point $x \in \mathbb{R}$ and a set $\Omega \subseteq \mathbb{R}$ we define the distance between x and Ω, denoted $d(x, \Omega)$, as

$$d(x, \Omega) \coloneqq \inf_{y \in \Omega} |x - y| \tag{2.1.2}$$

where $|\cdot|$ is the standard Euclidean distance induced by the 1-dimensional Lebesgue measure in $\mathbb{R}$.

Definition 2.1.5. Given a set $\Omega \subseteq \mathbb{R}$ and $t > 0$, we define the *inner tubular neighborhood of* Ω as

$$\Omega_t \coloneqq \{x \in \Omega \mid d(x, \partial\Omega) < t\}. \tag{2.1.3}$$

Now we set out to define the *Minkowski dimension* of a set which is a common "fractal dimension" (see Definition 1.0.2 in Chapter 1) used for analysis. We omit discussion of the Hausdorff dimension since it is not used our particular analysis, but an interested reader can find a detailed and approachable description in [Edg90]. The *Minkowski dimension* of a set is defined in terms of the *Minkowski content* of a set.

Definition 2.1.6. For any set $\Omega \subseteq \mathbb{R}$ and $d \geq 0$, the *upper d-dimensional Minkowski content of* Ω is

$$\mathcal{M}^{*d}(\Omega) \coloneqq \limsup_{t \to 0^+} \frac{|\Omega_t|}{t^{1-d}}. \tag{2.1.4}$$

The *lower d-dimensional Minkowski content of* Ω is defined analogously as

$$\mathcal{M}^{d}_{*}(\Omega) \coloneqq \liminf_{t \to 0^+} \frac{|\Omega_t|}{t^{1-d}}. \tag{2.1.5}$$

By definition we have $0 \leq \mathcal{M}^{d}_{*}(\Omega) \leq \mathcal{M}^{*d}(\Omega) \leq +\infty$. If these two values coincide, we simply call the value the *d-dimensional Minkowski content of* Ω and we can write

$$\mathcal{M}^{d}(\Omega) = \lim_{t \to 0^+} \frac{|\Omega_t|}{t^{1-d}}. \tag{2.1.6}$$

Note that, in general, the d-dimensional upper (or lower) Minkowski content is not a measure. Indeed, if we consider the set of rational numbers $\mathbb{Q}$,

$$\mathcal{M}^{*d}(\mathbb{Q}) = \mathcal{M}^{*d}\left(\overline{\mathbb{Q}}\right) = \mathcal{M}^{*d}(\mathbb{R}) > 0, \tag{2.1.7}$$

but $\mathbb{Q}$ is countable and so should have measure 0 by countable additivity (see, for example, [Fol99]). In particular, $\mathcal{M}^{*d}$ is not a measure in $\mathbb{R}^N$ unless $d = 0$ in which case

$$\mathcal{M}^{*0}(\Omega) = \limsup_{t \to 0^+} \frac{|\Omega_t|}{t} = \#(\Omega). \tag{2.1.8}$$

Similar arguments hold for $\mathcal{M}_*$. The fact that the Minkowski content is not a measure is beneficial in the study of fractal geometry since the fractality of an object can depend on countable sets.

Definition 2.1.7. We say a set $\Omega \subseteq \mathbb{R}$ is *Minkowski nondegenerate* if and only if $0 < \mathcal{M}_*^d(\Omega) \leq \mathcal{M}^{*d}(\Omega) < +\infty$, i.e. if and only if the Minkowski content is a nonzero finite number.

Definition 2.1.8. We say a set $\Omega \subseteq \mathbb{R}$ is *Minkowski measurable* if and only if $0 < \mathcal{M}_*^d(\Omega) \leq \mathcal{M}^{*d}(\Omega) < +\infty$ and $\mathcal{M}^{*d} = \mathcal{M}_*^d = \mathcal{M}^d$, i.e. if and only if Ω is Minkowski nondegenerate and the upper and lower Minkowski contents coincide.

Now that we have established the definition of the Minkowski content of a set, we can define the Minkowski dimension of a set.

Definition 2.1.9. For any set $\Omega \subseteq \mathbb{R}$, the *upper Minkowski dimension of* Ω is the unique real number $\overline{D} \coloneqq \overline{D}(\Omega) \coloneqq \overline{\dim}_B(\Omega)$ such that $\mathcal{M}^{*d}(\Omega) = +\infty$ for all $d < \overline{D}$, and $\mathcal{M}^{*d}(\Omega) = 0$ for all $d \geq \overline{D}$.[1]

The *lower Minkowski dimension of* Ω is defined analogously as the unique real number $\underline{D} \coloneqq \underline{D}(\Omega) \coloneqq \underline{\dim}_B(\Omega)$ such that $\mathcal{M}^{*d}(\Omega) = +\infty$ for all $d < \underline{D}$, and $\mathcal{M}^{*d}(\Omega) = 0$ for all $d \geq \underline{D}$.

[1] The subscript B is used because the Minkowski dimension of a set is equivalent to the box dimension of a set. For a proof of this, see [Lap91] Corollary 3.1.

If these two values coincide, we simply call the quantity the *Minkowski dimension of* Ω and write $D = D(\Omega) = \dim_B(\Omega)$.

Singling out the upper Minkowski dimension for a moment, the fact that such a number exists and is unique needs to be proven in order to establish the soundness of the definition. We do so below for the case when $\mathcal{M}^{*d}(\Omega) < +\infty$ and leave the case when $\mathcal{M}^{*d}(\Omega) = +\infty$ as an exercise to the reader. Moreover, if $d = D$ (or $d = \overline{D}$ or $d = \underline{D}$), then the Minkowski content can be any value in $[0, +\infty]$.

Lemma 2.1.1. The upper Minkowski dimension $\overline{D}$ of a set Ω exists and it is unique.

Proof. Let $\delta > 0$ and let $d \geq 0$. Suppose that $\mathcal{M}^{*d}(\Omega) < +\infty$. Since the limit superior always exists,

$$\begin{aligned} \mathcal{M}^{*(d+\delta)}(\Omega) &= \limsup_{t\to 0^+} \frac{|\Omega_t|}{t^{1-(d+\delta)}} = \limsup_{t\to 0^+} \frac{1}{t^{-\delta}} \cdot \frac{|\Omega_t|}{t^{1-d}} \\ &= \left(\limsup_{t\to 0^+} \frac{1}{t^{-\delta}}\right)\left(\limsup_{t\to 0^+} \frac{|\Omega_t|}{t^{1-d}}\right) = 0 \cdot \mathcal{M}^{*d}(\Omega) = 0. \end{aligned} \tag{2.1.9}$$

Similarly,

$$\begin{aligned} \mathcal{M}^{*(d-\delta)}(\Omega) &= \limsup_{t\to 0^+} \frac{|\Omega_t|}{t^{1-(d-\delta)}} = \limsup_{t\to 0^+} \frac{1}{t^{\delta}} \cdot \frac{|\Omega_t|}{t^{1-d}} \\ &= \left(\limsup_{t\to 0^+} \frac{1}{t^{\delta}}\right)\left(\limsup_{t\to 0^+} \frac{|\Omega_t|}{t^{1-d}}\right) = +\infty \cdot \mathcal{M}^{*d}(\Omega) = +\infty. \end{aligned} \tag{2.1.10}$$

Thus $d = \overline{D}$ is a real number such that $\mathcal{M}^{*d}(\Omega) = +\infty$ for all $d < \overline{D}$, and $\mathcal{M}^{*d}(\Omega) = 0$ for all $d > \overline{D}$. Moreover, this number is unique since, otherwise, if say $\overline{D}_1$ and $\overline{D}_2$ had such a property and were distinct, say $\overline{D}_1 < \overline{D}_2$, then $\mathcal{M}^*_{\frac{\overline{D}_1+\overline{D}_2}{2}}(\Omega) = 0$, contradicting the fact that $\mathcal{M}^*_d(\Omega) = +\infty$ for $d < \overline{D}_2$. □

Now that we have established the soundness of the definition of the upper (and lower) Minkowski dimension, we provide a characterization of this quantity that is helpful in the

analysis of the zeta functions we will see later. This characterization can also be taken as an equivalent definition.

Definition 2.1.10. For any set $\Omega \subseteq \mathbb{R}$,

$$\overline{D}(\Omega) = \inf\{d \geq 0 \mid \mathcal{M}^{*d}(\Omega) < \infty\} \tag{2.1.11}$$

$$= \inf\{d \geq 0 \mid \mathcal{M}^{*d}(\Omega) = 0\} \tag{2.1.12}$$

$$= \sup\{d \geq 0 \mid \mathcal{M}^{*d}(\Omega) = +\infty\}, \tag{2.1.13}$$

and a similar characterization of the lower Minkowski dimension holds by replacing $\overline{D}$ with $\underline{D}$.

Remark 2.1.1. The more irregular the boundary of $\partial\Omega$, the larger the Minkowski dimension D will be. Additionally, it is always the case that $0 \leq H \leq D \leq 1$ where H represents the Hausdorff dimension of a set. (See [Edg90] for a definition and exploration of the Hausdorff measure and dimension, and [Lap91] for a detailed comparison between the two notions of dimension.)

Remark 2.1.2 (Independence of Geometric Realization)**.** The reason to use the Minkowski dimension for our analysis as opposed to the Hausdorff dimension is that the Minkowski dimension is invariant under displacement of the intervals which comprise a fractal string $\mathcal{L}$, whereas this is not the case for the Hausdorff dimension (see [Lap91]). Thus, a fractal string $\mathcal{L}$ is completely determined by the sequence of lengths that comprise it. This independence also holds in higher dimensions, in particular for *relative fractal drums* (see Chapter 3).

2.2 The Cantor String

The quintessential example of a nontrivial ordinary fractal string is the Cantor String, $\mathcal{L}_{CS}$, partially depicted in Figure 2.2.1 and detailed at length in [LvF13]. Let $\Omega = CS$ be the

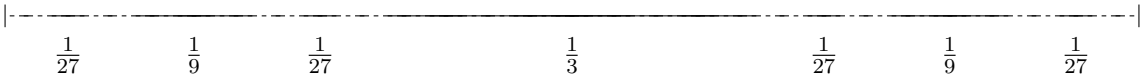

Figure 2.2.1: The Cantor string, CS [LvF13].

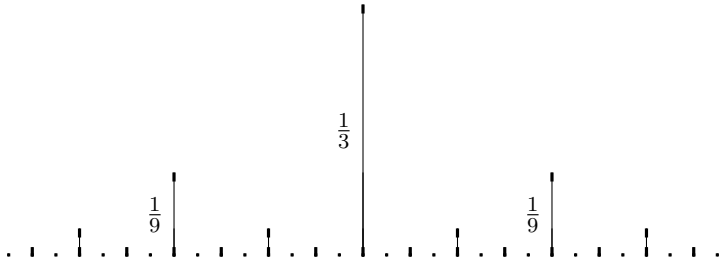

Figure 2.2.2: An inner ε-tubular neighborhood of the Cantor string, CS [LvF13].

complement in $[0,1]$ of the usual ternary Cantor set. In particular,

$$CS = \left(\frac{1}{3},\frac{2}{3}\right) \cup \left(\frac{1}{9},\frac{2}{9}\right) \cup \left(\frac{7}{9},\frac{8}{9}\right) \cup \left(\frac{1}{27},\frac{2}{27}\right) \cup \left(\frac{7}{27},\frac{8}{27}\right) \cup \left(\frac{19}{27},\frac{20}{27}\right) \cup \left(\frac{25}{27},\frac{26}{27}\right) \cup \cdots \tag{2.2.1}$$

and we can see here that the intervals are being counted according to multiplicity. Of particular interest is the volume of the inner tubular neighborhood of CS. In general, for any fractal string, the volume of the inner tubular ε-neighborhood of the boundary is given by

$$V(\varepsilon) = \sum_{j:\, l_j \geq 2\varepsilon} 2\varepsilon + \sum_{j:\, l_j < 2\varepsilon} l_j. \tag{2.2.2}$$

In essence, Equation 2.2.2 expresses the total inner ε-tubular volume as 2ε times the number of lengths that are greater than or equal in length to 2ε plus the sum of all the lengths that are less than 2ε. This makes sense because if $l_j \geq 2\varepsilon$, then we need only include the value 2ε, but if $l_j < 2\varepsilon$, then the interval corresponding to l_j is already shorter than 2ε in length so we must add the entire length itself (see Figure 2.2.2). Note that the volume of the inner tubular neighborhood is independent of geometric realization as well since it only depends on the lengths that comprise the string.

Let's find the inner tubular volume of the Cantor string. Let $\varepsilon \leq \frac{1}{2}$ be given and let $n = \lfloor -\log_3(2\varepsilon) \rfloor$. Then, after examining the Cantor string for a bit, we can deduce that

$$V_{CS}(\varepsilon) = 2\varepsilon \cdot (2^n - 1) + \sum_{k=n}^{\infty} 2^k \cdot 3^{-(k+1)} = 2\varepsilon \cdot 2^n + \left(\frac{2}{3}\right)^n - 2\varepsilon. \tag{2.2.3}$$

In order to obtain an *explicit formula* for $V_{CS}(\varepsilon)$, we observe that, for any $b > 0$ and $b \neq 1$,

$$b^n = b^{\lfloor -\log_3(2\varepsilon) \rfloor} = b^{-\log_3(2\varepsilon) - \{-\log_3(2\varepsilon)\}} = (2\varepsilon)^{-\log_3 b} \cdot b^{-\{-\log_3(2\varepsilon)\}}. \tag{2.2.4}$$

Using this result for $b = 2$ and $b = \frac{2}{3}$, and setting $D = \log_3 2 = \frac{\log 2}{\log 3}$[2], we can rewrite Equation 2.2.3 as

$$V_{CS}(\varepsilon) = (2\varepsilon)^{1-D} \left(\left(\frac{1}{2}\right)^{\{-\log_3(2\varepsilon)\}} + \left(\frac{3}{2}\right)^{\{-\log_3(2\varepsilon)\}} \right) - 2\varepsilon. \tag{2.2.5}$$

The function in parentheses is bounded, nonconstant, and multiplicatively periodic in that it takes on the same value at ε and $\frac{\varepsilon}{3}$. It doesn't have a limit as $\varepsilon \to 0^+$, and this is an example of what we refer to as *geometric oscillations*. We will see that this property is characteristic of fractals, and is related to the *complex dimensions* of a fractal. We can further explore the oscillatory behavior in Equation 2.2.5 by using the Fourier series of the map $u \mapsto b^{-\{u\}}$ for $b > 0$ and $b \neq 1$:

$$b^{-\{u\}} = \frac{b-1}{b} \sum_{n \in \mathbb{Z}} \frac{e^{2\pi i n u}}{\log b + 2\pi i n}. \tag{2.2.6}$$

Setting $\mathbf{p} = \frac{2\pi}{\log 3}$ and substituting Equation 2.2.6 into Equation 2.2.5 yields

$$V_{CS}(\varepsilon) = \frac{1}{2\log 3} \sum_{n \in \mathbb{Z}} \frac{(2\varepsilon)^{1-D-in\mathbf{p}}}{(D + in\mathbf{p})(1 - D - in\mathbf{p})} - 2\varepsilon. \tag{2.2.7}$$

The number $\mathbf{p}$ is called the *oscillatory period* of the Cantor string.

[2]Here and henceforth, the notation "log" refers to the natural logarithm.

2.3 The Geometric Zeta Function of a Fractal String

The definition of a geometric zeta function and many of its properties, some of which we will omit here, is introduced in [LvF13] Section 1.2. Let $\mathcal{L} = \{l_j\}_{j\geq 1}$ be a fractal string. By definition, the sum $\sum_{j=1}^{\infty} l_j^{\sigma}$ converges for $\sigma = 1$, so by passing to a complex variable $s \in \mathbb{C}$, the generalized Dirichlet series

$$\zeta_{\mathcal{L}}(s) = \sum_{j=1}^{\infty} l_j^s \tag{2.3.1}$$

defines a holomorphic function on $\{s \in \mathbb{C} : \text{Re } s > 1\}$ (see, for example, [Con78]).

Definition 2.3.1. The *geometric zeta function* of a fractal string $\mathcal{L}$ is defined as

$$\zeta_{\mathcal{L}}(s) = \sum_{j=1}^{\infty} l_j^s = \sum_{\ell} w_\ell \cdot \ell^s, \tag{2.3.2}$$

where w_ℓ is the multiplicity of the (distinct) length ℓ. Note that this series is only well-defined if it converges, and if it converges, then it does so absolutely since the lengths l_j are all nonnegative real numbers.

Remark 2.3.1 (Independence of Geometric Realization)**.** Note here that the geometric zeta function of a fractal string is also independent of geometric realization, an important attribute of this analytical tool. We will also see this for the *relative distance zeta function* discussed in Chapter 3 (see Remak 3.3.2).

Definition 2.3.2. The *abscissa of convergence* of the series in Equation 2.3.2 is defined as

$$\sigma = \inf \left\{ \alpha \in \mathbb{R} : \sum_{j=1}^{\infty} l_j^{\alpha} < +\infty \right\}. \tag{2.3.3}$$

In other words, $\{s \in \mathbb{C} : \text{Re } s > \sigma\}$ is the largest open half-plane on which this series converges. Moreover, the function $\zeta_{\mathcal{L}}(s)$ is holomorphic on this half-plane.

Theorem 2.3.1 ([LvF13] Theorem 1.10)**.** Suppose a fractal string $\mathcal{L}$ has infinitely many lengths. Then the abscissa of convergence of its geometric zeta function (the series in 2.3.2) coincides with $D = D_{\mathcal{L}}$, the Minkowski dimension of $\partial\mathcal{L}$.

We omit the proof of this theorem here, but a complete proof can be found in [LvF13]. Note that if $\mathcal{L}$ has finitely many lengths, then $D = 0$, but $\sigma = -\infty$ since $\zeta_{\mathcal{L}}(s)$ converges for all $s \in \mathbb{C}$. We also get the following corollary.

Corollary 2.3.1. The Minkowski dimension of an ordinary fractal string satisfies $0 \leq D \leq 1$.

The geometric zeta function of a fractal string is a fundamental tool of fractal analysis. It is holomorphic on some open half plane, but it may admit an analytic continuation to a larger set. In general, it will not have an analytic continuation to all of $\mathbb{C}$. In order to study it more carefully, we introduce the notions of a *screen* and a *window*.

Definition 2.3.3. We define the *screen* $\boldsymbol{S}$ to be the contour $\boldsymbol{S} \coloneqq \{s \in \mathbb{C} : s = S(t) + it, t \in \mathbb{R}\}$ where $S : \mathbb{R} \to [-\infty, D_{\mathcal{L}}]$ is a Lipschitz continuous function. We define the *window* W to be the part of the complex plane that is to the right of the screen, i.e. $W \coloneqq \{s \in \mathbb{C} : \operatorname{Re} s \geq S(\operatorname{Im} s)\}$. Note that W is a closed subset of $\mathbb{C}$ and $\boldsymbol{S} = \partial W$, the boundary of W. (See Figure 2.3.1.)

We will assume that $\zeta_{\mathcal{L}}$ is *admissible*, i.e. has a meromorphic extension to an open neighborhood of W and that $\zeta_{\mathcal{L}}$ does not have any singularity on the screen $\boldsymbol{S}$. (See Definition 3.3.7 in Chapter 3 for a more general definition.)

Definition 2.3.4. The set of *visible complex dimensions* of a fractal string $\mathcal{L}$ is

$$\mathcal{D}_{\mathcal{L}} \coloneqq \mathcal{D}_{\mathcal{L}}(W) \coloneqq \{\omega \in W : \zeta_{\mathcal{L}} \text{ has a singularity at } \omega\}. \tag{2.3.4}$$

If $W = \mathbb{C}$, then we call the set $\mathcal{D}_{\mathcal{L}}(\mathbb{C})$ simply the set of *complex dimensions* of $\zeta_{\mathcal{L}}$.

Remark 2.3.2. Note that the term *complex dimension* in this context is not the same as the one used in differential geometry where $\mathbb{C} = \mathbb{R}^2$ is often called a space of "complex

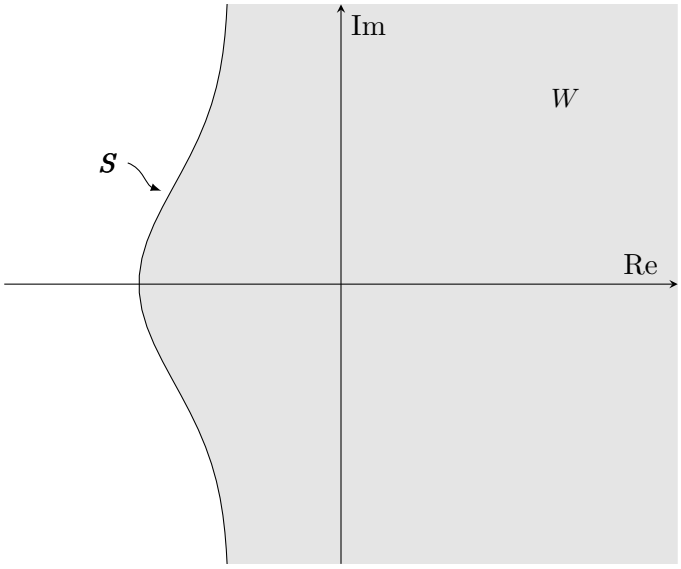

Figure 2.3.1: The *screen* $\boldsymbol{S}$ and the *window* W.

dimension 1". The term "complex dimensions" was settled upon since these singularities are directly associated with the "fractal dimension" of an object, in this case the Minkowski dimension, and, as we will see now, the existence of nonreal singularities.

Definition 2.3.5. A fractal string is defined as *fractal* if and only if the meromorphic continuation of its associated geometric zeta function has at least one nonreal complex dimension.

This powerful definition gives a way of properly characterizing fractality in $\mathbb{R}$ and we will see how it can be extended to $\mathbb{R}^N$ in Chapter 3. Let's return to the example of the Cantor string (see Section 2.2). By the definition of CS, the geometric zeta function of CS is

$$\zeta_{CS}(s) = \sum_{n=0}^{\infty} 2^n \cdot 3^{-(n+1)s} = \frac{3^{-s}}{1 - 2 \cdot 3^{-s}}. \tag{2.3.5}$$

This series is valid initially for all $s \in \mathbb{C}$ such that $\operatorname{Re} s > D_{CS} = D = \log_3 2$ by Theorem 2.3.1, but has a meromorphic continuation to all of $\mathbb{C}$, which we can write as the rational

function on the right in Equation 2.3.5. The singularities of $\zeta_{\mathcal{L}}$, i.e. the complex dimensions of CS, can be found by solving the complex exponential equation $1 - 2 \cdot 3^{-s} = 0$. This yields

$$\mathcal{D}_{CS} = \{D + in\mathbf{p} : \, n \in \mathbb{Z}\}, \tag{2.3.6}$$

where $D = \log_3 2$, the Minkowski dimension of the Cantor set, $\mathcal{C} = \partial CS$, and $\mathbf{p} = \frac{2\pi}{\log 3}$ is the oscillatory period of the Cantor string. Figure 2.3.2 depicts the poles of ζ_{CS} on the complex plane $\mathbb{C}$. Consequently, the Cantor set is a fractal by Definition 2.3.5.

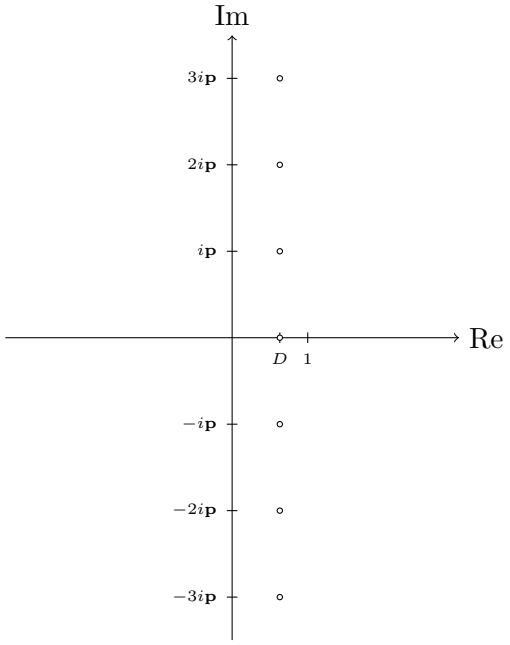

Figure 2.3.2: The complex dimensions of the Cantor set shown on the complex plane $\mathbb{C}$.

Remark 2.3.3. Heuristically speaking, nonreal complex dimensions above D indicate oscillations in the geometry of CS and the volume of the tubular neighborhood as well. We also see this oscillatory behavior in the geometric counting function of CS (Definition 2.1.2): for any $x \geq 1$, there are $1 + 2 + 4 + \cdots + 2^{n-1}$ lengths greater than x^{-1} where $n = \lfloor \log_3 x \rfloor$. Thus, $N_{CS}(x) = 2^n - 1$, and using the Fourier series in 2.2.6, we find

$$N_{CS}(x) = \frac{1}{2 \log 3} \sum_{n \in \mathbb{Z}} \frac{x^{D+in\mathbf{p}}}{D + in\mathbf{p}} - 1 = \frac{1}{2 \log 3} \sum_{\omega \in \mathcal{D}_{CS}} \frac{x^{\omega}}{\omega} - 1. \tag{2.3.7}$$

This oscillatory behavior is characteristic of fractals defined as in Definition 2.3.5, and we will explore it again in Chapter 6.

Naturally, one may be skeptical about the definition of fractality given in Definition 2.3.5. Why should this definition be taken over others? The a-string given in Counterexample 1.0.2 provides a clear reason: as detailed in [LvF13], Section 6.5.1, Theorem 6.21, the Minkowski dimension of the a-string is $\frac{1}{a+1}$, and the set of complex dimensions of the a-string is the following (or at least a subset of the following).

$$\mathcal{D}_a = \left\{ D = \frac{1}{a+1}, -\frac{1}{a+1}, -\frac{2}{a+1}, -\frac{3}{a+1}, \dots \right\} = \left\{ \frac{n}{a+1} : n \in \mathbb{Z}^+ \cup \{-1\} \right\}. \quad (2.3.8)$$

More specifically, all of the complex dimensions of the a-string are *real*, so it is, correctly, *not* classified as a fractal under Definition 2.3.5, even though it has a "fractal dimension" (Minkowski dimension) that is strictly greater than its topological dimension, 0. More evidence that this is the appropriate definition to describe fractality will be given in the next chapter where we generalize the theory to dimensions larger than 1.

Chapter 3

The Theory of Complex Dimensions in $\mathbb{R}^N$

3.1 Introduction

The following chapter details a natural generalization of the theory of complex dimensions to the higher-dimensional space, $\mathbb{R}^N$, for $N \in \mathbb{Z}^+$. In higher dimensions, the richness and beauty of the theory of complex dimensions becomes even more clear, and, naturally, we can recover the theory for $\mathbb{R}$ (when $N = 1$). This generalization to higher dimensions is critical for fractal analysis since many fractals have a dimension greater than 1, in particular, space-filling curves. As with Chapter 2, this preliminary exposition is similar to that found in the book *Fractal Zeta Functions and Fractal Drums: Higher-Dimensional Theory of Complex Dimensions* [LRŽ17] by Michel L. Lapidus, Goran Radunović, and Darko Žubrinić, and we encourage the interested reader to pick up a copy and explore. We begin with some preliminary definitions and theorems that are analogous to the ones seen Chapter 2.

3.2 The Distance Zeta Function of a Set in $\mathbb{R}^N$

Definition 3.2.1. For a point $x \in \mathbb{R}^N$ and a set $A \subseteq \mathbb{R}$ we define $d(x, A)$ as

$$d(x, A) \coloneqq \inf_{y \in A} |x - y|_N \tag{3.2.1}$$

where $|\cdot|_N$ is the standard Euclidean distance induced by the N-dimensional Lebesgue measure in $\mathbb{R}^N$.

Definition 3.2.2. Given a set $A \subseteq \mathbb{R}^N$ and $t > 0$, define the *tubular neighborhood of* A as

$$A_t \coloneqq \{x \in \mathbb{R}^N \mid d(x, \partial A) < t\}. \tag{3.2.2}$$

Remark 3.2.1. Note that this definition differs from Definition 2.1.5 in that x is not restricted to A, so rather than an *inner* tubular neighborhood, we are working with the *complete* tubular neighborhood. For our analysis this distinction will not matter, (see Remark 3.3.3 and Theorem 2.3.1) but for intuition in $\mathbb{R}^1$, the inner tubular neighborhood is more helpful. Also, now that we are in $\mathbb{R}^N$, the use of the word *tubular* is easier to intuit: suppose A is a line in $\mathbb{R}^3$. Then A_t is the open cylinder of radius t with axis the line A, i.e. the open tube surrounding the line A. If we instead consider $A = S^2$, the closed unit sphere, embedded in $\mathbb{R}^3$, then $A_t = (S^2)_t$ is the region between the two open spheres of radius $1 \pm t$ centered at the center of A.

Definition 3.2.3. For any set $A \subseteq \mathbb{R}^N$ and $d \geq 0$, the *upper d-dimensional Minkowski content of* A is

$$\mathcal{M}^{*d}(A) \coloneqq \limsup_{t \to 0^+} \frac{|A_t|_N}{t^{N-d}}. \tag{3.2.3}$$

The *lower d-dimensional Minkowski content of* A is defined analogously as

$$\mathcal{M}_*^{d}(A) \coloneqq \liminf_{t \to 0^+} \frac{|A_t|_N}{t^{N-d}}. \tag{3.2.4}$$

By definition we have $0 \leq \mathcal{M}_*^d(A) \leq \mathcal{M}^{*d}(A) \leq +\infty$. If these two values coincide, we simply call the value the *d-dimensional Minkowski content of A* and we can write

$$\mathcal{M}^d(A) = \lim_{t \to 0^+} \frac{|A_t|_N}{t^{N-d}}. \tag{3.2.5}$$

Remark 3.2.2. This definition differs from Definition 2.1.6 in that the N-dimensional Lebesgue measure is being used, and the exponent of the term in the denominator is $N - d$, where N is the dimension of the ambient space $\mathbb{R}^N$. Note that when $N = 1$, we recover Definition 2.1.6.

Definition 3.2.4. We say a set $A \subseteq \mathbb{R}^N$ is *Minkowski nondegenerate* if and only if $0 < \mathcal{M}_*^d(A) \leq \mathcal{M}^{*d}(A) < +\infty$, i.e. if and only if the Minkowski content is a nonzero finite number.

Definition 3.2.5. We say a set $A \subseteq \mathbb{R}^N$ is *Minkowski measurable* if and only if $0 < \mathcal{M}_*^d(A) \leq \mathcal{M}^{*d}(A) < +\infty$ and $\mathcal{M}^{*d} = \mathcal{M}_*^d = \mathcal{M}^d$, i.e. if and only if A is Minkowski nondegenerate and the upper and lower Minkowski contents coincide.

Definition 3.2.6. For any set $A \subseteq \mathbb{R}^N$, the *upper Minkowski dimension of A* is the unique real number $\overline{D} \coloneqq \overline{D}(A) \coloneqq \overline{\dim}_B(A)$ such that $\mathcal{M}^{*d}(A) = +\infty$ for all $d < \overline{D}$, and $\mathcal{M}^{*d}(A) = 0$ for all $d \geq \overline{D}$.

The *lower Minkowski dimension of A* is defined analogously as the unique real number $\underline{D} \coloneqq \underline{D}(A) \coloneqq \underline{\dim}_B(A)$ such that $\mathcal{M}^{*d}(A) = +\infty$ for all $d < \underline{\mathrm{D}}$, and $\mathcal{M}^{*d}(A) = 0$ for all $d \geq \underline{D}$

If these two values coincide, we simply call the quantity the *Minkowski dimension of A* and write $D = D(A) = \dim_B(A)$.

Definition 3.2.7. For any set $A \subseteq \mathbb{R}^N$,

$$\overline{D}(A) = \inf\{d \geq 0 \mid \mathcal{M}^{*d}(A) < \infty\} \tag{3.2.6}$$

$$= \inf\{d \geq 0 \mid \mathcal{M}^{*d}(A) = 0\} \tag{3.2.7}$$

$$= \sup\{d \geq 0 \mid \mathcal{M}^{*d}(A) = +\infty\}, \tag{3.2.8}$$

and a similar characterization of the lower Minkowski dimension holds by replacing $\overline{D}$ with $\underline{D}$.

In Definition 2.3.1, we defined the *geometric zeta function* of a bounded set $\Omega \subset \mathbb{R}$ in terms of the lengths comprising the string $\mathcal{L}$. The analogous generalization of this fractal zeta function to bounded sets $A \subset \mathbb{R}^N$ is given by the following definition.

Definition 3.2.8. Let $A \subset \mathbb{R}^N$ be a bounded set, and let $\delta > 0$ be arbitrary but fixed. The *distance zeta function* of A is

$$\zeta_A(s) \coloneqq \int_{A_\delta} d(x, A)^{s-N} \, \mathrm{d}x \tag{3.2.9}$$

for all $s \in \mathbb{C}$ sufficiently large. The integral is taken in the sense of Lebesgue and, as such, is absolutely convergent.

In essence, we are taking the distance from any point in a δ-neighborhood of A, raising that value to the complex exponent $s - N$, and integrating the result over the entire δ-neighborhood. In analogy to Definition 2.3.2 we have the following definition.

Definition 3.2.9. The *abscissa of convergence* of the integral in Equation 3.2.9 is defined as

$$D(\zeta_A) \coloneqq \inf\left\{\alpha \in \mathbb{R} : \int_{A_\delta} d(x, A)^{\alpha-N} \, \mathrm{d}x < \infty\right\}. \tag{3.2.10}$$

In other words, $\{s \in \mathbb{C} : \operatorname{Re} s > D(\zeta_A)\}$ is the largest open half-plane on which this series converges. Note also that $D(\zeta_A) \in \mathbb{R} \cup \{\pm\infty\}$, so the abscissa of convergence can be $\pm\infty$.

The following theorem establishes several important results about the distance zeta function, and part of it is analogous to Theorem 2.3.1. We simply state it here, but the interested reader can find a complete proof in [LRŽ17] subsection 2.1.2 (see Theorem 2.1.11).

Theorem 3.2.1 ([LRŽ17] Theorem 2.1.11)**.** Let $A \subset \mathbb{R}^N$ be a bounded set and let $\delta > 0$. Then

(a) The distance zeta function ζ_A defined in Equation 3.2.9 is holomorphic (i.e. analytic) in the open right half-plane $\{\text{Re } s > \overline{\dim}_B A\}$ and for all complex numbers in that region, its complex derivative is given as follows:

$$\zeta_A'(s) = \int_{A_\delta} d(x, A)^{s-N} \log d(x, A) \, \mathrm{d}x. \tag{3.2.11}$$

(b) The lower bound in the open right half-plane $\{\text{Re } s > \overline{\dim}_B A\}$ is optimal from the point of view of the (absolute) convergence of the Dirichlet-type integral defining ζ_A. In other words

$$\overline{\dim}_B(A) = D(\zeta_A), \tag{3.2.12}$$

where $D(\zeta_A)$ is the abscissa of convergence as defined in Equation 3.2.10. It follows that $D(\zeta_A) \in [0, N]$. Furthermore, the identity in Equation 3.2.9 contnues to hold in the half-plane of convergence $\{\text{Re } s > \overline{\dim}_B A\}$ of ζ_A. Moreover we have

$$D(\zeta_A) = \inf \left\{ \alpha \in [0, N] : \int_{A_\delta} d(x, A)^{\alpha - N} \, \mathrm{d}x < \infty \right\}. \tag{3.2.13}$$

(c) If the Minkowski (box) dimension $D := \dim_B A$ exists, $D < N$, and $\mathcal{M}_*^D(A) > 0$, then $\zeta_A(s) \to +\infty$ as $s \in \mathbb{R}$ converges to D from the right (so that D is a singularity of ζ_A).

3.3 The Relative Distance Zeta Function of a Set in $\mathbb{R}^N$

Now we introduce the *relative distance zeta function*, a fractal zeta function that gives us much more freedom in analyzing fractals of interest, and allows us to recover the theory in

$\mathbb{R}$. For a complete introduction as well as a bevy of interesting examples and connected topics, see [LRŽ17] Section 4.1.1.

Definition 3.3.1. Let $\Omega \subset \mathbb{R}^N$ be an open set, not necessarily bounded, but of finite N-dimensional Lebesgue measure. Let $A \subseteq \mathbb{R}^N$, also possibly unbounded, such that $\Omega \subseteq A_\delta$ for some $\delta > 0$. The *distance zeta function* $\zeta_{A,\Omega}$ *of* A *relative to* Ω (or the *relative distance zeta function*) is defined by

$$\zeta_{A,\Omega}(s) \coloneqq \int_\Omega d(x, A)^{s-N} \, \mathrm{d}x, \tag{3.3.1}$$

for all $s \in \mathbb{C}$ with Re s sufficiently large.

Definition 3.3.2. The ordered pair (A, Ω) in Definition 3.3.1 is called a *relative fractal drum*, abbreviated RFD.

Remark 3.3.1. In practice, A is typically the fractal of interest, and Ω is typically a set whose closure contains the fractal of interest, although this is not necessary for the relative distance zeta function in Definition 3.3.1 to be well-defined. The shape of the *drum* Ω is a choice, but the entirety of the drum must be contained in some tubular neighborhood of A to be valid. Consequently, when the role of δ needs to be emphasized, we can equivalently define the *relative distance zeta function* as

$$\zeta_{A,\Omega}(s; \delta) \coloneqq \int_{\Omega \cap A_\delta} d(x, A)^{s-N} \, \mathrm{d}x, \tag{3.3.2}$$

where $\delta > 0$ is a fixed number sufficiently large.

Remark 3.3.2 (Independence of Geometric Realization)**.** Note here that the relative distance zeta function is independent of geometric realization, just as we saw with the geometric zeta function in Chapter 2. In other words, this zeta function and the results obtained from its use, in particular the singularities, do not depend on an immutable geometric configuration of the fractal of interest.

Next we introduce the *relative Minkowski content* to continue our analysis.

Definition 3.3.3. For any set $A \subseteq \mathbb{R}^N$ and any $d \in \mathbb{R}$, we define the *upper d-dimensional Minkowski content of A relative to Ω* (or the *upper relative Minkowski content of the RFD* (A, Ω)) by

$$\mathcal{M}^{*d}(A, \Omega) \coloneqq \limsup_{t \to 0^+} \frac{|A_t \cap \Omega|_N}{t^{N-d}}. \tag{3.3.3}$$

The *lower d-dimensional Minkowski content of A relative to Ω* is defined analogously as

$$\mathcal{M}_*^d(A, \Omega) \coloneqq \liminf_{t \to 0^+} \frac{|A_t \cap \Omega|_N}{t^{N-d}}. \tag{3.3.4}$$

Note that now we have $-\infty \leq \mathcal{M}_*^d(A, \Omega) \leq \mathcal{M}^{*d}(A, \Omega) \leq +\infty$ whereas with Definitions 2.1.6 and 3.2.3 we have $0 \leq \mathcal{M}_*^d(A, \Omega) \leq \mathcal{M}^{*d}(A, \Omega) \leq +\infty$. If these two values coincide, we simply call the value the *d-dimensional Minkowski content of* (A, Ω) and we can write

$$\mathcal{M}^d(A, \Omega) = \lim_{t \to 0^+} \frac{|A_t \cap \Omega|_N}{t^{N-d}}. \tag{3.3.5}$$

Similar to the equivalent definition given in Definition 3.2.7, we also have:

Definition 3.3.4. For any relative fractal drum (A, Ω), we define the *upper d-dimensional Minkowski dimension of A relative to Ω* (or the *upper relative Minkowski dimension of the RFD* (A, Ω)) as

$$\overline{D}(A, \Omega) = \inf\{d \geq 0 \mid \mathcal{M}^{*d}(A, \Omega) < \infty\} \tag{3.3.6}$$

$$= \inf\{d \geq 0 \mid \mathcal{M}^{*d}(A, \Omega) = 0\} \tag{3.3.7}$$

$$= \sup\{d \geq 0 \mid \mathcal{M}^{*d}(A, \Omega) = +\infty\}, \tag{3.3.8}$$

and a similar characterization of the lower relative Minkowski dimension holds by replacing $\overline{D}$ with $\underline{D}$.

Definition 3.3.5. We say an RFD (A, Ω) is *Minkowski nondegenerate* if and only if $0 < \mathcal{M}_*^d(A, \Omega) \leq \mathcal{M}^{*d}(A, \Omega) < +\infty$, i.e. if and only if the Minkowski content is a nonzero finite number.

Definition 3.3.6. We say an RFD (A, Ω) is *Minkowski measurable* if and only if $0 < \mathcal{M}_*^d(A, \Omega) \leq \mathcal{M}^{*d}(A, \Omega) < +\infty$ and $\mathcal{M}^{*d} = \mathcal{M}_*^d = \mathcal{M}^d$, i.e. if and only if (A, Ω) is Minkowski nondegenerate and the upper and lower Minkowski contents coincide. (For a more detailed discussion of the relative Minkowski dimension, see [Lap91].)

Remark 3.3.3. Given some open set $\Omega \subseteq \mathbb{R}^N$, if we assume $A = \partial\Omega$, then $\overline{\dim}_B(\partial\Omega, \Omega)$ is the *inner Minkowski dimension of* $\partial\Omega$. If $N = 1$, this current scenario where $(A, \Omega) = (\partial\Omega, \Omega)$ allows us to recover the theory presented in Chapter 2. However, since we need not restrict ourselves to this special case, it may the case that $\overline{\dim}_B(A, \Omega)$ differs from $\overline{\dim}_B(A)$, where $\overline{\dim}_B(A)$ is as defined in Definition 3.2.6. More specifically, we have

$$\overline{\dim}_B(A, \Omega) \in [-\infty, \overline{\dim}_B(A)], \tag{3.3.9}$$

and similarly for the lower Minkowski dimension. In some cases, the inequality $\overline{\dim}_B(A, \Omega) \leq \overline{\dim}_B(A)$ may be strict (see Example 4.1.23 in Section 4.1.1 of [LRŽ17]).

Definition 3.3.7. A relative fractal drum (A, Ω) is said to be *admissible* if its relative distance zeta function $\zeta_{A,\Omega}$ can be meromorphically extended to an open connected neighborhood of some window W, and that $\zeta_{A,\Omega}$ does not have any singularity on the screen $\boldsymbol{S}$.

Now that we have all the tools we need, given any RFD (A, Ω), we can define the *relative complex dimensions* of A with respect to Ω. Like before, we will assume that $\zeta_{A,\Omega}$ is admissible.

Definition 3.3.8. The set of *visible relative complex dimensions* of an admissible RFD (A, Ω) is

$$\mathcal{D}_{A,\Omega} = \mathcal{D}_{A,\Omega}(W) \coloneqq \{\omega \in W : \zeta_{A,\Omega} \text{ has a singularity at } \omega\}.$$

If $W = \mathbb{C}$, then we call the set $\mathcal{D}_{A,\Omega}(\mathbb{C})$ simply the set of *relative complex dimensions* of $\zeta_{A,\Omega}$.

This natural extension yields the following robust definition of fractality.

Definition 3.3.9. A set $A \subseteq \mathbb{R}^N$ is defined as *fractal* if and only if there exists an associated relative fractal drum (A, Ω) (in the sense of Definitions 3.3.1 and 3.3.2) such that the meromorphic continuation of the associated relative distance zeta function has at least one nonreal complex dimension.

This definition expands the robustness of Definition 2.3.5 and allows us to properly classify some sets in $\mathbb{R}^2$ and above that have otherwise not been properly classified as fractals or nonfractals. In particular, it allows us to show that a class of *plane-filling curves* (see Chapter 4) satisfies this definition, and thus can be accurately, instead of just colloquially, classified as fractals for the first time.

Next, we have the following important result, analogous to Theorems 3.2.1 and 2.3.1.

Theorem 3.3.1 ([LRŽ17] Theorem 4.1.7)**.** Let Ω be an open subset of $\mathbb{R}^N$ of finite N-dimensional Lebesgue measure, and let $A \subseteq \mathbb{R}^N$ be such that $\Omega \subseteq A_\delta$ for some $\delta > 0$. Then the following properties hold:

(a) The relative distance zeta function $\zeta_{A,\Omega}$ defined in Equation 3.3.1 is holomorphic (i.e. analytic) in the open right half-plane $\{\text{Re } s > \overline{\dim}_B(A, \Omega)\}$ and for all complex numbers in that region, its complex derivative is given as follows:

$$\zeta'_{A,\Omega}(s) = \int_\Omega d(x, A)^{s-N} \log d(x, A) \, \mathrm{d}x. \tag{3.3.10}$$

(b) The lower bound in the open right half-plane $\{\text{Re } s > \overline{\dim}_B(A, \Omega)\}$ is optimal from the point of view of the (absolute) convergence of the Dirichlet-type integral defining $\zeta_{A,\Omega}$. In other words

$$\overline{\dim}_B(A, \Omega) = D(\zeta_{A,\Omega}), \tag{3.3.11}$$

where $D(\zeta_{A,\Omega})$ is the abscissa of convergence as defined in Equation 3.2.10.

(c) If the Minkowski dimension $D := \dim_B(A, \Omega)$ exists, $D < N$, and $\mathcal{M}_*^D(A, \Omega) > 0$, then $\zeta_{A,\Omega}(s) \to +\infty$ as $s \in \mathbb{R}$ converges to D from the right (so that D is a singularity of $\zeta_{A,\Omega}$).

Remark 3.3.4. One might wonder why we prefer to work with the upper Minkowski (or box) dimension instead of the lower, and the answer is that the upper Minkowski dimension enjoys *finite stability*. More specifically, given any two sets $A, B \subseteq \mathbb{R}^N$, we have $\overline{\dim}_B(A \cup B) = \max\left\{\overline{\dim}_B(A), \overline{\dim}_B(B)\right\}$. This is not the case for the lower Minkowski (or box) dimension (see [Fal90], or [LRŽ17] Section 6.1.2). Moreover, this result can be extended to the relative Minkowski dimension, i.e. for any two RFDs (A, Ω) and (B, Ω) sharing the same drum, we have $\overline{\dim}_B(A \cup B, \Omega) = \max\left\{\overline{\dim}_B(A, \Omega), \overline{\dim}_B(B, \Omega)\right\}$.

Next we have three other important and useful theorems about the relative distance zeta function that we will use in application in Chapter 5. First we state a basic definition.

Definition 3.3.10. Given a set $A \subseteq \mathbb{R}^N$ and a real number $k \in \mathbb{R}$, we define

$$kA := \{kx \in \mathbb{R}^N : x \in A\} = \{(kx_1, kx_2, \ldots, kx_N) : (x_1, x_2, \ldots, x_N) \in A\}. \tag{3.3.12}$$

Theorem 3.3.2. Let $\zeta_{A,\Omega}(s)$ be the relative distance zeta function of some relative fractal drum (A, Ω). Then for any real constant $k > 0$ we have that $D(\zeta_{kA,k\Omega}) = D(\zeta_{A,\Omega}) = \overline{\dim}_B(A, \Omega)$, and

$$\zeta_{kA,k\Omega}(s) = k^s \zeta_{A,\Omega}(s) \tag{3.3.13}$$

for $\operatorname{Re} s > \overline{\dim}_B(A, \Omega)$.

In other words, for positive scalars, the abscissa of convergence of the relative distance zeta function of the scaled RFD is the same as the abscissa of convergence of the relative distance zeta function of the unscaled RFD. Moreover, the zeta function of the scaled RFD can be written as a complex exponential multiple of the zeta function of the unscaled RFD.

Theorem 3.3.3. Assume that $\Omega = \bigcup_{j=1}^{\infty} B_j$ is an open subset in $\mathbb{R}^N$ of finite N-dimensional Lebesgue measure, where $\{B_j\}_{j=1}^{\infty}$ is a sequence of pairwise disjoint open subsets of $\mathbb{R}^N$.

Also assume that $A \subseteq \mathbb{R}^N$ and there exists a $\delta > 0$ such that $\Omega \subseteq A_\delta$. Then for all $s \in \mathbb{C}$ such that Re $(s) > \overline{\dim}_B(A, \Omega)$, we have

$$\zeta_{A,\Omega}(s) = \sum_{j=1}^{\infty} \zeta_{A,B_j}(s).$$

In other words, if our RFD is a disjoint union of *sub-RFDs* or *relative fractal subdrums*, then the relative distance zeta function of the union is the sum of the relative distance zeta functions of the individual subdrums, provided the subdrums are disjoint. This result combined with the result in Theorem 3.3.2 is very helpful when an RFD exhibits self-similarity at scale because, as long as the subdrums are disjoint, we can compute the zeta function of the entire RFD if we know the zeta functions of sub-RFDs.

Theorem 3.3.4 ([LRŽ17] 4.1.14)**.** Suppose that (A, Ω) is a Minkowski nondegenerate RFD in $\mathbb{R}^N$, (in particular $\dim_B(A, \Omega) = D$), and $D < N$. If $\zeta_{A,\Omega}(s)$ can be meromorphically extended to a connected open neighborhood of $\{\text{Re } (s) = D\}$, then D is necessarily a simple pole of $\zeta_{A,\Omega}$, the residue $\text{res}(\zeta_{A,\Omega}(s), D)$ is independent of δ and

$$\mathcal{M}_*^D(A, \Omega) \leq \frac{\text{res}(\zeta_{A,\Omega}(s), D)}{N - D} \leq \mathcal{M}^{*D}(A, \Omega). \tag{3.3.14}$$

Furthermore, if (A, Ω) is Minkowski measurable then this inequality yields

$$\mathcal{M}^D(A, \Omega) = \frac{\text{res}(\zeta_{A,\Omega}(s), D)}{N - D}. \tag{3.3.15}$$

This theorem is a helpful one because it allows us to express the D-dimensional relative Minkowski content of a set in terms of its relative distance zeta function. In particular, we will use this Theorem in Chapter 5 to assert the appropriateness of a class of relative fractal drums.

3.4 Examples of Relative Fractal Drums in $\mathbb{R}^2$

Examples are always illuminating, and this section consists of two examples that can help elucidate the application of the theory of complex dimensions in $\mathbb{R}^2$.

The Sierpiński Gasket

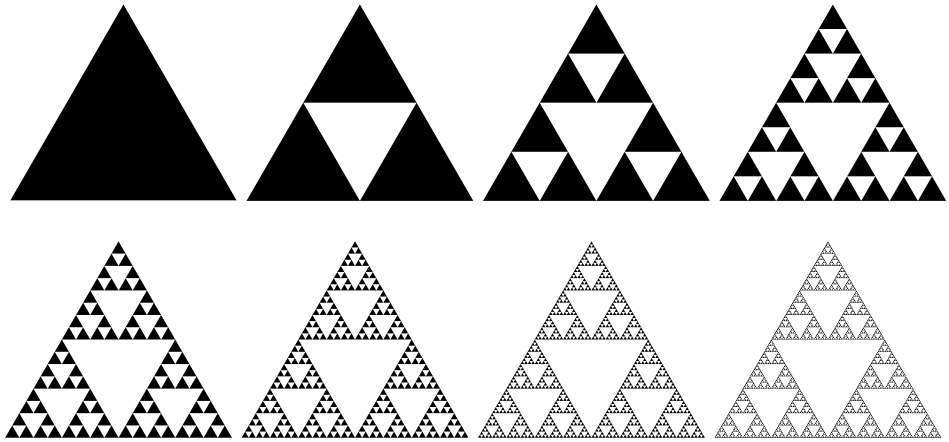

Figure 3.4.1: The first 8 approximations to the Sierpiński gasket (SG).

The Sierpiński gasket is a quintessential example of a fractal in $\mathbb{R}^2$, and in this section we will see how to construct an admissible RFD for the gasket, compute its relative distance zeta function, and find its complex dimensions. More details about this example can be found in [LRŽ17] Section 4.2.3, Example 4.2.24, where the use of *relative fractal sprays* is employed. One way of constructing the gasket is shown in Figure 3.4.1: one begins with the standard closed equilateral unit triangle, and then removes the successive open inner triangles formed by connecting the midpoints of the edges of the remaining triangles. Continue this process ad infinitum, and the set that remains is the Sierpiński gasket, SG. It is an interesting object for many reasons, but one intriguing property is that it has zero 2-dimensional Lebesgue measure (area) and infinite 1-dimensional Lebesgue meaure (length). This is often used as a motivating example for the development of the theory of fractal dimensions. One can calculate directly that the Minkowski dimension (and Hausdorff dimension) is $D_{SG} = \log_2 3$,

and we will see it recovered here. Note that $1 < \log_2 3 < 2$, so the higher-dimensional theory of complex dimensions is needed for our analysis. Now we proceed to compute the relative distance zeta function of $A = SG$. For a drum, we simply choose Ω to be the open unit triangle. Let $\delta > 1/6$ so that A_δ is simply connected, and we have that $\Omega \subset A_\delta$. To begin, the integral we are trying to compute is

$$\zeta_{SG,\Omega}(s) = \int_\Omega d(\mathbf{x}, SG)^{s-2}\, \mathrm{d}\mathbf{x}, \int_\Omega d((x,y), SG)^{s-2}\, \mathrm{d}y\, \mathrm{d}x, \tag{3.4.1}$$

so we need to analyze carefully what $d((x,y), SG)$ should be. Note that for any $(x,y) \in SG$ itself, $d((x,y), SG)^{s-2} = 0$, so the integral is 0 as well. Consequently, we need only compute the integral for points that lie off of SG, but inside the open unit triangle Ω. Looking at the construction of SG, we can see that $\Omega \setminus SG$ is a disjoint union of open equilateral triangles, each a scaled copy of the open unit equilateral triangle. Each of these triangles can be decomposed into six 30-60-90 subtriangles (see Figure 3.4.2), over which $d((x,y), SG)$ can be seen to be simply the distance to the long leg of the subtriangle. Looking at one of the six subtriangles in the unit triangle $\Omega = \Omega_0$, and centering the vertex of the 30° angle at the origin on a Cartesian plane with the long leg extending to the right along the positive direction of the x-axis, we can compute the relative distance zeta function of that subtriangle and SG as follows. (See Figure 3.4.3.)

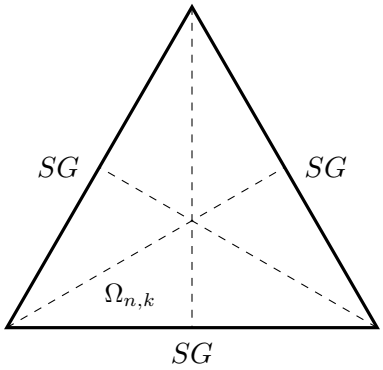

Figure 3.4.2: Decomposition of one cell of Ω_n into six right subtriangles.

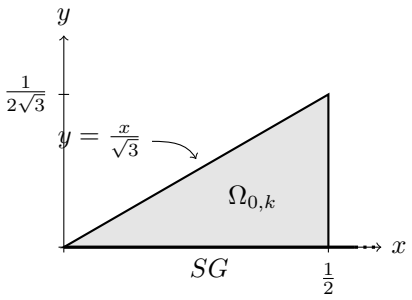

Figure 3.4.3: Region of integration for one of the six subtriangles in Ω_0.

$$\begin{aligned}\zeta_{SG,\Omega_{0,k}}(s) &= \int_{\Omega_{0,k}} d((x,y),SG)^{s-2}\,\mathrm{d}y\,\mathrm{d}x = \int_0^{1/2}\int_0^{x/\sqrt{3}} y^{s-2}\,\mathrm{d}y\,\mathrm{d}x \\ &= \int_0^{1/2}\left[\frac{1}{s-1}y^{s-1}\right]_0^{x/\sqrt{3}}\mathrm{d}x = \frac{(\sqrt{3})^{1-s}}{s-1}\int_0^{1/2} x^{s-1}\,\mathrm{d}x \\ &= \frac{(\sqrt{3})^{1-s}}{s-1}\left[\frac{1}{s}x^s\right]_0^{1/2} = \frac{(\sqrt{3})^{1-s}2^{-s}}{s(s-1)}.\end{aligned} \tag{3.4.2}$$

This is the relative distance zeta function for one of the six subtriangles in $\Omega = \Omega_0$. Now we can employ the help of Theorem 3.3.2 to compute the relative distance zeta function of any of the scaled (right) triangles, and then apply Theorem 3.3.3 to add up these zeta functions and yield the relative distance zeta function for (SG, Ω) itself. For any $n = 1, 2, 3, \ldots$ each open subtriangle removed in the construction of the nth approximation to SG is a copy of Ω_0 scaled by a factor of 2^{-n}. For each $n = 1, 2, 3, \ldots$, there are $6 \cdot 3^{n-1}$ right subtriangles that comprise the equilateral triangles removed. Thus, for any $k = 1, \ldots, 6 \cdot 3^{n-1}$, by Theorems 3.3.3 and 3.3.2, we have

$$\zeta_{SG,2^{-n}\Omega_{n,k}}(s) = (2^{-n})^s \zeta_{SG,\Omega_{0,k}}(s). \tag{3.4.3}$$

Therefore,

$$\begin{aligned}\zeta_{SG,\Omega}(s) &= \sum_{n=1}^{\infty}\sum_{k=1}^{6\cdot 3^{n-1}} \zeta_{SG,2^{-n}\Omega_{n,k}}(s) = \sum_{n=1}^{\infty} 6\cdot 3^{n-1}\cdot (2^{-n})^s \zeta_{SG,\Omega_{0,k}}(s) \\ &= \sum_{n=1}^{\infty} 2\cdot 3^n \cdot (2^{-n})^s \cdot \frac{(\sqrt{3})^{1-s}2^{-s}}{s(s-1)} \\ &= \frac{2(\sqrt{3})^{1-s}2^{-s}}{s(s-1)} \sum_{n=1}^{\infty} 3^n\cdot (2^{-s})^n = \frac{2(\sqrt{3})^{1-s}2^{-s}}{s(s-1)} \sum_{n=1}^{\infty} (3\cdot 2^{-s})^n \\ &= \frac{2(\sqrt{3})^{1-s}2^{-s}}{s(s-1)} \cdot \frac{3\cdot 2^{-s}}{1-3\cdot 2^{-s}} = \frac{6(\sqrt{3})^{1-s}2^{-s}}{s(s-1)(2^s-3)}.\end{aligned} \tag{3.4.4}$$

Immediately we can see that this zeta function has singularities (simple poles, in fact) at $s = 0$ and $s = 1$, and if we solve the complex exponential equation $2^s - 3 = 0$, the left hand side of which appears in our denominator, we find there are also (simple) poles at $s = \log_2 3 + in\mathbf{p}$ where $n \in \mathbb{Z}$ and $\mathbf{p} = \frac{2\pi}{\log 2}$. When $n = 0$, we recover $D_{SG} = D(\zeta_{SG,\Omega}) = \log_2 3$. Therefore, the set of complex dimensions of the Sierpiński gasket is

$$\mathcal{D}_{SG} = \{0, 1\} \cup \left\{\log_2 3 + \frac{2\pi}{\log 2} i\mathbb{Z}\right\}, \tag{3.4.5}$$

and the Sierpiński gasket is a fractal by Definition 3.3.9.

Heuristically, the pole $\omega = 0$ corresponds to the endpoints of the line segments that comprise SG, $\omega = 1$ corresponds to the line segments themselves, and $\omega = D = \log_2 3$ corresponds to the Minkowski dimension of the gasket. The presence of nonreal complex dimensions, namely when $n \in \mathbb{Z} \setminus \{0\}$ above, indicates that the Sierpiński gasket is, indeed, a fractal. Moreover, we can write the volume of the tubular neighborhood of SG as a sum over these complex dimensions as we did in Chapter 2 for the Cantor set (see Section 2.2, in particular Equation 2.2.7). Later on, in Chapter 6, we will discuss tube formulas in more detail.

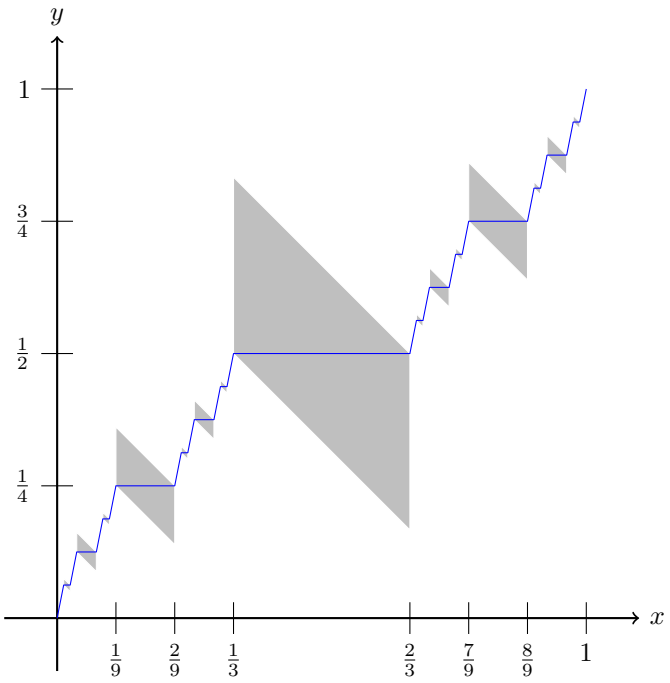

Figure 3.4.4: An approximate RFD for the Cantor-Lebesgue function (The Devil's Staircase).

The Devil's Staircase Revisited

Let us now return to the example of the Cantor-Lebesgue Function (the Devil's Staircase) (see Counterexample 1.0.1 from Chapter 1).

Example 3.4.1 (The Cantor-Lebesgue Function, or "The Devil's Staircase")**.** In Counterexample 1.0.1, we noted that the Cantor-Lebesgue function, denoted by f, did not satisfy conventional definitions of fractality, but it is certainly an object we would like to classify as fractal. We now proceed to construct an RFD for the staircase and compute its complex dimensions as in [LRŽ17], Section 5.5.4. Figure 3.4.4 shows the generating process for the RFD: for each horizontal line segment in the construction of the staircase, we attach two scaled, open, isosceles triangles as shown, each with one of the equal-length sides contacting a horizontal segment of the curve. Each triangle is a scaled copy of an original triangle called the *fundamental cell*, denoted by Ω_0. Corresponding to each generation n of the Cantor string CS, there are 2^n subtriangles, denoted Ω_i^n for $1 \leq i \leq 2^n$, each scaled by a factor of 3^{-n}. The complete drum is the union of these scaled, open triangular subdrums, denoted Ω:

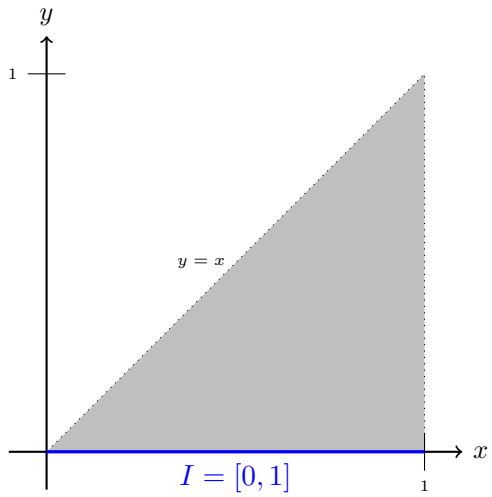

Figure 3.4.5: The *fundamental cell* for the Cantor-Lebesgue function (The Devil's Staircase).

$$\Omega = \bigcup_{n=1}^{\infty} \bigcup_{i=1}^{2^n} \Omega_i^n = \bigcup_{n=1}^{\infty} \bigcup_{i=1}^{2^n} 3^{-n}\Omega_0 \tag{3.4.6}$$

For convenience, we take the length of the congruent sides of Ω_0 to be 1. Placing an acute angle of Ω_0 at the origin in $\mathbb{R}^2$ and letting one congruent side coincide with $I = [0, 1]$ along the x-axis, we can compute the relative distance zeta function of (I, Ω_0) as follows.

$$\begin{aligned} \zeta_{I,\Omega_0}(s) &= \int_{\Omega_0} d(\mathbf{x}, I)^{s-2} \, \mathrm{d}\mathbf{x} \\ &= \int_0^1 \int_0^x y^{s-2} \, \mathrm{d}y \, \mathrm{d}x \\ &= \frac{1}{s-1} \int_0^1 x^{s-1} \, \mathrm{d}x \\ &= \frac{1}{s(s-1)}. \end{aligned} \tag{3.4.7}$$

Using Theorems 3.3.2 and 3.3.3, we can compute the following.

$$\begin{aligned}\zeta_{f,\Omega}(s) &= \sum_{n=1}^{\infty}\sum_{i=1}^{2^n}\zeta_{f,\Omega_i^n}(s) = \sum_{n=1}^{\infty}\sum_{i=1}^{2^n}(3^{-n})^s\zeta_{I,\Omega_0}(s) \\ &= \sum_{n=1}^{\infty}\sum_{i=1}^{2^n}(3^{-n})^s\frac{1}{s(s-1)} = \frac{1}{s(s-1)}\sum_{n=1}^{\infty}2^n(3^{-n})^s \\ &= \frac{1}{s(s-1)}\sum_{n=1}^{\infty}\left(\frac{2}{3^s}\right)^n = \frac{2}{s(3^s-2)(s-1)}.\end{aligned} \tag{3.4.8}$$

This function is valid initially for all $s \in \mathbb{C}$ with Re $s > 1$, and then for almost all $s \in \mathbb{C}$ after meromorphic continuation. Examining the denominator we can see that the set of complex dimensions of the Cantor-Lebesgue function is

$$\mathcal{D} = \{0, 1\} \cup \left\{\log_3 2 + \frac{2\pi}{\log 3}i\mathbb{Z}\right\}, \tag{3.4.9}$$

which contains at least one nonreal complex number. Therefore, the Cantor-Lebesgue function is, indeed, a fractal by Definition 3.3.9, despite other definitions (such as Definitions 1.0.1 and 1.0.2 in Chapter 1) failing to classify it as so. This example illustrates the versatility and accuracy of Definition 3.3.9 where others have fallen short.

Before we can discuss the new results of this dissertation regarding the complex dimensions of space-filling curves, we need to discuss the theory of space-filling curves itself.

Chapter 4

The Theory of Space-Filling Curves

4.1 Introduction

In this chapter we introduce the theory of space-filling curves necessary to explore the results of the subsequent chapters. The subject of space-filling curves is a rich and intriguing one, and the interested reader can find many texts on the subject. For our purposes, Hans Sagan's book *Space-Filling Curves* [Sag94], and Stein and Shakarchi's book *Real Analysis* [SS05], volume III, of their Princeton Lectures in Analysis, have all the necessary details. A note about Stein and Shakarchi's treatment of the Hilbert curve: they refer to the Hilbert construction and Hilbert curve as the Peano construction and the Peano curve, perhaps to pay homage to Peano who created the first space-filling curve, but the construction they detail is that of Hilbert's design. Either way, their treatment of the construction is excellent and ours follows a similar approach for brevity.

The subject of space-filling curves was first conceived by Italian mathematician Giuseppe Peano (1858 – 1932) in 1890 when he constructed a continuous and surjective mapping from the unit interval $I = [0, 1]$ to the unit square $I^2 = [0, 1] \times [0, 1] = [0, 1]^2$ in his paper *Sur une courbe, qui remplit toute une aire plane* [Pea90]. His research in this area was motivated by the work of Georg Cantor (1845 – 1918) who had shown previously, in 1878 [Can78], that I and I^2 have the same cardinality, i.e. there exists a bijection between I and I^2. A

natural question is whether or not such a mapping is continuous, and Eugen Netto (1848 – 1919) provided a negative answer to this question a year later in 1879 [Net79] when he showed that such a bijective mapping must always be discontinuous. A continuous injective mapping from I to I^2 is trivial to construct, but the question of the existence of a continuous surjective mapping from I to I^2 remained unanswered until Peano's construction in 1890. Peano discovered the first space-filling curve and described it analytically in terms of an operator from I to I^2 (see Section 4.3), but it was David Hilbert (1862 – 1943) who, in 1891 in [Hil91], provided a generalizable, geometric generating procedure for curves such as Peano's, resulting in an entire class of space-filling curves, the class consisting of curves which the present author will demonstrate must be fractals in the subsequent chapter. In a sense, Hilbert's original plane-filling curve is the canonical example of a space-filling curve, and it provides an illuminating example for the study of space-filling curves. First we need to establish some important preliminary definitions used in the general theory, definitions which can be found in [Sag94].

Definition 4.1.1. For $M, N \in \mathbb{Z}^+ \cup \{0\}$, if f is a function from $\mathbb{R}^M$ into $\mathbb{R}^N$, then we define the *direct image of A under f* as

$$f_*(A) = \{f(x) \in R(f) : x \in A \cap D(f)\} \subseteq \mathbb{R}^N, \tag{4.1.1}$$

where $A \subseteq \mathbb{R}^M$, $D(f)$ is the domain of f, and $R(f)$ is the range of f.

Definition 4.1.2. If $f : I \to \mathbb{R}^N$, $N \geq 0$ is continuous, then the direct image $f_*(I)$ is called a *curve*. $f(0)$ is called the *initial point* of the curve, and $f(1)$ is called the *endpoint* of the curve. We call $x = f(t)$ for all $t \in I$ a *parametric representation* of the curve $C = f_*(I)$.

Definition 4.1.3. If $f : I \to \mathbb{R}^N$ for $N \geq 1$ is continuous and the N-dimensional *Jordan content* of the direct image is strictly positive, i.e. $J_N(f_*(I)) > 0$, then $f_*(I)$ is called a *space-filling curve*.[1]

[1]Here $J_N(A)$ is the N-dimensional Jordan content of the set $A \subseteq \mathbb{R}^N$. The Jordan content is similar to the Lebesgue measure except the infimum is taken over coverings by finitely many rectangles. For a detailed introduction to the Jordan content, see [Fol99] Section 2.6.

Remark 4.1.1. The most general term in use is *space-filling curve* because the target space can be N-dimensional for $N \geq 1$. If $N = 1$, then the examples are trivial but are still examples, and this natural generality further suggests the need to use a more robust definition of fractality as provided in [LvF13] and Definition 3.3.9 so that nonexamples of fractals are not included in the definition of fractality. However the first space-filling curves were produced as surjections from I onto I^2, so they are often referred to as *plane-filling curves* in order to emphasize that the target space is $\mathbb{R}^2$.

Definition 4.1.4. A *contraction mapping* is a function f from a metric space (X, d) to itself with the property that there exists some nonnegative real number $0 \leq r < 1$ such that for all $x, y \in X$, we have $d(f(x), f(y)) \leq r \cdot d(x, y)$. The number r is called the *contraction ratio*.

Definition 4.1.5. An *iterated function system (IFS)* is a finite set of contraction mappings on a complete metric space.

4.2 The Hilbert Curve

Now we set about detailing the construction of the Hilbert curve and proving a few of its important properties. As mentioned previously and in Section 4.3, Peano discovered the first plane-filling curve, defining it in terms of an operator (see Formulas 4.3.1 and 4.3.2) but Hilbert recognized a geometric generating procedure innate to Peano's construction. In particular, he noticed that adjacent subintervals of I (in particular $[0, \frac{1}{9}]$, $[\frac{1}{9}, \frac{2}{9}]$, ..., $[\frac{8}{9}, 1]$) were mapped to adjacent subsquares of I^2 and produced his own, arguably simpler, plane-filling curve by exploiting this idea.

We begin with a heuristic explanation of the construction before proceeding to the details. Beginning with the unit square, I^2, we subdivide it into four congruent subsquares, as in Figure 4.2.1. Connect the centers of these four subsquares with a polygonal curve that does not intersect itself. This is a first approximation, $f_{1*}(I)$, to the Hilbert curve $f_{H*}(I)$. Continuing, subdivide the four subsquares of the first generation into four subsquares each,

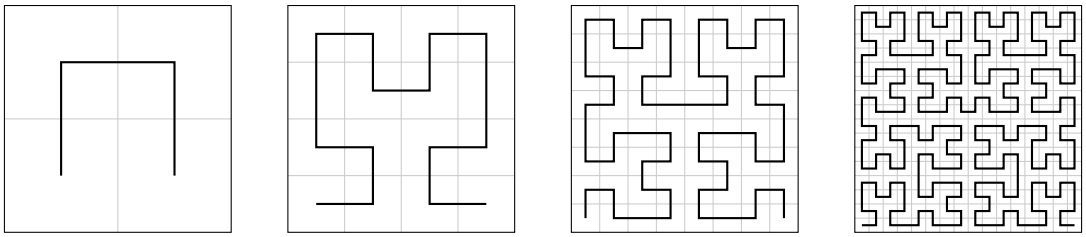

$n = 1$ $n = 2$ $n = 3$ $n = 4$

Figure 4.2.1: The first four approximations to the Hilbert curve.

for a total of sixteen subsquares in the unit square. Connect the centers of these sixteen subsquares with a polygonal curve as shown in Figure 4.2.1 that does not intersect itself. This is a second approximation, $f_{2*}(I)$, to the Hilbert curve $f_{H*}(I)$. Repeat this procedure ad infinitum, and we claim the resulting object is the plane-filling curve $f_{H*}(I)$ known as the Hilbert curve, and that it is a continuous surjective mapping from I to I^2.

There is much to be verified here: does this sequence of mappings and associated curves actually converge? If so, to what does it converge? Is the limit mapping well-defined? Is it a curve? Is it a space-filling curve? We proceed to answer all of these questions, first focusing on a specific regular partition of the unit interval I, then of the unit square I^2, and then establishing a correspondence between the subsets of the partitions. More details of this construction can be found in [SS05], Chapter 7, Section 3.

Definition 4.2.1. Given the closed unit interval I, we define the *quartic intervals* to be the closed intervals of the form $\left[\frac{k}{4^n}, \frac{k+1}{4^n}\right]$ for any positive integer $n \geq 1$ and any nonnegative integer $0 \leq k \leq 4^n - 1$. For example, the first generation of quartic intervals are

$$J_1 = \left[0, \frac{1}{4}\right] \qquad J_2 = \left[\frac{1}{4}, \frac{1}{2}\right] \qquad J_3 = \left[\frac{1}{2}, \frac{3}{4}\right] \qquad J_4 = \left[\frac{3}{4}, 1\right] \tag{4.2.1}$$

Definition 4.2.2. A *chain* of quartic intervals is a decreasing sequence $\{J^n\}_{n=1}^{\infty}$ of quartic intervals, i.e.

$$J^1 \supset J^2 \supset J^3 \supset \cdots \tag{4.2.2}$$

where J^n is a quartic interval of the nth generation.

Proposition 4.2.1. If $\{J^n\}$ is a chain of quartic intervals, then the following hold.

(i) There exists a unique $t \in I$ such that $t \in \bigcap_{n=1}^{\infty} J^n$

(ii) Conversely, given $t \in I$, there is a chain of quartic intervals $\{J^n\}$ such that $t \in \bigcap_{n=1}^{\infty} J^n$.

(iii) The set of $t \in I$ for which the sequence in part (ii) is not unique is a set of measure zero.

Proof. To show (i), note that $\{J^n\}$ is a decreasing sequence of nonempty compact sets, so it's intersection is nonempty and such a t exists. Moreover, the length of each interval is 4^{-n} which goes to 0 as $n \to \infty$ so such a t must be unique. Otherwise, if there were two distinct t_1 and t_2 in the intersection, then there exists a quartic interval J^m such that $t_1 \in J^m$, and $|J^m|_1 < |t_1 - t_2|_1$ which implies that t_2 is not in the intersection, a contradiction.

To show (ii), let $t \in [0, 1]$ be arbitrary but fixed. For any n, there exists at least one quartic interval J_i^n such that $t \in J_i^n$, hence t lies in the intersection $t \in \bigcap_{n_i=1}^{\infty} J^{n_i}$ where n_i is the index of the ith quartic interval in generation n that contains t.

If t is an endpoint of a quartic interval in the nth generation, then it belongs to at most two quartic intervals in the nth generation, and it has the form $\frac{i}{2^n}$ where $0 \leq i \leq 2^n$. In other words, t is a *dyadic rational*. The dyadic rational numbers are a subset of the rational numbers and so have measure 0, proving (iii). □

This result yields the fact that the unique point in the intersection of any chain of quartic intervals can be naturally described as a list of quaternary (base-4) digits, each digit corresponding to the index of the quartic subinterval in each generation in which t lies. More specifically, the quaternary representation of t is the following.

$$t = \sum_{n=1}^{\infty} \frac{q_i}{4^n} = 0.q_1q_2q_3\ldots \qquad \text{where } q_i \in \{0, 1, 2, 3\}. \tag{4.2.3}$$

Now we turn our attention to the unit square, I^2.

Definition 4.2.3. Given the closed unit square I^2, we define the *dyadic squares* as the closed squares formed by subdividing the unit square by successively bisecting the edges. In Figure 4.2.1, the gray lines indicate the lines of subdivision.

Definition 4.2.4. A *chain* of dyadic squares is a decreasing sequence $\{S^n\}_{n=1}^{\infty}$ of dyadic squares, i.e.

$$S^1 \supset S^2 \supset S^3 \supset \cdots \tag{4.2.4}$$

where S^n is a dyadic square of the nth generation.

Proposition 4.2.2. If $\{S^n\}$ is a chain of dyadic squares, then the following hold.

(i) There exists a unique $x \in I^2$ such that $x \in \bigcap_{n=1}^{\infty} S^n$

(ii) Conversely, given $x \in I^2$, there is a chain of dyadic squares $\{J^n\}$ such that $x \in \bigcap_{n=1}^{\infty} S^n$.

(iii) The set of x for which the sequence in part (ii) is not unique is a set of measure zero.

The proof of this proposition is analogous to that of Proposition 4.2.1 and is left as an exercise to the reader. Now that we have established how we are going to partition I and I^2, we can define a *dyadic correspondence*.

Definition 4.2.5. A *dyadic correspondence* is a mapping Φ from quartic intervals to dyadic squares that satisfies the following:

(i) Φ is bijective.

(ii) Φ respects generations, i.e. if J_i^n is a quartic interval of the nth generation, then $\Phi(J_i^n)$ is a dyadic square of the nth generation.

(iii) Φ respects inclusion, i.e. if $J^2 \subseteq J^1$, then $\Phi(J^2) \subseteq \Phi(J^1)$.

Note that there is a guaranteed bijection from any quartic interval to any dyadic square by the results of Cantor, so the defining characteristics of such a correspondence really lie in properties (ii) and (iii).

Remark 4.2.1. Given a dyadic correspondence Φ, it induces a mapping $\phi : I \to I^2$ as follows: given a chain of quartic intervals $\{J^n\}$, by Proposition 4.2.1 there is a unique t such that we can write $\{t\} = \bigcap_n J^n$. By definition, $\{\Phi(J^n)\}$ is a chain of dyadic squares and so we can define

$$\phi(t) = x \coloneqq \bigcap_{n=1}^{\infty} \Phi(J^n). \tag{4.2.5}$$

Remark 4.2.2. $\phi(t)$ is well-defined on I except on a countable set of measure 0: if we let A be the set of dyadic rational numbers in I and B be the set of points in I^2 that have a dyadic rational for at least one of their coordinates, then ϕ is well-defined on $I \setminus (A \cup \Phi^{-1}(B))$. To define ϕ on the sets A and $\Phi^{-1}(B)$, we must choose representative chains of quartic intervals and dyadic squares, respectively, for the points in those sets.

Remark 4.2.3. The pointwise-defined nature of the correspondence Φ induces oscillations in the 0-dimensional components of the curve, the points, which we will discuss in Chapters 5, 6, and 7. Moreover, without ambiguity, for any quartic interval J, we have

$$\begin{aligned} \phi(J) = \{\phi(t) : t \in J\} = \bigcup_{t \in J} \phi(t) \coloneqq \bigcup_{t \in J} \bigcap_{n=1}^{\infty} \Phi(J^n) \\ = \bigcup_{t \in J} \Phi\left(\bigcap_{n=1}^{\infty} J^n \right) = \bigcup_{t \in J} \Phi(\{t\}) = \Phi(J). \end{aligned} \tag{4.2.6}$$

The first part of Hilbert's contribution to the theory after Peano's discovery is encapsulated in Proposition 4.2.3 below.

Proposition 4.2.3. There is a unique dyadic correspondence Φ_H such that

(i) If J_1^n and J_2^n are two adjacent intervals of generation n, then $\Phi_H(J_1^n)$ and $\Phi_H(J_2^n)$ are two adjacent squares of generation n, and

(ii) In generation n, if J_-^n is the leftmost quartic interval and J_+^n is the rightmost quartic interval, then $\Phi_H(J_-^n)$ is the lower left dyadic square and $\Phi_H(J_+^n)$ is the lower right square.

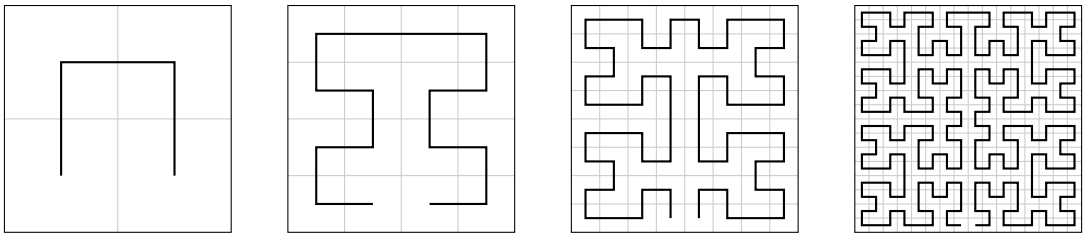

$n = 1$ $n = 2$ $n = 3$ $n = 4$

Figure 4.2.2: The first four approximations to the Moore curve.

Remark 4.2.4. Hilbert demonstrated that there exists a unique traversal (or ordering) of the dyadic squares of any generation n which begins at the lower left square and ends at the lower right square, and ensures that the adjacency mentioned in Proposition 4.2.3 holds. In the limit, the initial point of the Hilbert curve itself is $(0, 0)$ and the terminal point is $(1, 0)$. This traverse is only unique up to rotations by 90°, rotations which will correspondingly permute the initial and terminal points of the Hilbert curve around the vertices of the unit square. There is, however, another traverse of the dyadic squares discovered by E.H Moore in 1900 [Moo00] that induces a plane-filling curve, but the initial and terminal squares of the ordering are the bottom center subsquares, respectively, and so the initial and terminal points of the curve itself, in the limit, coincide at the point $\left(\frac{1}{2}, 0\right)$. Approximations to the Moore curve are pictured in Figure 4.2.2, and one can see how their structure is very similar to those of the Hilbert curve seen in Figure 4.2.1. Note also that the number of nth generational unit segments is the same as that of the Hilbert curve (see Definition 4.2.6 below).

Despite it's gravity with respect to the theory of space-filling curves, we omit the proof of Proposition 4.2.3 so as to not get too far off of the course of this dissertation, but a complete proof can be found in [SS05] Chapter 7, Section 3 where Proposition 4.2.3 is stated as Lemma 3.7 and proved thereafter.

Remark 4.2.5. As a helpful side note, if a reader is interested in producing images of these approximating polygons, Wolfram's *Mathematica* has a built in function that can do this. More specifically, the command `HilbertCurve[n]` will give a list of points in $[0, n] \times [0, n]$

of the nth generation that preserves the traverse given in Proposition 4.2.3. The command `Graphics[HilbertCurve[n]]` will generate an upscaled (by a factor of n) picture of the approximating polygon in generation n. This code, and others, for images found in the figures of this dissertation can be found in Appendix A.

Now that we have established (or at least accepted) that such a dyadic correspondence exists, we can precisely define the Hilbert curve, and verify that it is indeed a space-filling curve. Let Φ_H be the dyadic correspondence given in Proposition 4.2.3. Let $\{S_k\}_{k=1}^{4^n}$ be the sequence of dyadic squares of the nth generation, ordered according to the traverse in Proposition 4.2.3 and depicted in Figure 4.2.1. More specifically, let $\Phi_H(J_k) = S_k$. For $k = 2, 3, \ldots, 4^n - 1$, let t_k be the midpoint of J_k:

$$t_k = \frac{k - \frac{1}{2}}{4^n}, \tag{4.2.7}$$

and for $k = 1$ and $k = 4^n$ let t_k be the leftmost and rightmost endpoint of J_k, respectively. Let x_k be the center of square S_k, and for all $k = 1, 2, \ldots, 4^n$, define

$$f_n(t_k) \coloneqq x_k. \tag{4.2.8}$$

Connecting the centers x_k by vertical and horizontal line segments according to the ordering described by Φ_H allows us to extend $f_n(t)$ continuously to all of $I = [0, 1]$.

Proposition 4.2.4. The sequence of continuous functions $\{f_n\}$ converges uniformly to a continuous function f_H. Moreover, $f_H : I \to I^2$ is surjective so that $f_{H*}(I) = I^2$ is a space-filling curve.

Proof. This proof follows the proof given after the proof of Lemma 3.7 in Chapter 7, Section 3 of [SS05]. First note that f_n is continuous for any $n \geq 1$ by construction, and in fact is differentiable almost everywhere except when $t = t_k$ since it is composed of line segments.

Next, for any $n \geq 1$ and any k such that $1 \leq k \leq 4^n$, we have

$$|x_k - x_{k+1}| \leq 2^{-n} \qquad \text{and} \qquad |t_k - t_{k+1}| \leq 4^{-n}. \tag{4.2.9}$$

Consequently, for all $t \neq t_k$,

$$\frac{df_n}{dt} = \frac{|x_k - x_{k+1}|}{|t_k - t_{k+1}|} \leq \frac{2^{-n}}{4^{-n}} = 2^n. \tag{4.2.10}$$

By the definition of f_n, for all $s, t \in I$, we have

$$|f_n(t) - f_n(s)| \leq 2^n |t - s|. \tag{4.2.11}$$

Additionally,

$$|f_{n+1}(t) - f_n(t)| \leq \sqrt{2} \cdot 2^{-n} \tag{4.2.12}$$

because $f_{n+1}(t)$ and $f_n(t)$ lie in the same dyadic square in generation n due to the fact that Φ_H is a dyadic correspondence. As a result, $\{f_n\}$ is uniformly convergent. Next, writing

$$f_H(t) = \lim_{n\to\infty} f_n(t) = f_1(t) + \lim_{n\to\infty} \sum_{i=1}^{n} f_{i+1}(t) - f_i(t), \tag{4.2.13}$$

we obtain

$$\begin{aligned} |f_H(t)| &\leq |f_1(t)| + \lim_{n\to\infty} \sum_{i=1}^{n} |f_{i+1}(t) - f_i(t)| \\ &\leq |f_1(t)| + \sum_{i=1}^{\infty} \sqrt{2} \cdot 2^{-n} \\ &= |f_1(t)| + \sqrt{2} < \infty. \end{aligned} \tag{4.2.14}$$

Thus, f_H exists, and it is a continuous function since each f_n is continuous and $\{f_n\}$ is uniformly convergent. Finally, by Proposition 4.2.3 and by construction, every f_n visits every dyadic square of generation n as t passes from 0 to 1. Thus, f_H is dense in the unit square I^2 because it meets every open set that intersects I^2. Equivalently, its closure is the

unit square. Since it is continuous, $f_H(I)$ is the continuous image of a compact set and so is compact. In particular $f_H(I)$ is closed so it is equal to its closure, the unit square. Thus f_H is surjective, and we have that $f_{H*}(I)$ is a space-filling curve. □

Remark 4.2.6. We could have instead used the induced mapping ϕ_H for the proof of Proposition 4.2.4 because, due to the ordering given by Φ_H, ϕ_H is well-defined for all $t \in I$. Suppose that $t \in \bigcap_n J_1^n$ and $t \in \bigcap_n J_2^n$ where $\{J_1^n\}, \{J_2^n\}$ are chains of quartic intervals. Then J_1^n and J_2^n are adjacent for sufficiently large n, whence $\Phi_H(J_1^n)$ and $\Phi_H(J_2^n)$ are adjacent for sufficiently large n, and so $\phi_H(t) = \bigcap_n \Phi(J_1^n) = \bigcap_n \Phi(J_2^n)$. Thus,

$$\phi_H(t) = \bigcap_{n=1}^{\infty} \Phi(J^n) = \bigcap_{n=1}^{\infty} S^n = \lim_{n\to\infty} f_n(t) = f_H(t). \tag{4.2.15}$$

Remark 4.2.7. By construction, in any generation n the length of any line segment connecting the centers of two consecutive subsquares is 2^{-n}, and there are $4^n - 1$ of these segments. Thus the total length of any approximating polygon is $2^n - 2^{-n}$. Naturally, this length goes to infinity as n goes to infinity.

Definition 4.2.6. We call the length of a line segment connecting the centers of consecutive subsquares in generation n the *nth generational unit length* or the *unit length of generation* n, and we refer to one of these line segments as an *nth generational unit segment* or a *unit segment of generation* n.

The construction of f_H (and ϕ_H) and the proof of Proposition 4.2.4 reveal the delicate and elegant structure needed to produce a space-filling curve. Restated succinctly, the ordering asserted by Φ_H in Proposition 4.2.3 guarantees that image points of consecutive generations of approximating polygons "don't wander too far" from each other, which yields the uniform convergence of the sequence. This yields the existence of the limit curve, and the continuity of the approximating polygons under this uniform convergence yields the continuity of the limit curve. The ordering (traversal) also guarantees that the center of every subsquare of I^2 in any generation is visited, so the image of the limit curve is dense

since it will meet any open set in intersecting I^2. I is closed, so the limit curve is closed and dense in I^2, so it must be I^2 itself.

Remark 4.2.8. The Hilbert curve construction is extendable to $\mathbb{R}^N$ for $N > 2$ as well so that $f_{H*}(I) = I^N$, but we will not detail it here. We will breifly address the case of the Hilbert curve that fills I^3 in Chapter 7, but other such constructions will be addressed in later work.

Remark 4.2.9. There are many variations on the Hilbert curve, and popular variations involve extending the approximating polygons given in the proof of 4.2.4 to the points $(0, 0)$ and $(1, 0)$ in some fashion. This is not necessary to produce the Hilbert curve, but this practice allows the approximations to be produced via a convenient iterated function system, which has the unit square as its attractor (see System 4.2.16 below). This is a good reason why fractality should not be strictly defined in terms of iterated functions systems; sometimes they are not necessary to produce a "fractal". In light of this, one can call the construction of the Hilbert curve using the polygons described in the proof of Proposition 4.2.4 the *canonical construction* of the Hilbert curve, or the *minimal construction* of the Hilbert curve, because the approximating polygons have minimal length and satisfy all of the necessary requirements to converge to the unit square. They are also the polygons depicted in Hilbert's original paper on the curve, [Hil91].

In [Sag94], Sagan details the use of the following iterated function system acting on the unit square to produce a myriad of Hilbert curve variations.

$$\begin{aligned} H_0(z) &= \frac{1}{2}\bar{z}i & H_2(z) &= \frac{1}{2}(z+1+i) \\ H_1(z) &= \frac{1}{2}(z+i) & H_3(z) &= \frac{1}{2}(-\bar{z}i+i)+1 \end{aligned} \tag{4.2.16}$$

For modeling purposes, this iterated function system and can help elucidate the extent of the oscillations of points mentioned in Remark 4.2.3, but this discussion will be reserved for Chapter 6.

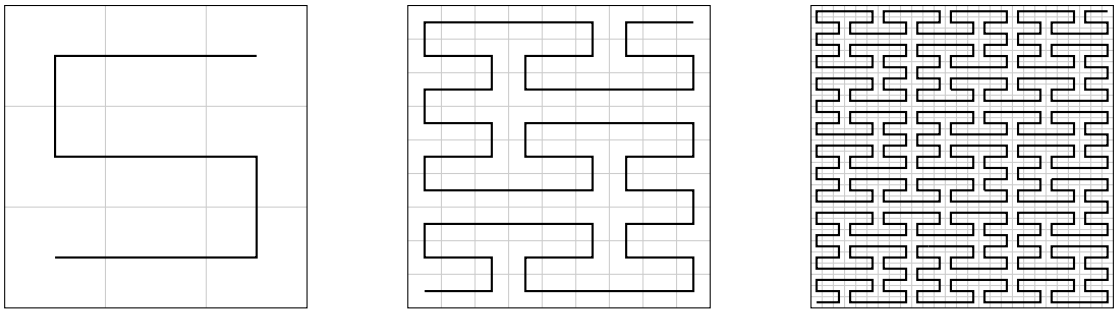

Figure 4.3.1: The first three approximations to the Peano curve.

Now we turn our attention to the Peano curve, and the generalization of the geometric generating procedure described in the construction of the Hilbert curve.

4.3 The Peano Curve, and a Class of Space-Filling Curves

In 1890, Peano defined a map $f_p : I \to I^2$ in terms of the operator

$$kt_j = 2 - t_j \qquad \text{for } t_j = 0, 1, 2, \tag{4.3.1}$$

where, given any ternary representation of a point $x \in I$, written $x = 0.t_1t_2t_3\ldots$, $f_p(x)$ is given as

$$f_p(x) = f_p(0.t_1t_2t_3\ldots) = \begin{pmatrix} 0.t_1(k^{t_2}t_3)(k^{t_2+t_4}t_5)\cdots \\ 0.(k^{t_1}t_2)(k^{t_1+t_3}t_4)\cdots \end{pmatrix}, \tag{4.3.2}$$

where k^α denotes the αth iterate of k. In his paper, [Pea90], he showed this mapping is continuous and surjective, but did not give a geometric interpretation of it. However, David Hilbert noticed there was a *triadic correspondence* induced by this operator that defined a mapping similar to that in Proposition 4.2.3 between the ternary intervals of I and the triadic squares of I^2. This led him to construct the Hilbert curve, and produce a general geometric generating procedure. For clarity, we need some definitions.

Definition 4.3.1. In $\mathbb{R}^N$, a *tessellation* is a covering of $\mathbb{R}^N$ using one or more geometric shapes, called *cells*, with no overlaps and no gaps. Intuitive examples can be readily found in $\mathbb{R}^2$ where the cells are called *tiles* (e.g., tiled floors or walls).

Definition 4.3.2. A *regular tessellation* is a tessellation using congruent cells, i.e. all of the cells in the tessellation are the same.

Definition 4.3.3. In $\mathbb{R}^N$, a *rectilinear tessellation* is a tessellation using N-dimensional rectangles, not necessarily cubes.

Definition 4.3.4. In $\mathbb{R}^N$, a *regular rectilinear tessellation* is a tessellation using N-dimensional cubes.

These definitions are detailed explicitly so that different classes of space-filling curves and their complex dimensions can be discussed without ambiguity. For example, regular *non*rectilinear tessellations and *ir*regular rectilinear tessellations can produce space-filling curves, and conjectures for these classes of space-filling curves are discussed in Chapter 7.

Returning to regular rectilinear tessellations, the, or perhaps more appropriately, a, Peano curve is produced similarly to the Hilbert curve. This is achieved by connecting the centers of the triadic subsquares in each generation by a continuous curve that follows an appropriate traverse, and taking the limit of this sequence of approximations. The image of this limit curve is the unit square, I^2. There are several differences between the Hilbert curve and the Peano curve, but one notable difference is that there exist many triadic correspondences between I and I^2 that can produce a space-filling curve, and differ by more than a simple rotation of the square. In other words, there is more than one traverse (ordering) of the triadic squares that results in a space-filling curve, so there is more than one "Peano mapping" and in some sense more than one "Peano curve". In contrast, the Hilbert curve induced by the ordering in Proposition 4.2.3 is unique (up to rotations by 90°). The existence of multiple Peano curves was proved by Walter Wunderlich (1910 – 1998) in his 1973 paper *Über Peano-Kurven* [Wun73]. In fact, he was able to demonstrate that there are 274 ways of producing a Peano curve. 272 of those ways he referred to as the "switchback type", and the other 2 he referred to as the "meandering type".

Remark 4.3.1. Examples of these two types are given in Figures 4.3.1 and 4.3.2, and in each example the image points of consecutive generations of approximating polygons "don't

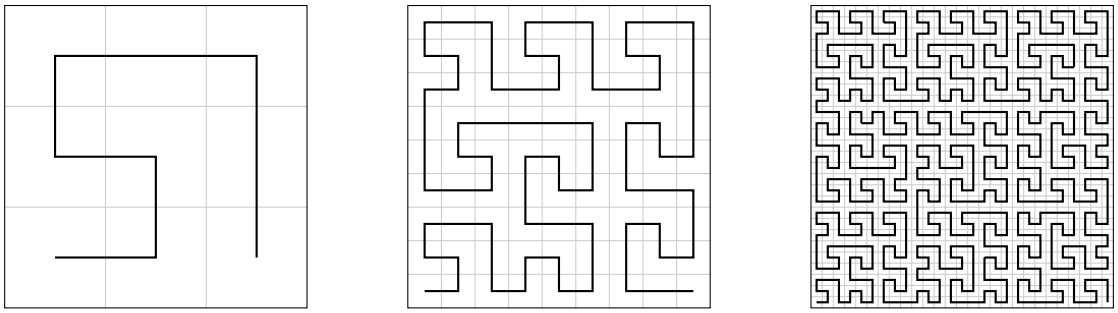

$n = 1$ $n = 2$ $n = 3$

Figure 4.3.2: The first three approximations to a Peano curve of the meandering type.

wander too far" from each other, as required. Note also that, regardless of the traverse used, the minimum number generational unit segments needed to connect the centers of consecutive subsquares and produce a *minimal construction* of the Peano curve is the same in each case.

Remark 4.3.2. The unit length of generation n (see Definition 4.2.6) for the Peano curve is 3^{-n} and there are $9^n - 1$ of these generational unit segments, so the total length of any minimal approximating polygon is $3^n - 3^{-n}$, similar to the Hilbert curve.

Definition 4.3.5. More generally, given any positive nonunital integer $\lambda \in \{2, 3, 4, \ldots\}$, there exists a corresponding regular rectilinear tessellation whence we can subdivide the unit square I^2 into λ^{2n} subsquares for any $n \in \mathbb{Z}^+$. Using an appropriate λ-adic correspondence Φ_λ between the λ-ary subintervals of I and the λ-adic subsquares of I^2, we can produce a sequence of approximating curves that converges to a space-filling curve as we have seen above. We denote the set of plane-filling curves produced as described above by $\mathcal{S}_2(\lambda)$, and the class of these sets, indexed by λ, is denoted by $\mathfrak{R}_2$.

Remark 4.3.3. The subscript 2 in Definition 4.3.5 denotes the dimension of the space the curves fill; more generally, we have $\mathcal{S}_N(\lambda)$ and $\mathfrak{R}_N$. This dissertation and most of the new mathematical results herein involve plane-filling curves in the class $\mathfrak{R}_2$, but the present author has conjectures for how these new results will extend to higher dimensions, and other classes of space-filling curves that are induced by differerent tessellations (see Chapter 7).

This concludes the discussion of the theory of space-filling curves that we will need to access the results of the following chapters, but it does not need to be the end of your exploration. The present author encourages the interested reader to read more about space-filling curves since they are interesting objects that challenge our intuition about what dimension really means.

Chapter 5

Relative Fractal Drums (RFDs) for a Class of Plane-Filling Curves

Now that we have all the necessary background, we are ready to create a class of *relative fractal drums* (RFDs) that will allow us to detect the complex dimensions of a class of space-filling curves and prove that they are, indeed, fractals. Professor Lapidus and the present author have always agreed that such curves must be fractals, and Professor Lapidus suggested that a relative fractal drum in $\mathbb{R}^3$ could be successful in detecting the complex dimensions. This chapter details such successful constructions.

Recall from Counterexample 1.0.3 in Chapter 1 that space-filling curves in the class $\mathfrak{R}_2$, i.e. plane-filling curves generated via regular rectilinear tessellations of I^2 (see Definition 4.3.5 in Chapter 4), are not classified as fractals under the conventional definitions discussed in Definitions 1.0.1 and 1.0.2 in Chapter 1, even though they are colloquially referred to as fractals because mathematicians would like to label them as such. Recall also from Chapter 3 the following definition of fractality.

Definition 3.3.9. A set $A \subseteq \mathbb{R}^N$ is defined as *fractal* if and only if there exists an associated relative fractal drum (A, Ω) (in the sense of Definitions 3.3.1 and 3.3.2) such that

the meromorphic continuation of the associated relative distance zeta function has at least one nonreal complex dimension.

The difficulty is in devising a valid RFD for a plane-filling curve in $\mathfrak{R}_2$ because the image of the curve is the complete unit square, I^2. For example, if we take $\Omega = (I^2)_t$, the t-tubular neighborhood of I^2 in $\mathbb{R}^2$ where $t > 0$, the *relative distance zeta function* of $(I^2, (I^2)_t)$ (see Definition 3.3.1) is

$$\begin{aligned}\int_{(I^2)_t} d((\mathbf{x}, I^2)^{s-2}\ \mathrm{d}\mathbf{x} &= \int_{I^2} d((x,y), I^2)^{s-2}\ \mathrm{d}x\ \mathrm{d}y + \int_{(I^2)_t \setminus I^2} d((x,y), I^2)^{s-2}\ \mathrm{d}x\ \mathrm{d}y \\ &= \int_{(I^2)_t \setminus I^2} d((x,y), I^2)^{s-2}\ \mathrm{d}x\ \mathrm{d}y\end{aligned} \tag{5.0.1}$$

since $d((x,y), I^2 = 0$ for all $(x,y) \in I^2$. The remaining integral is taken over the open tubular neighborhood surrounding the unit square, and this can be computed by breaking the integral up into four equivalent integrals taken over the four rectangles with one side a side of the unit square, and another four integrals taken over the quarter-circular wedges centered at the four vertices of the unit square. More specifically, we have

$$4\int_0^1 \int_0^t x^{s-2}\ \mathrm{d}x\ \mathrm{d}y = \frac{4t^{s-1}}{s-1} \tag{5.0.2}$$

for the integrals over the rectangles, and

$$4\int_0^{\frac{\pi}{2}} \int_0^t r^{s-2} \cdot r\ \mathrm{d}r\ \mathrm{d}\theta = \frac{8\pi t^s}{s} \tag{5.0.3}$$

for the integrals over the quarter-circular wedges. Adding these up, we have

$$\int_{(I^2)_t} d((x,y), I^2)^{s-2}\ \mathrm{d}x\ \mathrm{d}y = \frac{4t^{s-1}}{s-1} + \frac{8\pi t^s}{s}, \tag{5.0.4}$$

and we can see that the set of complex dimensions given by this RFD is simply $\{0, 1\}$. This makes sense because the RFD is only picking up the topological dimensions associated

with the line segments that comprise the boundary of the unit square and the points that comprise the set of vertices of the unit square. It is not detecting any complex dimensions associated with the dimension of the unit square itself, i.e. $\omega = 2$, because this RFD is not robust enough. We could recover the 2nd dimension by using another fractal tube function called the *tube zeta function* as described in [LRŽ17] (cf. Section 2.2.2, Definition 2.2.8), but we will not be using this fractal zeta function in our analysis. Moreover, neither of these zeta functions (the distance or tube zeta functions) reveal any *nonreal* complex dimensions, which indicates, unsurprisingly, that the unit square is not a fractal.

After some thought, it becomes clear that a better approach is to embed I^2 in $\mathbb{R}^3$. With this extra space, one may consider instead choosing $\Omega = I^3 \setminus \partial I^3$, the open unit cube in $\mathbb{R}^3$, so that the closure of one face of $I^3 \setminus \partial I^3$ coincides with I^2. Let's observe what happens in this case. We have

$$\int_{I^3 \setminus \partial I^3} d(\mathbf{x}, I^2)^{s-3} \, \mathrm{d}\mathbf{x} = \int_0^1 \int_0^1 \int_0^1 z^{s-3} \, \mathrm{d}z \, \mathrm{d}y \, \mathrm{d}x = \frac{1}{s-2}. \tag{5.0.5}$$

Here the only complex dimension we pick up is $\omega = 2$. If we instead integrate over a "puffed up" cube, i.e. a t-tubular neighborhood of I^3, we would also pickup dimensions 1 and 0 corresponding to the edges and vertices, respectively, but we still would not detect any nonreal complex dimensions, as expected.

The problem with these choices of Ω is that they are not refined enough to elicit the fractal qualities of a space-filling curve in $\mathfrak{R}_2$. One issue in particular is that these choices of drum do not *respect the generations* that are characteristic of the constructions of space-filling curve, so they cannot detect the oscillations induced by these constructions.

The next section will detail the construction of a specific relative fractal drum for the Hilbert curve; an original construction developed by the present author that will then be generalized and proved valid in several ways.

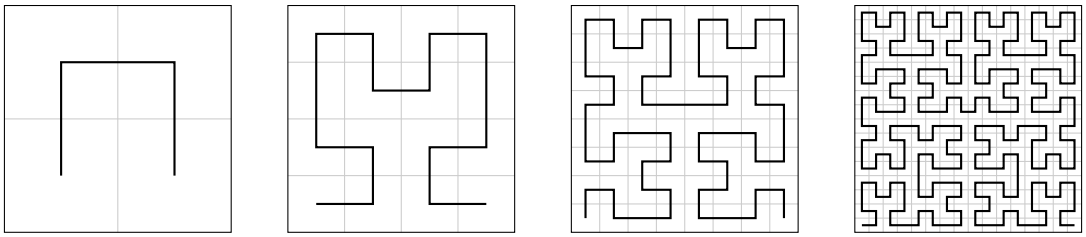

$n = 1$ $n = 2$ $n = 3$ $n = 4$

Figure 4.2.1: The first four approximations to the Hilbert curve. (Repeated from page 41.)

5.1 The Hilbert Curve RFD

As mentioned in Chapter 4, the Hilbert curve is, in some senses, the canonical plane-filling curve, and it serves as a perfect object with which to demonstrate the validity of the following RFD. Recall the construction of the Hilbert curve, illustrated again in Figure 4.2.1. The *Hilbert curve RFD* is constructed as follows.

Remark 5.1.1. Let $n = 1, 2, 3, \ldots$ represent the nth generation of approximation to the Hilbert curve. Figure 5.1.1 depicts what we refer to as the *fundamental cell*, Ω_0, for the Hilbert curve RFD. It is defined as the open region in $\mathbb{R}^3$ bounded by the 2-dimensional planes given by $z = y$, $z = 1 - y$, $x = 0$, $x = 1$, and $y = 0$. This cell is the "base drum" for the RFD in the sense that all of the other subdrums in the RFD are scaled copies of this one. In particular, for each of the $4^n - 1$ unit segments of generation n (see Definition 4.2.6), we associate/attach an appropriately scaled copy of Ω_0 to the unit segment so that the segment is the boundary of the lower edge of the triangular prism shown in Figure 5.1.1. For $n \geq 1$, this line segment is contained in I^2, so these prisms are touching the unit square only at these edges of generational unit length. Repeat this process for each generation n: scale the fundamental cell by a factor of 2^{-n} and attach a prism to each generational unit segment. Define the union of all of the scaled copies of the fundamental cell to be Ω, and we claim $(f_{H*}(I), \Omega) \coloneqq (H, \Omega) = (I^2, \Omega)$ is the appropriate *Hilbert curve RFD*.

Remark 5.1.2. More specifically, for any $n \geq 1$, let Ω_i^n be a copy of the fundamental cell Ω_0 scaled by a factor of 2^{-n}, where $1 \leq i \leq 4^n - 1$. Then $\Omega_i^n = 2^{-n}\Omega_0$ (see Definition 3.3.10),

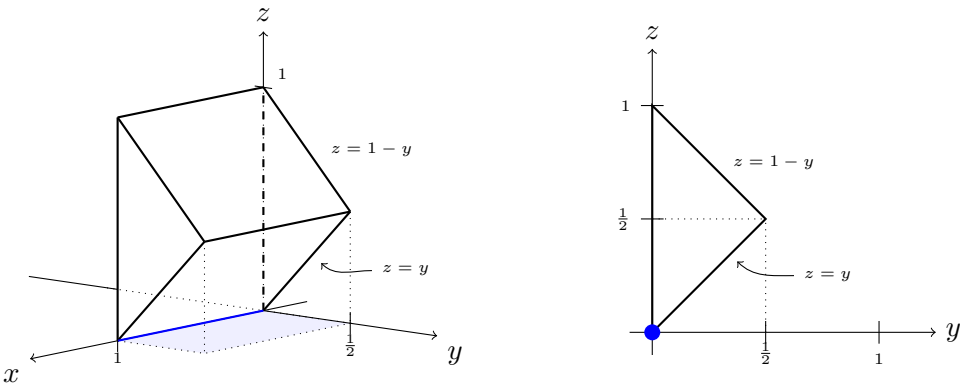

Figure 5.1.1: Isometric and side views of the fundamental cell, Ω_0, for the Hilbert Curve

and we can write

$$\Omega = \bigcup_{n=1}^{\infty} \bigcup_{i=1}^{4^n-1} \Omega_i^n = \bigcup_{n=1}^{\infty} \bigcup_{i=1}^{4^n-1} 2^{-n}\Omega_0. \tag{5.1.1}$$

Before we can assert that this is a valid RFD, let alone the one we are seeking for the Hilbert curve, we need the following corollary. It is a corollary of Proposition 5.2.1, which is proved below. For now we assume this corollary to be true and verify it later.

Corollary 5.1.1. The prisms comprising Ω in the construction of the Hilbert curve RFD can be taken to be disjoint and arranged in a configuration such that only the lower edge of each touches the plane $\mathbb{R}^2$, and the projection of Ω onto the plane is contained entirely in the unit square, I^2. In other words, a valid *geometric realization* of the relative fractal drum (H, Ω) exists.

Remark 5.1.3. Figures 5.1.2 to 5.1.9 show a model of the RFD that has been scaled by a factor of $\frac{1}{2}$ to emphasize how the structure of the RFD complements the structure of the Hilbert curve, and to show that it is plausible that there is enough space to fit all of the prisms above and below the unit square so they do not intersect each other. Some other, more stunning images of this can be found in Appendix A. An unscaled version is pictured in Figures 5.3.4 and 5.3.5 in Section 5.3 below where there is also a discussion of another valid RFD for the Hilbert curve. All of these models were made with Mathematica, and the Mathematica code itself can be found in Appendix A as well.

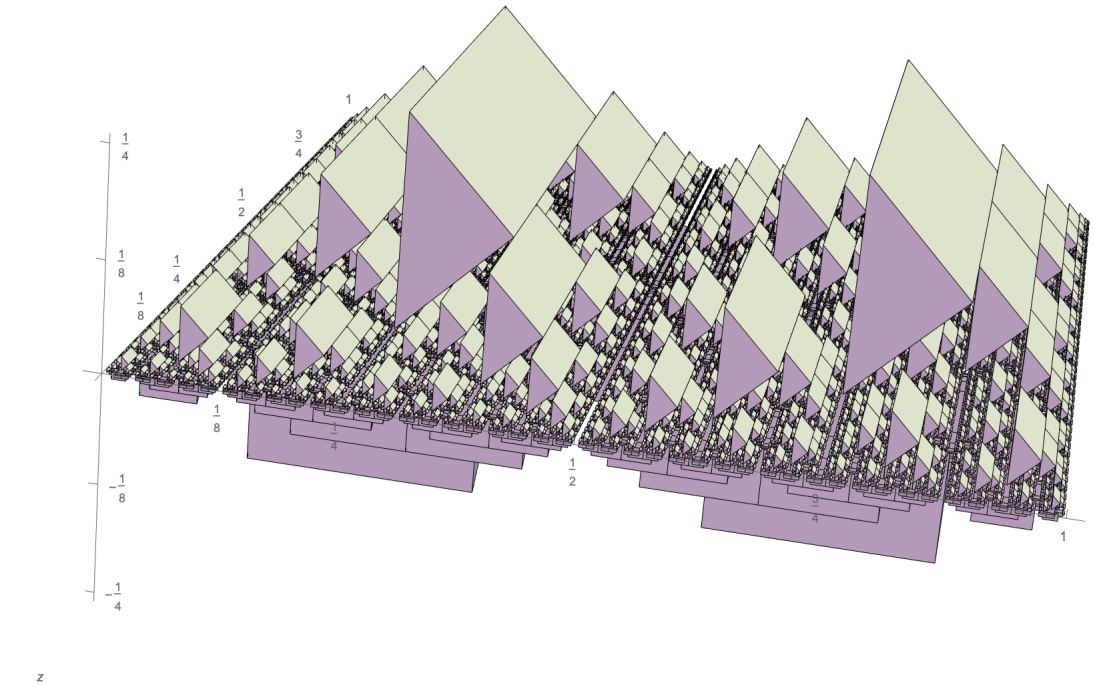

Figure 5.1.2: A 3D model of the Hilbert Curve RFD with the prisms scaled down by a factor of $\frac{1}{2}$, viewed from above.

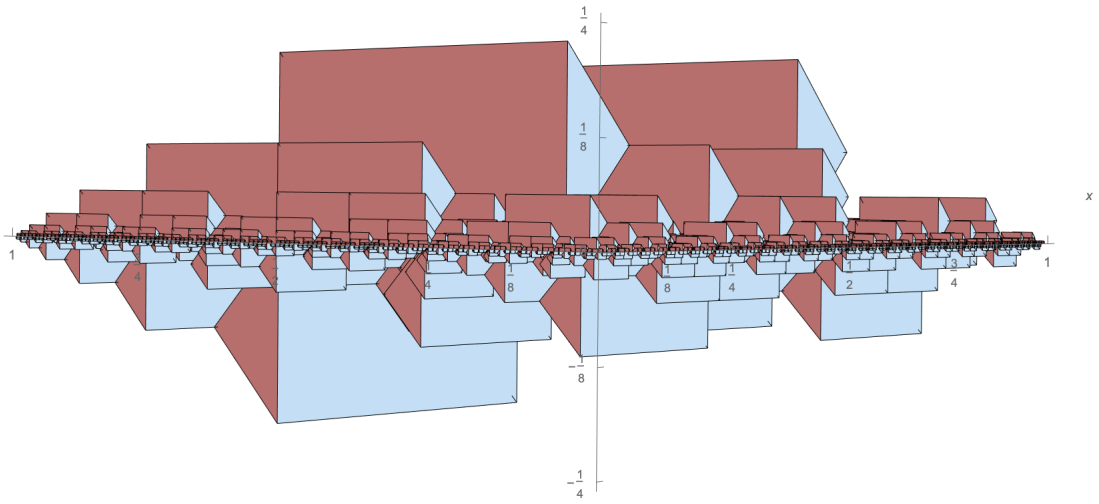

Figure 5.1.3: A 3D model of the Hilbert Curve RFD with the prisms scaled down by a factor of $\frac{1}{2}$, viewed from the side.

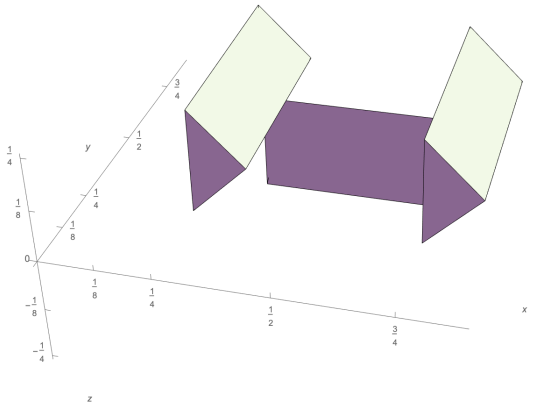

Figure 5.1.4: Scaled Hilbert curve RFD, generation 1.

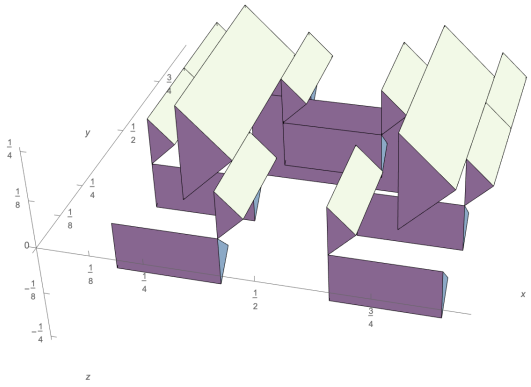

Figure 5.1.5: Scaled Hilbert curve RFD, generations 1 and 2.

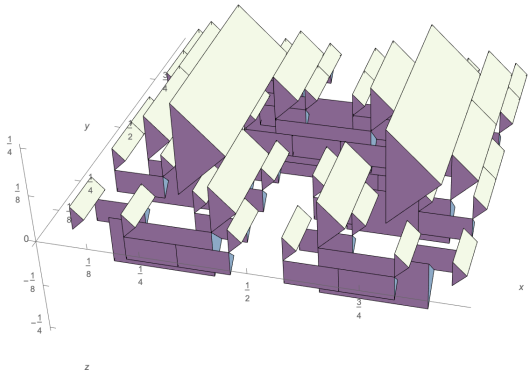

Figure 5.1.6: Scaled Hilbert curve RFD, generations 1–3.

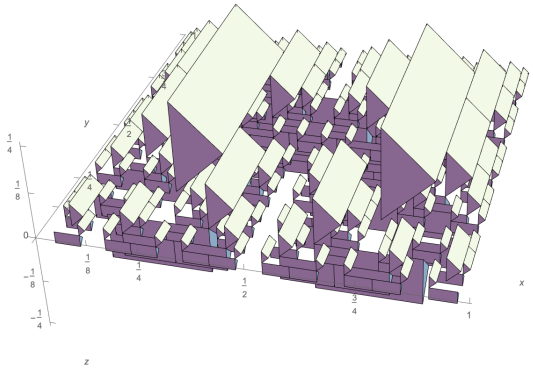

Figure 5.1.7: Scaled Hilbert curve RFD, generations 1–4.

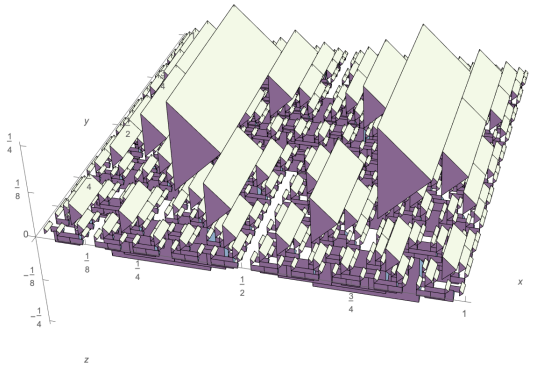

Figure 5.1.8: Scaled Hilbert curve RFD, generations 1–5.

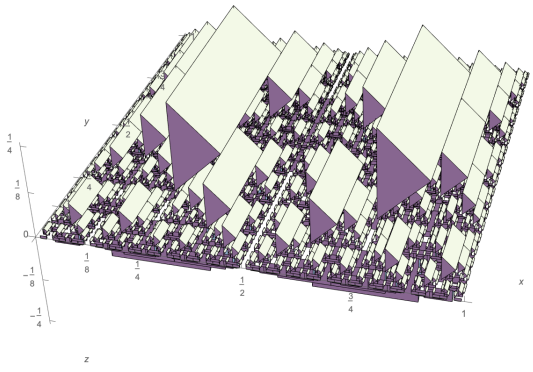

Figure 5.1.9: Scaled Hilbert curve RFD, generations 1–6.

Note that when $n = 1$, the generational unit length is $\frac{1}{2}$, so for any $\delta \geq \frac{1}{2}$ we have $\Omega \subset H_\delta$, where H_δ is the δ-tubular neighborhood of $H = I^2$, i.e. Ω is contained in a sufficiently large open neighborhood of the unit square embedded in $\mathbb{R}^3$. Additionally, since the 3-dimensional Lebesgue measure of Ω_0 is $\frac{1}{2}$, by countable additivity we have that the 3-dimensional Lebesgue measure of Ω is

$$\begin{aligned}
|\Omega|_3 &= \left| \bigcup_{n=1}^{\infty} \bigcup_{i=1}^{4^n-1} \Omega_i^n \right|_3 = \sum_{n=1}^{\infty} \sum_{i=1}^{4^n-1} |\Omega_i^n|_3 = \sum_{n=1}^{\infty} \sum_{i=1}^{4^n-1} |2^{-n}\Omega_0|_3 \\
&= \sum_{n=1}^{\infty} (4^n - 1)2^{-3n} \cdot \frac{1}{4} = \frac{1}{4} \sum_{n=1}^{\infty} 2^{-n} - 2^{-3n} = \frac{1}{4} \left(\frac{\frac{1}{2}}{1 - \frac{1}{2}} - \frac{\frac{1}{8}}{1 - \frac{1}{8}} \right) \\
&= \frac{1}{4} \left(1 - \frac{1}{7} \right) = \frac{3}{14} < \infty.
\end{aligned} \tag{5.1.2}$$

Now we have established that $\Omega \subset H_\delta$ and $|\Omega|_3 < \infty$, we can compute the relative distance zeta function of (H, Ω). First we compute the relative distance zeta function for the fundamental cell, Ω_0:

$$\begin{aligned}
\zeta_{H,\Omega_0}(s) &= \int_{\Omega_0} d(\mathbf{x}, H)^{s-3} \, \mathrm{d}\mathbf{x} = \int_0^1 \int_0^{\frac{1}{2}} \int_y^{1-y} z^{s-3} \, \mathrm{d}z \, \mathrm{d}y \, \mathrm{d}x \\
&= \frac{1}{s-2} \int_0^{\frac{1}{2}} (1-y)^{s-2} - y^{s-2} \, \mathrm{d}y \\
&= \frac{1}{(s-2)(s-1)} \left[-(1-y)^{s-1} - y^{s-1} \right]_0^{\frac{1}{2}} \\
&= \frac{1}{(s-2)(s-1)} \left[-\left(\frac{1}{2}\right)^{s-1} - \left(\frac{1}{2}\right)^{s-1} + 1 \right] \\
&= \frac{1}{(s-2)(s-1)} [-2 \cdot 2^{1-s} + 1] = \frac{1 - 2^{2-s}}{(s-2)(s-1)}.
\end{aligned} \tag{5.1.3}$$

Remark 5.1.4. Note that the distance function in this case is simply $d(\mathbf{x}, H) = z$ since the fractal of interest, H, is the unit square in the plane $z = 0$ which lies directly below any point in Ω_0. This also holds for any subdrum Ω_i^n. In particular, $d(\mathbf{x}, H) = d(\mathbf{x}, 2^{-n}H)$ for any $\mathbf{x} \in \Omega_i^n$. Also note that the only singularity of $\zeta_{H,\Omega_0}(s)$ is $s = 1$ because the possible at

singularity $s = 2$ is canceled by the factor of $1 - 2^{2-s}$ in the numerator. It is expected that there is a singularity at $s = 1$ since the contacting edge is a 1-dimensional line segment.

Now, each subdrum Ω_i^n is a scaled copy of Ω_0, and since $d(\mathbf{x}, 2^{-n}H) = z = d(\mathbf{x}, H)$ for any point $\mathbf{x} \in \Omega_i^n$, it follows that

$$\int_{\Omega_i^n} d(\mathbf{x}, 2^{-n}H)^{s-3}\, \mathrm{d}\mathbf{x} = \int_{\Omega_i^n} d(\mathbf{x}, H)^{s-3}\, \mathrm{d}\mathbf{x}. \tag{5.1.4}$$

Thus Theorem 3.3.2, the scaling property of the relative distance zeta function, yields

$$\zeta_{H,\Omega_i^n}(s) = \zeta_{2^{-n}H,\Omega_i^n}(s) = \zeta_{2^{-n}H,2^{-n}\Omega_0}(s) = (2^{-n})^s \zeta_{H,\Omega_0}(s). \tag{5.1.5}$$

We can also apply Theorem 3.3.3 given in Chapter 3 since these prisms are all disjoint when properly configured. With these two results in hand, we have the following.

$$\begin{aligned}
\zeta_{H,\Omega}(s) &= \sum_{n=1}^{\infty} \sum_{i=1}^{4^n-1} \zeta_{H,\Omega_i^n}(s) = \sum_{n=1}^{\infty} \sum_{i=1}^{4^n-1} (2^{-n})^s \zeta_{H,\Omega_0}(s) \\
&= \sum_{n=1}^{\infty} \sum_{i=1}^{4^n-1} (2^{-n})^s \frac{(1-2^{2-s})}{(s-2)(s-1)} = \frac{(1-2^{2-s})}{(s-2)(s-1)} \sum_{n=1}^{\infty} 2^{-sn}(4^n - 1) \\
&= \frac{(1-2^{2-s})}{(s-2)(s-1)} \sum_{n=1}^{\infty} \left[(2^{2-s})^n - (2^{-s})^n \right] = \frac{(1-2^{2-s})}{(s-2)(s-1)} \left[\frac{2^{2-s}}{1-2^{2-s}} - \frac{2^{-s}}{1-2^{-s}} \right] \\
&= \frac{\cancel{(1-2^{2-s})}}{(s-2)(s-1)} \left[\frac{2^{2-s} - \cancel{2^{-s}2^{2-s}} - 2^{-s} + \cancel{2^{-s}2^{2-s}}}{\cancel{(1-2^{2-s})}(1-2^{-s})} \right] = \frac{2^{-s}(4-1)}{(s-2)(s-1)(1-2^{-s})} \\
&= \frac{3}{(s-2)(s-1)(2^s-1)}.
\end{aligned} \tag{5.1.6}$$

In other words, the relative distance zeta function of the Hilbert curve RFD is

$$\zeta_{H,\Omega}(s) = \frac{3}{(s-2)(s-1)(2^s-1)}. \tag{5.1.7}$$

This function is valid initially for all $s \in \mathbb{C}$ such that Re $s > 2$, but it can be extended meromorphically to all of $\mathbb{C}$ via analytic continuation (see Theorem 3.3.1). From Equation 5.1.7 we can read off the singularities of $\zeta_{H,\Omega}(s)$, and we have that the set of relative complex dimensions of the Hilbert curve must be

$$\mathcal{D}(\zeta_{H,\Omega}) = \left\{0 + \frac{2\pi}{\log 2} i\mathbb{Z}\right\} \cup \{1, 2\}. \tag{5.1.8}$$

Since this set contains nonreal numbers, it is shown that the Hilbert curve is indeed a fractal according to Definition 3.3.9, and its oscillatory period is $\mathbf{p} = \frac{2\pi}{\log 2}$.

Remark 5.1.5. There is a beautiful reaction occurring in this construction. Since the Hilbert curve $H = I^2$ is a 2-dimensional object, we expect to see the pole $s = 2$, and this pole did not manifest via the relative distance zeta function of Ω_0 because it is cancelled out. However, after taking the union of all of the scaled subdrums, a factor of $1 - 2^{2-s}$ appears in the denominator due to the geometric series that results from summing the zeta functions of all of the subdrums. Moreover, the factor of $2^s - 1$ appears precisely because the minimal representation of any nth approximation only requires $4^n - 1$ generational unit segments. This is one reason why it is important to distinguish between the necessary conditions to produce a space-filling curve and the convenient conditions, as mentioned in Remark 4.2.9.

Now that we have seen this construction, there are some natural questions to ask.

1. Is Corollary 5.1.1 true, i.e. does a valid geometric realization exist?

2. Is this RFD unique, i.e. does there exist another RFD that is capable of correctly detecting the complex dimensions of the Hilbert curve?

3. Why is this RFD the one that correctly detects the complex dimensions of the Hilbert curve?

4. Can this construction be generalized to space-filling curves produced by other regular rectilinear tessellations of the unit square I^2?

5. Can this construction be generalized to space-filling curves produced by other nonrectilinear tessellations of subsets of the plane $\mathbb{R}^2$?

6. Can this construction be extended to higher dimensional Hilbert curves, and more generally, other higher dimensional space-filling curves?

We proceed to answer the first four questions in the next two sections, and leave the discussion of the last two questions for Chapter 7.

5.2 A Generalized RFD

The construction of the Hilbert curve RFD given in the previous section can indeed be generalized to any regular rectilinear tessellation of I^2, and once we have done so, we will affirm the validity of not only the Hilbert curve RFD, but an entire class of RFDs associated with $\mathfrak{R}_2$, the class of all space-filling curves generated via regular rectilinear tessellations of the plane. Once we have produced the generalization, we will demonstrate that a valid geometric realization exists for any regular rectilinear tessellation.

To begin, recall Definition 4.3.5, and let $\lambda \in \{2, 3, 4, \ldots\}$[1], that is, let λ be a positive integer greater than or equal to 2. For $n = 1, 2, 3, \ldots$, we can construct a regular rectilinear tessellation of I^2 by subdividing the unit square into λ^{2n} subsquares, and, by choosing an appropriate λ-adic correspondence (traverse) Φ_λ, create an associated space-filling curve $\Lambda \in \mathcal{S}_2(\lambda)$. For example, in the construction of the Hilbert curve, $\lambda = 2$, and in the construction of the Peano curve, detailed in Section 5.3 below, $\lambda = 3$. In order to produce an associated relative fractal drum analogous to that of the Hilbert RFD, we need to use the correct *fundamental cell*. In Figure 5.2.1, we see the fundamental cell, Ω_0, for any curve in $\mathcal{S}_2(\lambda)$. In particular, it is the open region in $\mathbb{R}^3$ bounded by the 2-dimensional planes $z = 1 - y$, $z = \frac{1}{1-\lambda} y$, $x = 0$, $x = 1$, and $y = 0$. Some examples of fundamental cells for other choices of λ are shown in Figure 5.2.2.

[1]From this point forward, anytime λ is used, it is assumed to be a positive integer greater than or equal to 2. See Section 7.2 in Chapter 7 for a brief discussion of the cases when λ is a real number greater than or equal to 2.

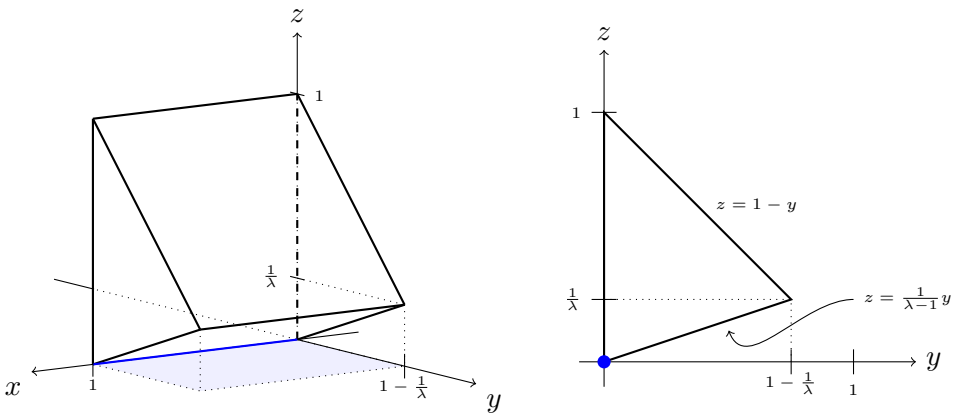

Figure 5.2.1: Isometric and side views of the fundamental cell, Ω_0, for any curve in $\mathcal{S}_2(\lambda)$

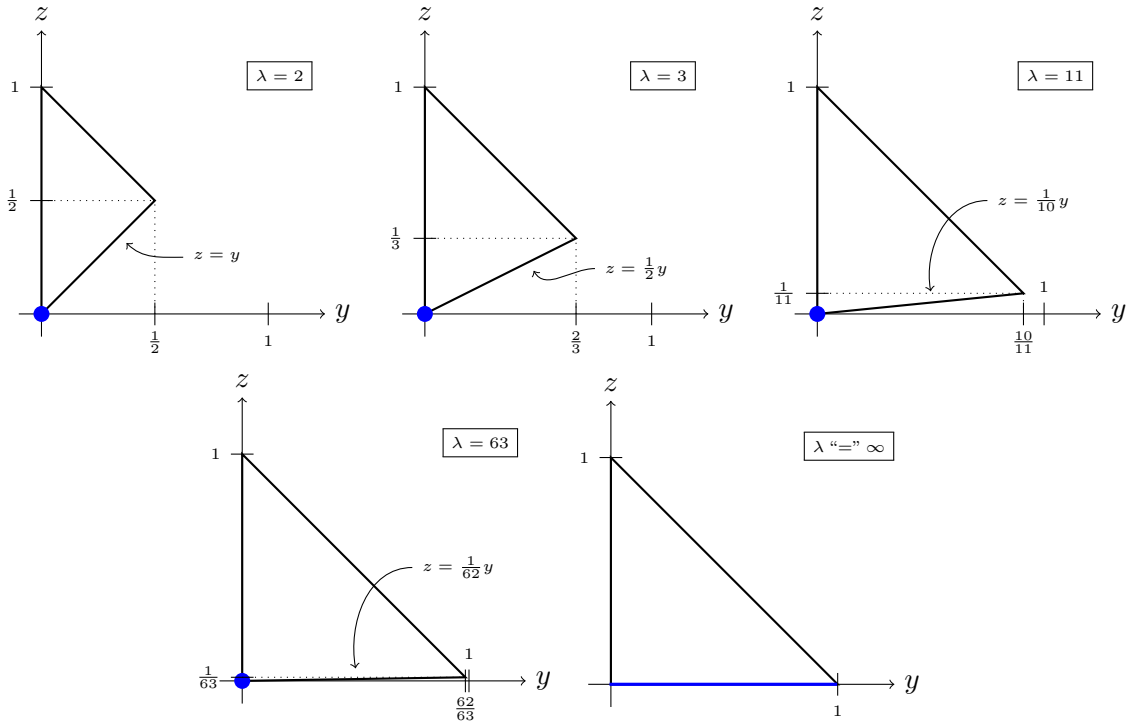

Figure 5.2.2: Side views of the fundamental cells for some values of λ.

Seeing the side views of some of the fundamental cells for large values of λ in Figure 5.2.2 makes it clear that the existence of a valid geometric realization is not a trivial matter since the volume of space beneath these cells is decreasing as λ increases. However, the subdrums are also getting thinner as λ increases. We now show that a valid geometric realization exists by proving the following Proposition.

Proposition 5.2.1. Let $\lambda \in \{2, 3, \ldots\}$, and let Ω_0 be the associated fundamental cell. Then the volume of space above and below the unit square I^2 is sufficient to accommodate the disjoint union of all of the prisms in all of the generations in the construction of the associated RFD so that each prism touches the unit square along one edge of generational unit length. In other words, a valid geometric realization of this RFD exists for any $\lambda \in \{2, 3, \ldots\}$.

Proof. This amounts to a 3-dimensional "prism packing" problem which reduces to a problem of available 2-dimensional area in the unit square: the maximum height of the cavity under a prism restricts how many prisms of the subsequent generations can fit underneath and still contact the plane in which the unit square is embedded, and this space restriction is in one-to-one correspondence with a restricted projected area under each prism. A simple calculation shows that, for any λ, the area covered (or shadowed) by a single scaled prism in the nth generation is given by Formula 5.2.1 below. See Figures 5.2.3 and 5.2.4 for a visualization of the area restrictions.

$$A_n = \frac{\lambda - 1}{\lambda^{2n+1}}. \tag{5.2.1}$$

In each generation, there is a minimum amount of area within the unit square that must be accessible for intersection with the projected area of the prisms yet to be placed. We denote this minimum area by $m(n)$. Since there are $\lambda^{2n} - 1$ prisms in any generation n, we must be able to access a minimum area of

$$m(n) = A_n \cdot (\lambda^{2n} - 1) = \frac{\lambda - 1}{\lambda^{2n+1}} \cdot (\lambda^{2n} - 1). \tag{5.2.2}$$

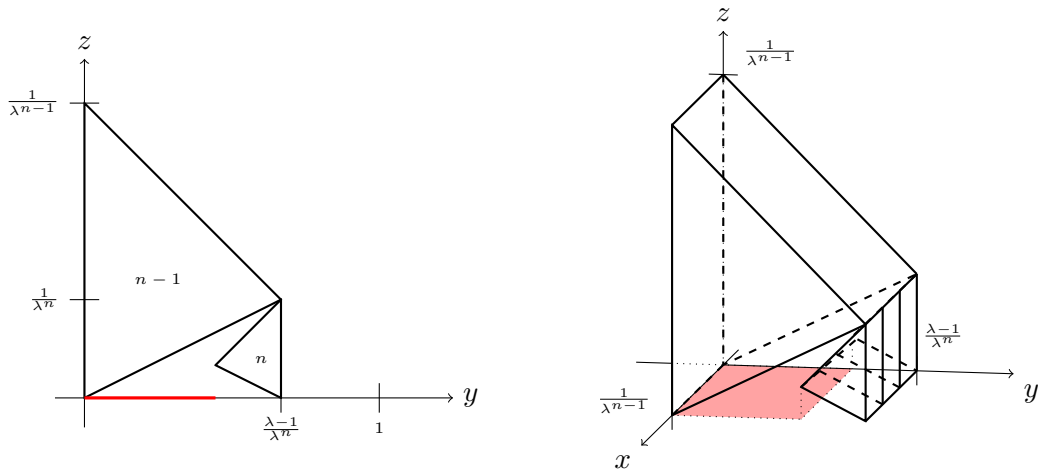

Figure 5.2.3: The area under a prism in generation $n-1$ restricted from the prisms in generation n for $n \geq 2$.

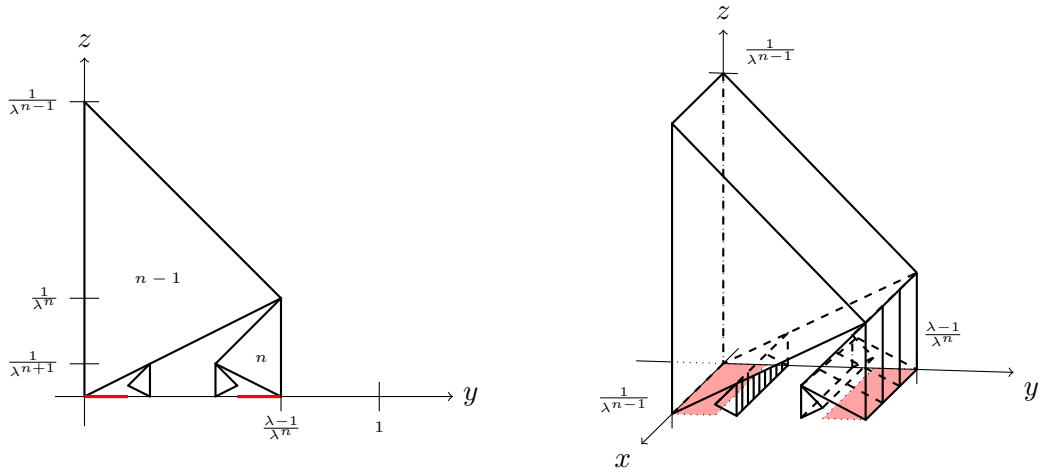

Figure 5.2.4: The area under prisms in generations $n-1$ and n restricted from the prisms in generation $n+1$ for $n \geq 2$.

In each generation n, there is also some amount of area that is geometrically inaccessible due to the placement of the prisms from all of the previous generations combined. We denote this accumulated, inaccessible (or restricted) area by $r(n)$. As long as $r(n)$ does not meet or exceed $m(n)$, i.e. $r(n) < m(n)$, a valid geometric realization will exist since there will be enough space to place all of the prisms in each generation, and thus enough room to place all of the prisms in the RFD.

To determine the formula for $r(n)$, note that a prism in the $(n-1)$th generation restricts $\frac{\lambda-1}{\lambda}$ of the area it covers from being accessed (or shadowed) by a prism in the nth generation (see Figures 5.2.3 and 5.2.4). More specifically, the area restricted from prisms in generation n by a single prism in generation $n-1$, is

$$\frac{\lambda-1}{\lambda} \cdot A_{n-1} = \frac{\lambda-1}{\lambda} \cdot \frac{\lambda-1}{\lambda^{2n-1}} = \frac{(\lambda-1)^2}{\lambda^{2n}}. \tag{5.2.3}$$

The total area restricted from the nth generation, $r(n)$, is the sum of the areas restricted by all previous generations. The restriction relationship between *consecutive* generations enables us to count how much *accumulated* area is restricted for each generation. More specifically, we find the following.

$$r(n) = \frac{\lambda-1}{\lambda} \cdot A_{n-1} \sum_{k=1}^{n} \lambda^{k-1} \left((\lambda^2)^{n-k} - 1 \right) \tag{5.2.4}$$

Simplifying Formula 5.2.4, we find

$$\begin{aligned} r(n) &= \frac{\lambda-1}{\lambda} \cdot A_{n-1} \sum_{k=1}^{n} \lambda^{k-1} \left((\lambda^2)^{n-k} - 1 \right) = \frac{\lambda-1}{\lambda} \cdot \frac{\lambda-1}{\lambda^{2n-1}} \cdot \frac{1}{\lambda} \sum_{k=1}^{n} \lambda^k \left(\lambda^{2n-2k} - 1 \right) \\ &= \frac{(\lambda-1)^2}{\lambda^{2n+1}} \sum_{k=1}^{n} \left(\lambda^{2n-k} - \lambda^k \right) = \frac{(\lambda-1)^2}{\lambda^{2n+1}} \cdot \frac{(\lambda^n-1)(\lambda^n-\lambda)}{\lambda-1} \\ &= \frac{(\lambda^n-1)(\lambda^{n-1}-1)(\lambda-1)}{\lambda^{2n}}. \end{aligned} \tag{5.2.5}$$

Now we can proceed by showing that $r(n) < m(n)$ for all $n \geq 2$. We have the following chain of equivalent inequalities.

$$r(n) < m(n)$$

$$\frac{(\lambda^n - 1)(\lambda^{n-1} - 1)(\lambda - 1)}{\lambda^{2n}} < \frac{\lambda - 1}{\lambda^{2n+1}}(\lambda^{2n} - 1)$$

$$(\lambda^n - 1)(\lambda^{n-1} - 1) < \lambda^{2n-1} - \lambda^{-1}$$

$$\lambda^{2n-1} - \lambda^n - \lambda^{n-1} + 1 < \lambda^{2n-1} - \lambda^{-1}$$

$$\lambda^{n+1} + \lambda^n - \lambda > 1. \tag{5.2.6}$$

Inequality 5.2.6 holds for all $\lambda > 1$, and all $n \geq 1$. Consequently, there is always enough room available in the unit square to place the $\lambda^{2n} - 1$ scaled prisms that are required for the nth generation of the construction, even after all of the previous prisms have been placed. In other words, a valid geometric realization of this RFD exists for any λ. □

Since a valid geometric realization exists for any λ, we have also proved Corollary 5.1.1, i.e. that the Hilbert curve RFD is valid construction.

Remark 5.2.1. Now is a good time to point out that the exact placement of the prisms does not need to follow the traverse of the approximating polygons because the unit square is filled by the space-filling curve itself, not by any approximation. As mentioned in Remark 5.1.4, this is what allows us to choose the distance function $d(\mathbf{x}, H) = z$. Moreover, as mentioned in Remarks 3.3.2, 2.3.1, and 2.1.2, all of our analytical tools are independent of geometric realization. The question of whether or not it is necessary to move them is addressed in Section 5.3 below.

Remark 5.2.2. As a side note, referring back to Formulas 5.2.2 and 5.2.5, observe that

$$\lim_{n\to\infty} r(n) = \lim_{n\to\infty} m(n) = \frac{\lambda - 1}{\lambda}, \tag{5.2.7}$$

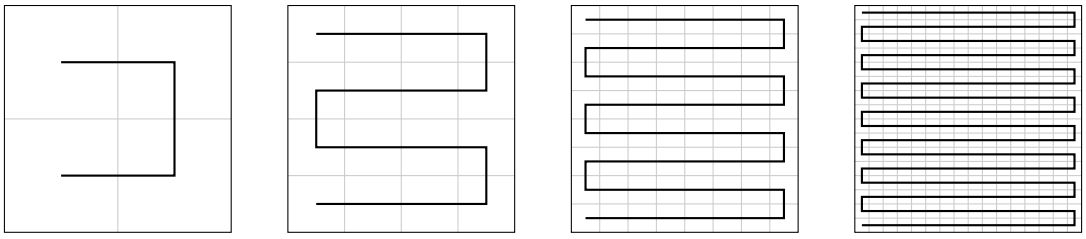

$n = 1$ $n = 2$ $n = 3$ $n = 4$

Figure 5.2.5: The first four "approximations" to an accordion "curve".

so the accumulated restricted area coincides with the minimum area needed at infinity, which is to be expected. Moreover, this limiting value, $\frac{\lambda-1}{\lambda}$, goes to 1 as $\lambda \to \infty$, as we would also expect. This is a piece of evidence that suggests this construction of a generalized RFD is the correct one, addressing Question 3 to some extent.

Before we come to the main result of this dissertation, it is edifying to explore the following counterexample which also serves as evidence that this construction of a generalized RFD is the correct one.

Counterexample 5.2.1 (The Accordion "Curve")**.** The first four "approximations" to one of these accordion "curves" (or scan curves) when $\lambda = 2$ are shown in Figure 5.2.5, and they consist of a simple scanning traverse from left to right and then right to left, moving up or down one square when an edge square is reached. In the same sense as the a-string discussed in Counterexample 1.0.2, accordion "curves" are not generally considered to be fractals. However, for each n, these polygons have the same number of generational unit segments as the Hilbert curve so in light of Proposition 5.2.1 and Remark 5.2.1 one might suspect that the relative distance zeta function for this "curve" would be the same as that of the Hilbert curve, given in Equation 5.1.7. Thus our definition of fractality would erroneously include these "non-fractal" objects. But the accordion "curve" is not a space-filling curve. In fact, "it" is not a curve at all. The sequence of mappings whose images are depicted in Figure 5.2.5 does not converge, and the distance between images of points in consecutive generations can differ by over $1 - 2^{-n}$, i.e. points can "wander too far" for the sequence to converge. Since this sequence of mappings does not converge to the unit square, we cannot

choose the distance function $d(\mathbf{x}, I^2)$ to be simply z as we did for the Hilbert curve, and the relative distance zeta function we derived does not apply here. If we instead took our distance function to be the distance from a point in a subdrum to the segment which it contacts in the unit square, a simple pole of $s = 1$ would arise since the topological dimension of a generational unit segment is 1. Moreover, the union of all the subdrums in a given generation would also yield a pole at $s = 1$, but the union of all of the generations of scaled subdrums would not have any geometric significance as it does for the Hilbert curve.

We are now ready to assert and prove the main result of this dissertation.

Theorem 5.2.1 (A.D. Richardson, 2021)**.** Let $\lambda \in \{2, 3, 4, \ldots\}$ and let $\Lambda \in \mathcal{S}_2(\lambda)$ be a plane-filling curve. Let (Λ, Ω) be the associated RFD, constructed as above. Then a relative distance zeta function for (Λ, Ω) is

$$\zeta_{\Lambda,\Omega}(s) = \frac{\lambda^2 - 1}{(s-2)(s-1)(\lambda^s - 1)}. \tag{5.2.8}$$

Consequently, the set of relative complex dimensions of Λ is

$$\mathcal{D}(\zeta_{\Lambda,\Omega}) = \left\{0 + \frac{2\pi}{\log \lambda} i\mathbb{Z}\right\} \cup \{1, 2\}, \tag{5.2.9}$$

and therefore Λ is a fractal by Definition 3.3.9. Since this is true for any $\lambda \in \{2, 3, 4, \ldots\}$, it follows that every space-filling curve in $\mathfrak{R}_2$ is a fractal by Definition 3.3.9.

Proof. Given $\Lambda \in \mathcal{S}_2(\lambda)$, we first compute the relative distance zeta function for the fundamental cell Ω_0 (see Figure 5.2.1):

$$\begin{aligned}
\zeta_{\Lambda,\Omega_0}(s) &= \int_0^1 \int_0^{1-\frac{1}{\lambda}} \int_{\frac{1}{\lambda-1}y}^{1-y} z^{s-3}\, \mathrm{d}z\, \mathrm{d}y\, \mathrm{d}x = \frac{1}{s-2} \int_0^{1-\frac{1}{\lambda}} (1-y)^{s-2} - (\lambda-1)^{2-s} y^{s-2}\, \mathrm{d}y \\
&= \frac{1}{(s-2)(s-1)} \left[-(1-y)^{s-1} - (\lambda-1)^{2-s} y^{s-1} \right]_0^{1-\frac{1}{\lambda}} \\
&= \frac{1}{(s-2)(s-1)} \left[-\left(\frac{1}{\lambda}\right)^{s-1} - (\lambda-1)^{2-s} \left(\frac{\lambda-1}{\lambda}\right)^{s-1} + 1 \right] \\
&= \frac{1}{(s-2)(s-1)} \left[-\left(\frac{1}{\lambda}\right)^{s-1} - (\lambda-1) \left(\frac{1}{\lambda}\right)^{s-1} + 1 \right] \\
&= \frac{1}{(s-2)(s-1)} \left[-\lambda \cdot \lambda^{1-s} + 1 \right] = \frac{(1-\lambda^{2-s})}{(s-2)(s-1)}.
\end{aligned} \tag{5.2.10}$$

Just like before, each subdrum Ω_i^n is a scaled copy of Ω_0, so we can apply Theorems 3.3.2 and 3.3.3, yielding

$$\begin{aligned}
\zeta_{\Lambda,\Omega}(s) &= \sum_{n=1}^{\infty} \sum_{i=1}^{\lambda^{2n}-1} \zeta_{H,\Omega_i^n}(s) = \sum_{n=1}^{\infty} \sum_{i=1}^{\lambda^{2n}-1} (\lambda^{-n})^s \zeta_{H,\Omega_0}(s) \\
&= \frac{(1-\lambda^{2-s})}{(s-2)(s-1)} \sum_{n=1}^{\infty} \lambda^{-sn}(\lambda^{2n}-1) = \frac{(1-\lambda^{2-s})}{(s-2)(s-1)} \sum_{n=1}^{\infty} \left[(\lambda^{2-s})^n - (\lambda^{-s})^n \right] \\
&= \frac{(1-\lambda^{2-s})}{(s-2)(s-1)} \left[\frac{\lambda^{2-s}}{1-\lambda^{2-s}} - \frac{\lambda^{-s}}{1-\lambda^{-s}} \right] \\
&= \frac{\cancel{(1-\lambda^{2-s})}}{(s-2)(s-1)} \left[\frac{\lambda^{2-s} - \cancel{\lambda^{-s}\lambda^{2-s}} - \lambda^{-s} + \cancel{\lambda^{-s}\lambda^{2-s}}}{\cancel{(1-\lambda^{2-s})}(1-\lambda^{-s})} \right] \\
&= \frac{(\lambda^2-1)\lambda^{-s}}{(s-2)(s-1)(1-\lambda^{-s})} = \frac{\lambda^2-1}{(s-2)(s-1)(\lambda^s-1)}.
\end{aligned} \tag{5.2.11}$$

Thus, we have Equation 5.2.8 and we can read off the set of relative complex dimensions of Λ as:

$$\mathcal{D}(\zeta_{\Lambda,\Omega}) = \left\{ 0 + \frac{2\pi}{\log \lambda} i\mathbb{Z} \right\} \cup \{1, 2\}. \tag{5.2.12}$$

Since this set contains at least one nonreal complex number, Λ is a fractal by Definition 3.3.9. Since λ was chosen arbitrarily, every plane-filling curve in $\mathfrak{R}_2$ is a fractal by Definition 3.3.9. □

At last the fractality of such curves has been established! The value $\mathbf{p} = \frac{2\pi}{\log \lambda}$ is the *oscillatory period* of $\zeta_{\Lambda,\Omega}$. Note that all of the complex dimensions are simple poles, and we can compute the residues:

$$\operatorname{res}(\zeta_{\Lambda,\Omega}(s), 2) = \lim_{s\to 2} \frac{\lambda^2 - 1}{(s-1)(\lambda^s - 1)} = 1, \tag{5.2.13}$$

$$\operatorname{res}(\zeta_{\Lambda,\Omega}(s), 1) = \lim_{s\to 1} \frac{\lambda^2 - 1}{(s-2)(\lambda^s - 1)} = \frac{(\lambda-1)(\lambda+1)}{-(\lambda-1)} = -(\lambda+1), \text{ and} \tag{5.2.14}$$

$$\begin{aligned}
\operatorname{res}(\zeta_{\Lambda,\Omega}(s), 0 + in\mathbf{p}) &= \lim_{s\to in\mathbf{p}} \frac{(s - in\mathbf{p})(\lambda^2 - 1)}{(s-2)(s-1)(\lambda^s - 1)} \\
&= \lim_{s\to in\mathbf{p}} \frac{\lambda^2 - 1}{(s-2)(s-1)} \cdot \lim_{s\to in\mathbf{p}} \frac{s - in\mathbf{p}}{\lambda^s - 1} \\
&= \frac{\lambda^2 - 1}{(in\mathbf{p} - 2)(in\mathbf{p} - 1)} \cdot \lim_{s\to in\mathbf{p}} \frac{1}{(\log \lambda)\lambda^s} \\
&= \frac{\lambda^2 - 1}{\log \lambda (in\mathbf{p} - 2)(in\mathbf{p} - 1)}
\end{aligned} \tag{5.2.15}$$

for all $n \in \mathbb{Z}$.

Now we can, at least initially, address Question 3 by recalling Theorem 3.3.4:

Theorem 3.3.4 ([LRŽ17] 4.1.14)**.** Suppose that (A, Ω) is a Minkowski nondegenerate RFD in $\mathbb{R}^N$, (in particular $\dim_B(A, \Omega) = D$), and $D < N$. If $\zeta_{A,\Omega}(s)$ can be meromorphically extended to a connected open neighborhood of $\{\text{Re } (s) = D\}$, then D is necessarily a simple pole of $\zeta_{A,\Omega}$, the residue $\operatorname{res}(\zeta_{A,\Omega}(s), D)$ is independent of δ and

$$\mathcal{M}_*^D(A, \Omega) \leq \frac{\operatorname{res}(\zeta_{A,\Omega}(s), D)}{N - D} \leq \mathcal{M}^{*D}(A, \Omega). \tag{3.3.14}$$

Furthermore, if (A, Ω) is Minkowski measurable then this inequality yields

$$\mathcal{M}^D(A, \Omega) = \frac{\operatorname{res}(\zeta_{A,\Omega}(s), D)}{N - D}. \tag{3.3.15}$$

In light of the results in Theorem 5.2.1, we use Equation 5.2.13 to conclude that

$$\mathcal{M}^2(\Lambda, \Omega) = \frac{\operatorname{res}(\zeta_{\Lambda,\Omega}(s), 2)}{3 - 2} = 1, \tag{5.2.16}$$

as expected of the unit square. Of course it still remains to be shown that (Λ, Ω) is Minkowski measurable, but this is proven in detail in Proposition 6.2.1 in Chapter 6.

Remark 5.2.3. Note that the complex dimensions with nonzero imaginary part are precisely those with real part equal to 0. In other words, the oscillatory behavior of this fractal is associated with the 0-dimensional objects, the points. This is an artifact of the fact that the λ-adic mapping Φ_λ is defined pointwise using chains of λ-ary intervals. Based on the appearance of the images of approximations to these curves (see, for example, Figures 4.2.1 and 4.3.1) one might wonder if there are oscillations associated with topological dimensions 1 and 2. It is clear that there are no oscillations associated with dimension 2 because that is the topological dimension of the unit square itself. The intuition for why there are not oscillations associated with dimension 1 is less immediate, and is easier to intuit when working with curves that fill a space of dimension greater than 2, so we reserve this discussion for Remark 7.1.1 in Chapter 7.

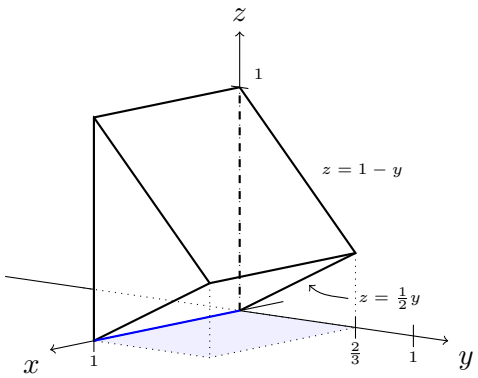

Figure 5.3.1: The fundamental cell for a Peano curve RFD.

5.3 The Peano Curve RFD, and another Hilbert Curve RFD

We begin this section with an example of another RFD for a plane-filling curve, a Peano curve.

Example 5.3.1 (The Peano curve RFD)**.** Let $\lambda = 3$ and let $P = I^2$ represent (the direct image of) a Peano curve. Then Equation 5.2.8 gives

$$\zeta_{P,\Omega}(s) = \frac{8}{(s-2)(s-1)(3^s-1)}, \tag{5.3.1}$$

and the set of complex dimensions for a Peano curve is

$$\mathcal{D}(\zeta_{P,\Omega}) = \left\{0 + \frac{2\pi}{\log 3} i\mathbb{Z}\right\} \cup \{1, 2\}. \tag{5.3.2}$$

We can also compute this directly by computing the zeta function for the fundamental cell, and summing up the zeta functions as before. Those calculations are included below because they can help illuminate where certain factors arise in computation of the relative distance zeta function.

$$
\begin{aligned}
\zeta_{P,\Omega_0}(s) &= \int_0^1 \int_0^{\frac{2}{3}} \int_{\frac{1}{2}y}^{1-y} z^{s-3}\, \mathrm{d}z\, \mathrm{d}y\, \mathrm{d}x \\
&= \frac{1}{s-2} \int_0^{\frac{2}{3}} (1-y)^{s-2} - 2^{2-s} y^{s-2}\, \mathrm{d}y \\
&= \frac{1}{(s-2)(s-1)} \left[-(1-y)^{s-1} - 2^{2-s} y^{s-1} \right]_0^{\frac{2}{3}} \\
&= \frac{1}{(s-2)(s-1)} \left[-\left(\frac{1}{3}\right)^{s-1} - 2^{2-s} \left(\frac{2}{3}\right)^{s-1} + 1 \right] \\
&= \frac{1}{(s-2)(s-1)} [-3^{1-s} - 2 \cdot 3^{1-s} + 1] = \frac{(1-3^{2-s})}{(s-2)(s-1)}.
\end{aligned}
\tag{5.3.3}
$$

$$
\begin{aligned}
\zeta_{P,\Omega}(s) &= \sum_{n=1}^{\infty} \sum_{i=1}^{9^n-1} \zeta_{P,\Omega_i^n}(s) = \sum_{n=1}^{\infty} \sum_{i=1}^{9^n-1} (3^{-n})^s \zeta_{P,\Omega_0}(s) \\
&= \frac{(1-3^{2-s})}{(s-2)(s-1)} \sum_{n=1}^{\infty} 3^{-sn}(3^{2n}-1) = \frac{(1-3^{2-s})}{(s-2)(s-1)} \sum_{n=1}^{\infty} \left[(3^{2-s})^n - (3^{-s})^n \right] \\
&= \frac{(1-3^{2-s})}{(s-2)(s-1)} \left[\frac{3^{2-s}}{1-3^{2-s}} - \frac{3^{-s}}{1-3^{-s}} \right] \\
&= \frac{\cancel{(1-3^{2-s})}}{(s-2)(s-1)} \left[\frac{3^{2-s} - \cancel{3^{-s}3^{2-s}} - 3^{-s} + \cancel{3^{-s}3^{2-s}}}{\cancel{(1-3^{2-s})}(1-3^{-s})} \right] \\
&= \frac{3^{-s}(9-1)}{(s-2)(s-1)(1-3^{-s})} = \frac{8}{(s-2)(s-1)(3^s-1)}.
\end{aligned}
\tag{5.3.4}
$$

In Remark 5.2.1, it is mentioned that the exact placement of the prisms in the RFD does not need to follow the traverse of the approximating polygons as long as the edge of each one is contacting the unit square. A natural question to ask is whether or not it is *necessary* to move the prisms around to accommodate all of them, or if they can be taken to follow the traverse of the approximating polygons. Figure 5.3.2 shows the first three approximations to a Peano curve of the switchback type, overlayed and colored green, red, and blue for generations $n = 1, 2, 3$ respectively. It illustrates that there is nontrivial overlap of the approximating curves. More specifically, if we lay each generation of approximating

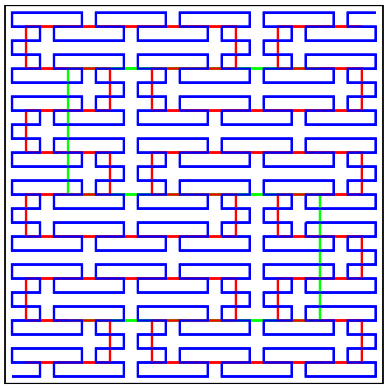

Figure 5.3.2: The first three approximations to a Peano curve of the switchback type, overlayed and colored according to generation.

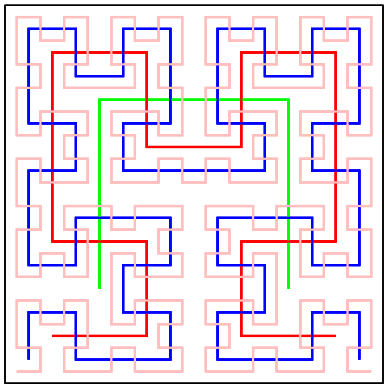

Figure 5.3.3: The first four approximations to the Hilbert curve, overlayed and colored according to generation.

polygons on top of each other, there will be line segments that are covered by segments from an infinite number of generations. This means that infinitely many of the prisms in the corresponding RFD will have a nonempty region of intersection in $\mathbb{R}^3$ that has positive 3-dimensional Lebesgue measure. In this event, we cannot invoke Theorem 3.3.3 so our RFD would not be valid. However, the independence of geometric realization allows us to translate and rotate these prisms to accommodate them all, so for curves such as a Peano curve, this translation is necessary.

In contrast, Figure 5.3.3 shows the first four approximations to the Hilbert curve, overlayed and colored green, red, blue, and pink for generations $n = 1, 2, 3, 4$ respectively. In this case, we see that there is only trivial overlap of the polygons at points. In this event,

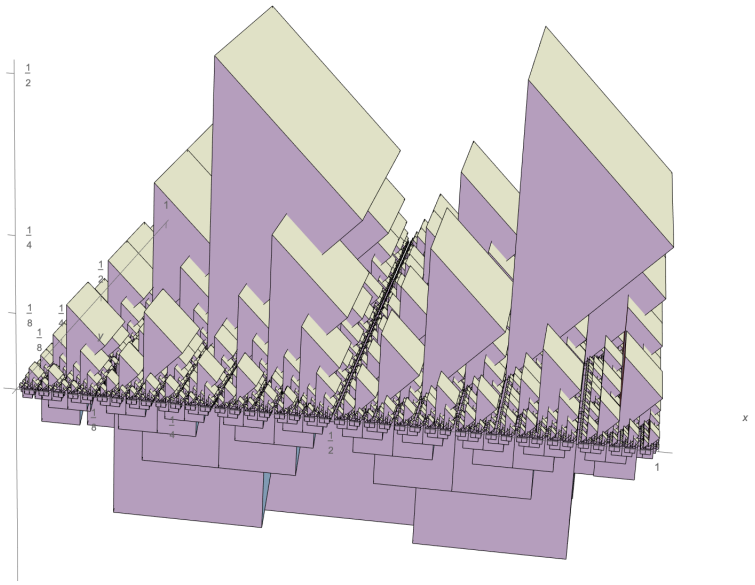

Figure 5.3.4: A 3D model of the Hilbert Curve RFD with the prisms unscaled, viewed from above.

as long as the prisms in the RFD are not so tall that they overlap in $\mathbb{R}^3$, translation of the prisms would not be necessary. However, as mentioned in Remark 5.1.3, the model of the Hilbert curve RFD depicted in Figures 5.1.2 and 5.1.3 has the prisms scaled down by a factor of $\frac{1}{2}$ to illustrate the relationship between the prisms and the approximations to the Hilbert curve itself. Figures 5.3.4 and 5.3.5 depict the actual size of the prisms in the Hilbert RFD as described in Remark 5.1.1, and illustrate that these prisms, too, must be translated to accommodate all of them.

One might wonder if the scaled down version of the Hilbert curve RFD would still be valid since it is convenient and more intriguing to have a construction that does not require the prisms to be moved around. While it is still an admissible RFD, it is not quite appropriate. In particular, the Minkowski content of $H = I^2$ relative to the scaled-down RFD Ω is $\frac{1}{2}$, not 1 as we would expect since our fractal of interest has the unit square as its image. This is not to say that the scaled RFD, by any scalar, is not a worthy object of study, but as we will see now, there is another Hilbert curve RFD that is perhaps more appropriate for that particular curve.

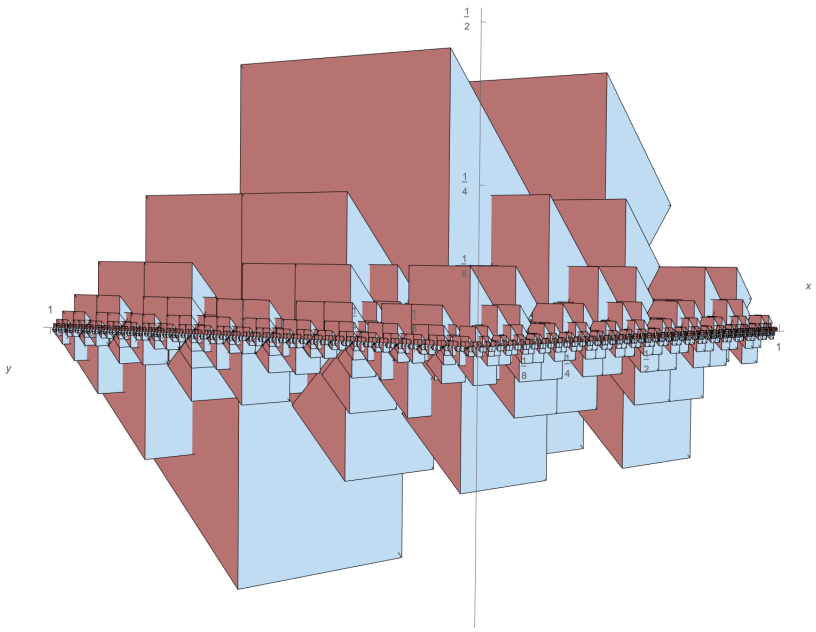

Figure 5.3.5: A 3D model of the Hilbert Curve RFD with the prisms unscaled, viewed from the side.

Remark 5.3.1. The Hilbert curve is unique in that the fundamental cell for the Hilbert curve RFD has symmetry that we can exploit; symmetry that is not enjoyed by the fundamental cells for RFDs associated with curves induced by $\lambda > 2$ tessellations. More specifically, by scaling the original fundamental cell for the Hilbert curve RFD down by a factor of $\frac{1}{2}$, the number of prisms needed in each generation doubles as well because the length of the contacting edge is reduced by $\frac{1}{2}$. But in doing so, the area covered by any prism is also cut in half, and so the area covered by any generation of prisms is cut in half. This means there is room for (at least) another duplicate set of prisms in any generation, and since the original fundamental cell for the Hilbert curve RFD is exactly half of a rectangular prism, we can instead choose our fundamental cell to be a rectangular prism. The rectangular prism is exactly double our original fundamental cell, Ω_0, and it contacts one-half of a generational unit segment. The resulting zeta function will be slightly different as we will see, but it will yield the same complex dimensions and relative Minkowski content. Moreover, *the rectangular prisms will not need to be rotated or translated to accommodate them.* Figures

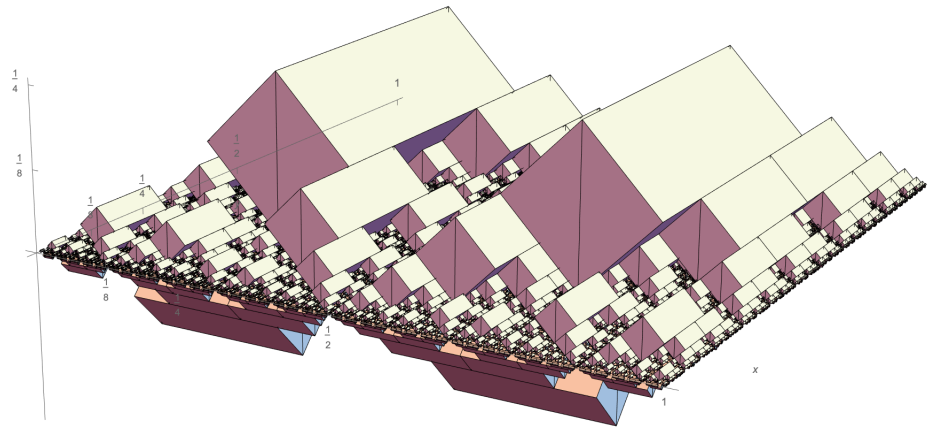

Figure 5.3.6: A 3D model of a Hilbert Curve RFD using rectangular prisms instead of triangular prisms, viewed from above.

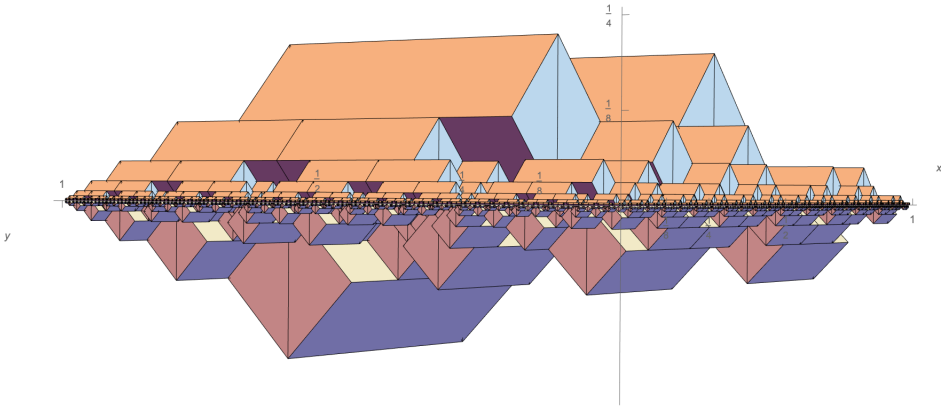

Figure 5.3.7: A 3D model of a Hilbert Curve RFD using rectangular prisms instead of triangular prisms, viewed from the side.

5.3.6 and 5.3.7 show a 3D model of the RFD itself, and more images can be found in Appendix A, Section A.3. In this case, this model is unaltered, and even though the closed faces of the prisms may intersect, recall that the construction uses *open* subdrums, so all of these prisms are in fact disjoint from one another. We proceed to detail the calculation of the relative distance zeta function for this RFD, denoted (H, Θ).

First we compute the relative distance zeta function for the fundamental cell Θ_0 which is pictured in Figure 5.3.8.

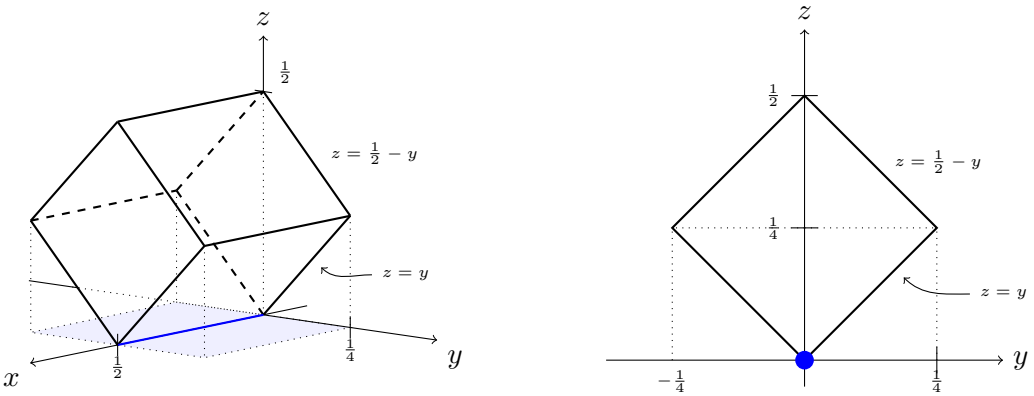

Figure 5.3.8: Isometric and side views of a different fundamental cell, Θ_0, for the Hilbert Curve.

$$
\begin{aligned}
\zeta_{H,\Theta_0}(s) &= \int_{\Theta_0} d(\mathbf{x}, H)^{s-3}\, \mathrm{d}\mathbf{x} = \int_0^{\frac{1}{2}} \int_0^{\frac{1}{4}} \int_{|y|}^{\frac{1}{2}-|y|} z^{s-3}\, \mathrm{d}z\, \mathrm{d}y\, \mathrm{d}x \\
&= 2\int_0^{\frac{1}{2}} \int_0^{\frac{1}{4}} \int_y^{\frac{1}{2}-y} z^{s-3}\, \mathrm{d}z\, \mathrm{d}y\, \mathrm{d}x \\
&= \frac{1}{s-2}\int_0^{\frac{1}{4}} \left(\frac{1}{2}-y\right)^{s-2} - y^{s-2}\, \mathrm{d}y \\
&= \frac{1}{(s-2)(s-1)}\left[-\left(\frac{1}{2}-y\right)^{s-1} - y^{s-1}\right]_0^{\frac{1}{4}} \\
&= \frac{1}{(s-2)(s-1)}\left[-\left(\frac{1}{4}\right)^{s-1} - \left(\frac{1}{4}\right)^{s-1} + \left(\frac{1}{2}\right)^{s-1}\right] \\
&= \frac{1}{(s-2)(s-1)}\left[-2\left(\frac{1}{4}\right)^{s-1} + \left(\frac{1}{2}\right)^{s-1}\right] \\
&= \frac{2^{1-s}}{(s-2)(s-1)}[-2\cdot 2^{1-s}+1] \\
&= \frac{2^{1-s}(1-2^{2-s})}{(s-2)(s-1)}.
\end{aligned}
\tag{5.3.5}
$$

Notice the additional factor of 2^{1-s} in the numerator that is not present in Equation 5.1.3, the relative distance zeta function for (H, Ω_0). In each generation n, there are now $2\cdot(4^n-1)$ of these rectangular prisms; two to cover each generational unit segment. Just

like before, each subdrum Θ_i^n is a scaled copy of Θ_0, so we can apply Theorems 3.3.2 and 3.3.3, yielding

$$\begin{aligned}
\zeta_{H,\Theta}(s) &= \sum_{n=1}^{\infty}\sum_{i=1}^{2\cdot 4^n-1}\zeta_{H,\Theta_i^n}(s) = \sum_{n=1}^{\infty}\sum_{i=1}^{2\cdot 4^n-1}(2^{-n})^s\zeta_{H,\Theta_0}(s)\\
&= \sum_{n=1}^{\infty}\sum_{i=1}^{2\cdot 4^n-1}(2^{-n})^s\frac{2^{1-s}(1-2^{2-s})}{(s-2)(s-1)} = \frac{2^{2-s}(1-2^{2-s})}{(s-2)(s-1)}\sum_{n=1}^{\infty}2^{-sn}(4^n-1)\\
&= \frac{2^{2-s}(1-2^{2-s})}{(s-2)(s-1)}\sum_{n=1}^{\infty}\left[(2^{2-s})^n-(2^{-s})^n\right] = \frac{2^{2-s}(1-2^{2-s})}{(s-2)(s-1)}\left[\frac{2^{2-s}}{1-2^{2-s}}-\frac{2^{-s}}{1-2^{-s}}\right]\\
&= \frac{2^{2-s}\cancel{(1-2^{2-s})}}{(s-2)(s-1)}\left[\frac{2^{2-s}-\cancel{2^{-s}2^{2-s}}-2^{-s}+\cancel{2^{-s}2^{2-s}}}{\cancel{(1-2^{2-s})}(1-2^{-s})}\right] = \frac{2^{2-s}\cdot 2^{-s}(4-1)}{(s-2)(s-1)(1-2^{-s})}\\
&= \frac{3\cdot 2^{2-s}}{(s-2)(s-1)(2^s-1)}.
\end{aligned} \tag{5.3.6}$$

This function is valid initially for all $s\in\mathbb{C}$ such that Re $s>2$, but it can be extended meromorphically to all of $\mathbb{C}$ via analytic continuation. From Equation 5.3.6 we can read off the singularities of $\zeta_{H,\Theta}(s)$, and we have that the set of relative complex dimensions of the Hilbert curve still must be

$$\mathcal{D}(\zeta_{H,\Theta}) = \left\{0+\frac{2\pi}{\log 2}i\mathbb{Z}\right\}\cup\{1,2\}. \tag{5.3.7}$$

Moreover,

$$\operatorname{res}(\zeta_{H,\Theta}(s),2) = \lim_{s\to 2}\frac{3\cdot 2^{2-s}}{(s-1)(2^s-1)} = \frac{3\cdot 2^{2-2}}{(1)(3)} = 1, \tag{5.3.8}$$

so by Theorem 3.3.4 again, we have the desired result

$$\mathcal{M}^2(\Lambda,\Theta) = \frac{\operatorname{res}(\zeta_{\Lambda,\Theta}(s),2)}{3-2} = 1. \tag{5.3.9}$$

Remark 5.3.2. This provides a negative answer to Question 2 since there is, indeed, at least one other RFD that is appropriate for detecting the complex dimensions of the Hilbert curve, but its construction is dependent on a symmetry that cannot be exploited for $\lambda>3$,

so the present author believes this is a special case exclusive to curves in $\mathcal{S}_2(2)$. However, this construction may have some intriguing applications since the Hilbert curve is a plane-filling curve and these associated prisms follow the traverse of the approximations in a disjoint way through $\mathbb{R}^3$. Additionally, the volume of the tubular neighborhood relative to this RFD (and the others depicted above) has lower order oscillations as we will see in the next chapter.

Remark 5.3.3. Speaking more generally, it is still an open problem whether or not other such constructions exist for $\lambda > 3$, but questions of uniqueness are typically more difficult to answer than questions of existence. However, the present author has explored many variations of fundamental cells in the course of their research and, while some other fundamental cells were discovered which produce the necessary factor of $1 - \lambda^{2-s}$ (or simply $1 - 2^{2-s}$ in the case of the Hilbert curve) seen in Equation 5.2.10, they yielded other intractable characteristics; some failed to admit a valid geometric realization because there was not enough room to accommodate all of the prisms necessary for the construction, and some could not be generalized to large λ without the volume of the RFD going to infinity.

With this collection of new results in hand, we turn now to an exploration of the oscillatory behavior of space-filling curves in the next chapter.

Chapter 6

Languidity, and the Oscillatory Behavior of Space-Filling Curves

In this chapter we will explore and detail the oscillatory behavior of space-filling curves, but first we need to define the notion of a *languid* relative fractal drum. Languidity is a condition necessary for us to utilize a powerful theorem from [LRŽ17] that allows us to recover pointwise explicit formulas for the volume of the tubular neighborhood of an RFD as well as antiderivatives of these formulas. For convenience, we repeat Definitions 3.2.2, 2.3.3, and 3.3.7 below.

Definition 3.2.2. Given a set $A \subseteq \mathbb{R}^N$ and $t > 0$, define the *tubular neighborhood of* A as

$$A_t \coloneqq \{x \in \mathbb{R}^N \mid d(x, \partial A) < t\}. \tag{3.2.2}$$

Definition 2.3.3. We define the *screen* $\boldsymbol{S}$ to be the contour $\boldsymbol{S} \coloneqq \{s \in \mathbb{C} : s = S(t) + it, t \in \mathbb{R}\}$ where $S : \mathbb{R} \to [-\infty, D_{\mathcal{L}}]$ is a Lipschitz continuous function. We define the *window* W to be the part of the complex plane that is to the right of the screen, i.e. $W \coloneqq \{s \in \mathbb{C} : \operatorname{Re} s \geq S(\operatorname{Im} s)\}$. Note that W is a closed subset of $\mathbb{C}$ and $\boldsymbol{S} = \partial W$, the boundary of W. (See Figure 2.3.1.)

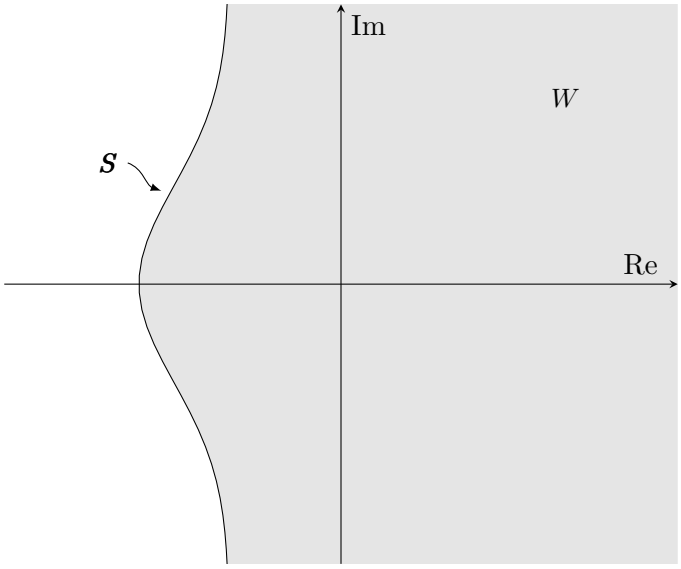

Figure 2.3.1: The *screen* $\boldsymbol{S}$ and the *window* W. (Repeated from page 17.)

Definition 3.3.7. A relative fractal drum (A, Ω) is said to be *admissible* if its relative distance zeta function $\zeta_{A,\Omega}$ can be meromorphically extended to an open connected neighborhood of some window W, and that $\zeta_{A,\Omega}$ does not have any singularity on the screen $\boldsymbol{S}$.

6.1 Languidity of Relative Fractal Drums Associated with Space-Filling Curves

We begin with the definitions of *d-languidity* and *strong d-languidity*. See [LRŽ17] Section 5.3.2 for more details about these definitions and more results related to them.

Definition 6.1.1. An admissible relative fractal drum (A, Ω) in $\mathbb{R}^N$ is said to be *d-languid* if for some fixed $\delta > 0$, its relative distance zeta function $\zeta_{A,\Omega}(\,\cdot\,; \delta)$ satisfies the following growth conditions:

There exists a real constant $\kappa_d \in \mathbb{R}$, the *d-languidity exponent*, and a two-sided sequence $(T_n)_{n\in\mathbb{Z}}$ of real numbers such that $T_{-n} < 0 < T_n$ for $n \geq 1$, and

$$\lim_{n\to\infty} T_n = +\infty \qquad \text{and} \qquad \lim_{n\to\infty} T_{-n} = -\infty \tag{6.1.1}$$

satisfying the following two hypotheses **L1** and **L2**:

L1: For a real fixed constant $c > N > \overline{\dim}_B(A,\Omega)$, there exists a positive constant $C > 0$ such that for all $n \in \mathbb{Z}$ and all σ in the open interval $(S(T_n), c)$,

$$|\zeta_{A,\Omega}(\sigma + iT_n; \delta)| \leq C(|T_n| + 1)^{\kappa_d}. \tag{6.1.2}$$

L2: For all $t \in \mathbb{R}$, $|t| \geq 1$,

$$|\zeta_{A,\Omega}(S(t) + it; \delta)| \leq C|t|^{\kappa_d}, \tag{6.1.3}$$

where C is a positive constant which (without loss of generality) can be chosen to be the same one as in condition **L1**.

Definition 6.1.2. In addition, an admissible relative fractal drum (A,Ω) in $\mathbb{R}^N$ is said to be *strongly d-languid* if for some fixed $\delta > 0$, its relative distance zeta function $\zeta_{A,\Omega}(\cdot;\delta)$ satisfies condition **L1** with $S(T_n) \equiv -\infty$, i.e. for every $\sigma < c$, and additionally there exists a sequence of screens $\mathbf{S}_m : t \mapsto S_m(t) + it$ for $m \geq 1$, $t \in \mathbb{R}$ with $\sup S_m \to -\infty$ as $m \to \infty$ and with a uniform Lipschitz bound $\sup_{m\geq 1} \|S_m\|_{\text{Lip}} < \infty$ such that the following condition holds:

L2': There exist constants $B, C > 0$ such that for all $t \in \mathbb{R}$ and $m \geq 1$,

$$|\zeta_{A,\Omega}(S_m(t) + it; \delta)| \leq CB^{|S_m(t)|}(|t| + 1)^{\kappa_d}. \tag{6.1.4}$$

Remark 6.1.1. The "*d*" in the definitions of *d-languidity* and strong *d-languidity* denotes that the zeta function being used is the relative distance zeta function. This is because the condition of *languidity* developed in [LRŽ17] and [LvF13] uses the *tube zeta function*, but we

do not use that zeta function in the analysis presented in this dissertation. The interested reader can find a detailed and analogous discussion of languidity based on the tube zeta function in Section 5.1.1 of [LRŽ17].

Remark 6.1.2. Hypothesis **L1** is a polynomial growth condition along horizontal line segments in the complex plane, while hypotheses **L2** and **L2'** are polynomial growth conditions along the vertical direction of the screen(s). These hypotheses are necessary prerequisites for determining the pointwise and distributional fractal tubular volume formulas with and without error term. More specifically, if (A, Ω) is a strongly d-languid RFD, then there is an exact, generalized pointwise formula (in terms of t) for $V_{\Lambda,\Omega}(t) = |A_t \cap \Omega|_N$, and the primitives (antiderivatives) $V^{[k]}_{\Lambda,\Omega}(t)$ of that formula for $k > \kappa_d - 1$.

Proposition 6.1.1. Let (Λ, Ω) be a relative fractal drum associated with a plane-filling curve in $\mathfrak{R}_2$ and constructed as described in Remark 5.1.1 and generalized in Section 5.2. Then (Λ, Ω) is strongly d-languid.

Proof. Let $\lambda \geq 2$ and let $\Lambda \in \mathcal{S}_2(\lambda)$. By Theorem 5.2.1, the relative distance zeta function for (Λ, Ω) is

$$\zeta_{\Lambda,\Omega}(s) = \frac{\lambda^2 - 1}{(s-2)(s-1)(\lambda^s - 1)}. \tag{6.1.5}$$

For any $s \in \mathbb{C}$ that is not a singularity of $\zeta_{\Lambda,\Omega}$, we have

$$\left|\zeta_{\Lambda,\Omega}(s)\right| = \left|\frac{\lambda^2 - 1}{(s-2)(s-1)(\lambda^s - 1)}\right| \leq \frac{\lambda^2}{|s-2||s-1||\lambda^s - 1|}. \tag{6.1.6}$$

We will verify condition **L1** first. Choose our sequence $(T_n)_{n\in\mathbb{Z}}$ to be given by

$$T_n = \frac{(2n+1)\pi}{\log \lambda}. \tag{6.1.7}$$

It follows immediately that $T_{-n} < 0 < T_n$ for $n \geq 1$, and that

$$\lim_{n\to\infty} T_n = \lim_{n\to\infty} \frac{(2n+1)\pi}{\log \lambda} = +\infty \qquad \text{and} \qquad \lim_{n\to\infty} T_{-n} = \lim_{n\to\infty} \frac{(-2n+1)\pi}{\log \lambda} = -\infty. \tag{6.1.8}$$

Moreover, this choice of T_n avoids any singularities of $\zeta_{\Lambda,\Omega}$ since $T_n \neq n\mathbf{p} = n\frac{2\pi}{\log\lambda}$ for any n.

Fix a number $c \in \mathbb{R}$ such that $c > 3 > \overline{\dim}_B(\Lambda, \Omega) = 2$. For any $\sigma < c$, by application of the triangle inequality and the definition of a complex exponential, we have

$$\begin{aligned}\left|\zeta_{\Lambda,\Omega}(\sigma + iT_n; \delta)\right| &\leq \frac{\lambda^2}{|\sigma - 2 + iT_n||\sigma - 1 + iT_n||\lambda^\sigma \lambda^{iT_n} - 1|} \\ &\leq \frac{\lambda^2}{|T_n||T_n|\left|e^{(\log\lambda)\sigma}e^{i(\log\lambda)T_n} - 1\right|}.\end{aligned} \tag{6.1.9}$$

By our choice of sequence (T_n), $e^{i(\log\lambda)T_n} = e^{i(2n+1)\pi} = -1$ for all $n \in \mathbb{Z}$. Consequently,

$$\left|e^{(\log\lambda)\sigma}e^{i(\log\lambda)T_n} - 1\right| = \left|e^{(\log\lambda)\sigma} + 1\right| \geq 1 \tag{6.1.10}$$

for all $\sigma < c$. Thus, Inequality 6.1.9 becomes

$$\left|\zeta_{\Lambda,\Omega}(\sigma + iT_n; \delta)\right| \leq \frac{\lambda^2}{|T_n|^2}. \tag{6.1.11}$$

Now, for any $x \in \mathbb{R}$ and any $\lambda > 1$, if $|x| \geq 1$, then $\lambda|x| \geq |x| + 1$. Consequently, $\frac{1}{|x|^2} \leq \frac{\lambda^2}{(|x|+1)^2}$. Since $\min_{n\in\mathbb{Z}}\{|T_n|\} = |T_0| = \frac{\pi}{\log\lambda} > 1$, it follows that

$$\left|\zeta_{\Lambda,\Omega}(\sigma + iT_n; \delta)\right| \leq \frac{\lambda^2}{|T_n|^2} \leq \frac{\lambda^5}{(|T_n| + 1)^2} = \lambda^5(|T_n| + 1)^{-2}. \tag{6.1.12}$$

Choosing $C = \lambda^5$ and $\kappa_d = -2$, we see that we have verified condition **L1**.

Next, to show condition **L2'**, let our sequence of screens be given by

$$\mathbf{S}_m = \{S_m(t) + it : m \in \mathbb{N},\, t \in \mathbb{R}\} = \{-m + it : m \in \mathbb{N},\, t \in \mathbb{R}\}. \tag{6.1.13}$$

Then clearly $\sup S_m \to -\infty$ as $m \to \infty$ and $\sup_{m\geq 1} \|S_m\|_{\text{Lip}} = 1 < \infty$. For any $m \in \mathbb{N}$, the triangle inequality yields

$$
\begin{aligned}
|\zeta_{\Lambda,\Omega}(S_m(t)+it;\delta)| &= \left|\frac{\lambda^2-1}{(s-2)(s-1)(\lambda^s-1)}\right|_{s\in\mathbf{S}_m} \\
&\leq \frac{\lambda^2}{|-m-2+it||-m-1+it||\lambda^{-m}\lambda^{it}-1|} \\
&\leq \frac{\lambda^2}{|m||m||\lambda^{-m}-1|}.
\end{aligned} \tag{6.1.14}
$$

Since $m \geq 1$, $\lambda^{-m} < \lambda^{-1} < 1$. Thus $|\lambda^{-m}-1| > \lambda^{-1}$, whence $\dfrac{1}{|\lambda^{-m}-1|} \leq \lambda$, so

$$
|\zeta_{\Lambda,\Omega}(S_m(t)+it;\delta)| \leq \frac{\lambda^3}{|m|^2} \leq \frac{\lambda^5}{(|m|+1)^2} = \lambda^5(|m|+1)^{-2} \leq \lambda^5(|t|+1)^{-2}. \tag{6.1.15}
$$

Choosing $B = 1$, we have $B^{|S_m(t)|} = 1$ for all $m \geq 1$, and so Inequality 6.1.14 yields

$$
\left|\zeta_{\Lambda,\Omega}(S_m(t)+it;\delta)\right| \leq \lambda^5(|t|+1)^{-2}. \tag{6.1.16}
$$

This verifies condition **L2'** and, therefore, (Λ,Ω) is strongly d-languid. □

6.2 Oscillatory Behavior of Space-Filling Curves

In this section we will elucidate the oscillatory behavior associated with plane-filling curves in $\mathfrak{R}_2$. This oscillatory behavior is also expected for curves in $\mathfrak{R}_N$, and a conjecture about this phenomenon is detailed in Chapter 7. In the first section we show that there are *subcritical oscillations* in the volume of the tubular neighborhood of (Λ,Ω), i.e. oscillations in the lower order terms of the tubular volume formula. We compute this formula directly for the generalized RFD constructed in Chapter 5, and then, using the result of strong d-languidity established in Proposition 6.1.1, recover the volume formula from the general theory of fractal tube formulas detailed in Chapter 5 of [LRŽ17].

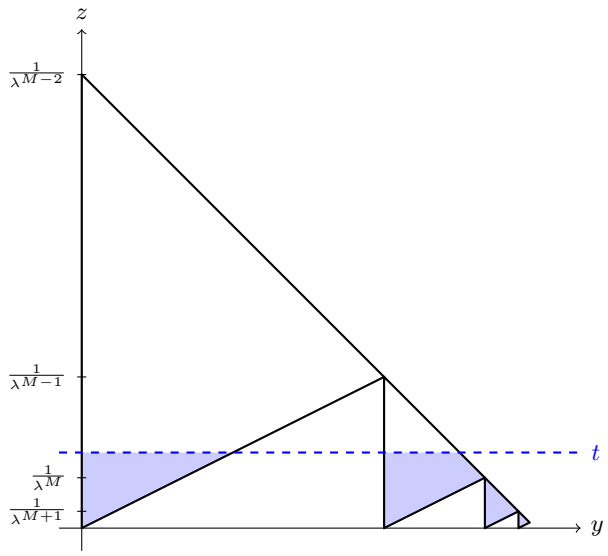

Figure 6.2.1: Side view of the RFD submerged to the "water line" $z = t$.

Oscillations in the Volume of the Tubular Neighborhood

Let $\lambda \geq 2$ and let $\Lambda \in \mathcal{S}_2(\lambda) \subset \mathfrak{R}_2$. Let (Λ, Ω) be the associated relative fractal drum. Define $V_{\Lambda,\Omega}(t) \coloneqq |\Lambda_t \cap \Omega|_3$, i.e. the pointwise volume of the tubular neighborhood of $\Lambda = I^2$ relative to Ω. Since the drum lies entirely above and below the unit square, for $t > 0$, we have

$$\Lambda_t \cap \Omega = [0,1]^2 \times (-t, t) \cap \Omega. \tag{6.2.1}$$

By counting prisms (subdrums) according to multiplicity in each generation n, we can write

$$\Lambda_t \cap \Omega = [0,1]^2 \times [0, t) \cap \Omega. \tag{6.2.2}$$

More intuitively, this allows us to view $\Lambda_t \cap \Omega$ as being the part of the RFD that is submerged up to some "water line" $z = t$. Figure 6.2.1 illustrates this idea.

For any $t > 0$, there exists an $M \in \mathbb{N}$ such that

$$\frac{1}{\lambda^M} \leq t < \frac{1}{\lambda^{M-1}}, \tag{6.2.3}$$

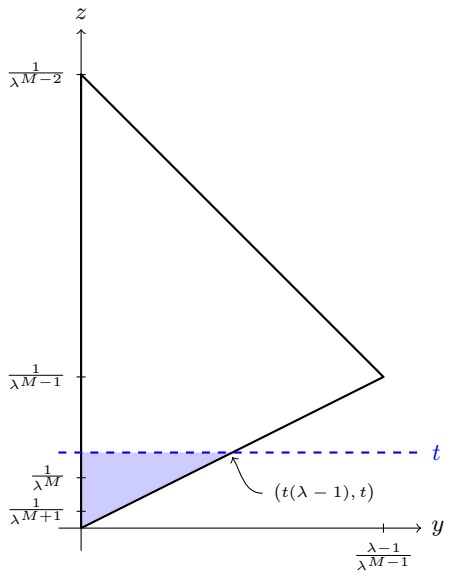

Figure 6.2.2: A prism in Ω_1 submerged up to the line $z = t$.

in particular,

$$M = \left\lceil \log_\lambda \left(\frac{1}{t} \right) \right\rceil \tag{6.2.4}$$

where $\lceil \cdot \rceil$ indicates the ceiling function (see Definition 2.1.3 in Chapter 2). The choice of t partitions Ω into three disjoint collections of prisms, Ω_1, Ω_2, and Ω_3, so that $\Omega = \Omega_1 \cup \Omega_2 \cup \Omega_3$ where

$$\Omega_1 = \bigcup_{n=1}^{M-2} \bigcup_{i=1}^{\lambda^{2n}-1} \Omega_i^n, \tag{6.2.5}$$

$$\Omega_2 = \bigcup_{i=1}^{\lambda^{2(M-1)}-1} \Omega_i^{M-1}, \text{ and} \tag{6.2.6}$$

$$\Omega_3 = \bigcup_{n=M}^{\infty} \bigcup_{i=1}^{\lambda^{2n}-1} \Omega_i^n \tag{6.2.7}$$

This allows us to compute the total volume of the tubular neighborhood in three parts, by computing the volume of submerged portion of each collection separately and adding the results.

First we compute $|\Lambda_t \cap \Omega_1|_3$. See Figure 6.2.2 for a visual reference. The cross-section of the submerged section of any prism in Ω_1 is a triangle that has area

$$A = \frac{1}{2} t \cdot t(\lambda - 1) = \frac{t^2(\lambda - 1)}{2}. \tag{6.2.8}$$

The base of any (3-dimensional) prism has length $\frac{1}{\lambda^n}$, thus the volume of the submerged portion is

$$V_n = \frac{t^2(\lambda - 1)}{2\lambda^n}. \tag{6.2.9}$$

There are $\lambda^{2n} - 1$ prisms Ω_i^n in any nth generation contained in Ω_1, so we have the following.

$$\begin{aligned} |\Lambda_t \cap \Omega_1|_3 &= \sum_{n=1}^{M-2} (\lambda^{2n} - 1) \cdot V_n = \sum_{n=1}^{M-2} (\lambda^{2n} - 1) \frac{t^2(\lambda - 1)}{2\lambda^n} \\ &= \frac{t^2(\lambda - 1)}{2} \sum_{n=1}^{M-2} \left(\lambda^n - \frac{1}{\lambda^n} \right) \\ &= \frac{t^2 \cancel{(\lambda - 1)}}{2} \left[\frac{\lambda^{M-1} + \lambda^{2-M} - \lambda - 1}{\cancel{\lambda - 1}} \right] \\ &= \frac{t^2}{2} \left[\lambda^{M-1} + \lambda^{2-M} - \lambda - 1 \right]. \end{aligned} \tag{6.2.10}$$

Next we compute $|\Lambda_t \cap \Omega_2|_3$. See Figure 6.2.3 for reference. The cross-section of these prisms is a quadrilateral Q which can be decomposed into a right triangle T and a trapezoid Z:

$$Q = T \cup Z \tag{6.2.11}$$

We have

$$|T|_2 = \frac{1}{2} \cdot \frac{1}{\lambda^M} \cdot \frac{\lambda - 1}{\lambda^M} = \frac{\lambda - 1}{2\lambda^{2M}}, \tag{6.2.12}$$

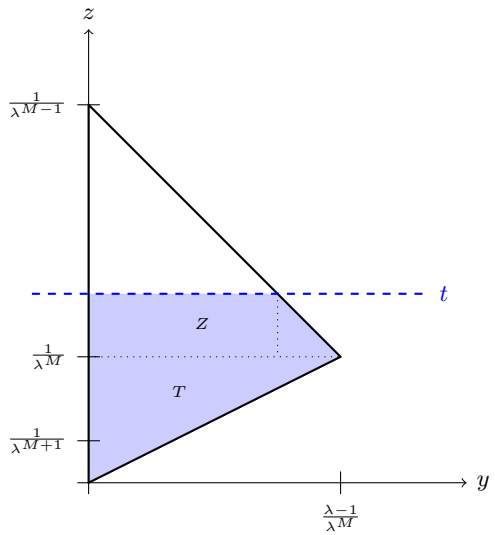

Figure 6.2.3: A prism in Ω_2 submerged up to the line $z = t$.

and

$$\begin{aligned}
|Z|_2 &= \frac{1}{2}h(b_1 + b_2) \\
&= \frac{1}{2}\left(t - \frac{1}{\lambda^M}\right)\left[\frac{\lambda-1}{\lambda^M} + \frac{\lambda-1}{\lambda^M} - \left(t - \frac{1}{\lambda^M}\right)\right] \\
&= \frac{1}{2}\left(t - \frac{1}{\lambda^M}\right)\left(\frac{2\lambda-1}{\lambda^M} - t\right) \\
&= \frac{1}{2\lambda^M}\left((2\lambda-1)t - \lambda^M t^2 - \frac{2\lambda-1}{\lambda^M} + t\right).
\end{aligned} \tag{6.2.13}$$

Adding these results together, we have

$$\begin{aligned}
|Q|_2 &= |T|_2 + |Z|_2 \\
&= \frac{\lambda-1}{2\lambda^{2M}} + \frac{1}{2\lambda^M}\left((2\lambda-1)t - \lambda^M t^2 - \frac{2\lambda-1}{\lambda^M} + t\right) \\
&= \frac{1}{2\lambda^M}\left(\frac{\lambda-1}{\lambda^M} + (2\lambda-1)t - \lambda^M t^2 - \frac{2\lambda-1}{\lambda^M} + t\right) \\
&= \frac{1}{2\lambda^M}\left(-\frac{1}{\lambda^{M-1}} + 2\lambda t - \lambda^M t^2\right) \\
&= \frac{t}{\lambda^{M-1}} - \frac{1}{2\lambda^{2M-1}} - \frac{t^2}{2}.
\end{aligned} \tag{6.2.14}$$

Therefore,

$$\begin{aligned} |Q|_3 &= \frac{1}{\lambda^{M-1}} \cdot |Q|_2 = \frac{1}{\lambda^{M-1}} \left[\frac{t}{\lambda^{M-1}} - \frac{1}{2\lambda^{2M-1}} - \frac{t^2}{2} \right] \\ &= \frac{t}{\lambda^{2M-2}} - \frac{1}{2\lambda^{3M-2}} - \frac{t^2}{2\lambda^{M-1}}. \end{aligned} \tag{6.2.15}$$

Since there are exactly $\lambda^{2(M-1)} - 1$ prisms in Ω_2, we have

$$\begin{aligned} |\Lambda_t \cap \Omega_2|_3 &= \left(\lambda^{2(M-1)} - 1 \right) \cdot |Q|_3 \\ &= \left(\lambda^{2M-2} - 1 \right) \left(\frac{t}{\lambda^{2M-2}} - \frac{1}{2\lambda^{3M-2}} - \frac{t^2}{2\lambda^{M-1}} \right). \end{aligned} \tag{6.2.16}$$

Lastly, we compute $|\Lambda_t \cap \Omega_3|_3$. The entirety of any prism in Ω_3 is included in $\Lambda_t \cap \Omega$. The volume of any prism in generation n is

$$V_n = \frac{1}{2} \cdot \frac{1}{\lambda^n} \cdot \frac{\lambda - 1}{\lambda^{n+1}} \cdot \frac{1}{\lambda^n} = \frac{\lambda - 1}{2\lambda^{3n+1}}. \tag{6.2.17}$$

There are $\lambda^{2n} - 1$ prisms in any generation n, so we have

$$\begin{aligned} |\Lambda_t \cap \Omega_3|_3 &= \sum_{n=M}^{\infty} (\lambda^{2n} - 1) \cdot V_n = \sum_{n=M}^{\infty} (\lambda^{2n} - 1) \cdot \frac{\lambda - 1}{2\lambda^{3n+1}} \\ &= \frac{\lambda - 1}{2\lambda} \sum_{n=M}^{\infty} \left(\frac{1}{\lambda^n} - \frac{1}{\lambda^{3n}} \right) \\ &= \frac{\cancel{\lambda - 1}}{2\cancel{\lambda}} \left[\frac{\lambda^{-3M} \left(\lambda^{2M+1} + \lambda^{2M+2} + \lambda^{2M} - \lambda^2 \right)}{\cancel{(\lambda - 1)}(\lambda^2 + \lambda + 1)} \right] \\ &= \frac{\lambda^{-3M} \left(\lambda^{2M+1} + \lambda^{2M+2} + \lambda^{2M} - \lambda^2 \right)}{2(\lambda^2 + \lambda + 1)} \end{aligned} \tag{6.2.18}$$

Now that we have all three subvolumes calculated, we combine Equations 6.2.10, 6.2.15, and 6.2.18, yielding

$$
\begin{aligned}
|\Lambda_t \cap \Omega|_3 &= |\Lambda_t \cap (\Omega_1 \cup \Omega_2 \cup \Omega_3)|_3 \\
&= |\Lambda_t \cap \Omega_1|_3 + |\Lambda_t \cap \Omega_2|_3 + |\Lambda_t \cap \Omega_3|_3 \\
&= \frac{t^2}{2}\left[\lambda^{M-1} + \lambda^{2-M} - \lambda - 1\right] \\
&+ \left(\lambda^{2M-2} - 1\right)\left(\frac{t}{\lambda^{2M-2}} - \frac{1}{2\lambda^{3M-2}} - \frac{t^2}{2\lambda^{M-1}}\right) \\
&+ \frac{\lambda^{-3M}\left(\lambda^{2M+1} + \lambda^{2M+2} + \lambda^{2M} - \lambda^2\right)}{2(\lambda^2 + \lambda + 1)}.
\end{aligned}
\tag{6.2.19}
$$

After simplifying, we arrive at the following.

$$
|\Lambda_t \cap \Omega|_3 = \frac{1}{2}\left(\frac{(\lambda^{1-M})^3(1+\lambda)}{1+\lambda+\lambda^2} - 2t(\lambda^{1-M})^2 + (\lambda^{1-M} - 1)(1+\lambda)t^2 + 2t\right). \tag{6.2.20}
$$

Next, observe that

$$
\lambda^M = \lambda^{\lceil -\log_\lambda t \rceil} = \lambda^{-\log_\lambda t + (1 - \{-\log_\lambda t\})} = \lambda^{-\log_\lambda t} \cdot \lambda^{1-\{-\log_\lambda t\}} = \frac{1}{t} \cdot \lambda^{1-\{-\log_\lambda t\}} \tag{6.2.21}
$$

where $\{\cdot\}$ indicates the fractional part of a number (See Definition 2.1.3 in Chapter 2). Thus,

$$
\lambda^{1-M} = t \cdot \lambda^{\{-\log_\lambda t\}} \tag{6.2.22}
$$

Substituting Equation 6.2.22 into Equation 6.2.20 yields that

$$
\begin{aligned}
V_{\Lambda,\Omega}(t) = |\Lambda_t \cap \Omega|_3 &= \frac{1}{2}\left(\frac{(\lambda^{1-M})^3(1+\lambda)}{1+\lambda+\lambda^2} - 2t(\lambda^{1-M})^2 + (\lambda^{1-M} - 1)(1+\lambda)t^2 + 2t\right) \\
&= \frac{1}{2}\left(\frac{t^3 \cdot \lambda^{3\{-\log_\lambda t\}}(1+\lambda)}{1+\lambda+\lambda^2} - 2t^3 \cdot \lambda^{2\{-\log_\lambda t\}} + t^3 \cdot \lambda^{\{-\log_\lambda t\}}(1+\lambda)\right) \\
&\quad - \frac{1}{2}\Big((1+\lambda)t^2 - 2t\Big), \text{ so}
\end{aligned}
$$

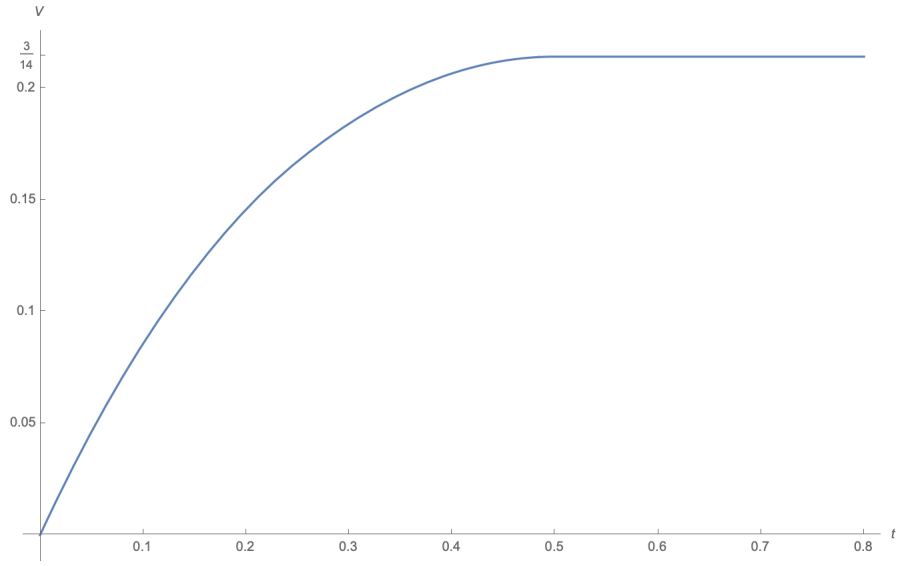

Figure 6.2.4: A plot of $V_{H,\Omega}(t)$, the volume of the tubular neighborhood of (H, Ω).

$$V_{\Lambda,\Omega}(t) = t - \frac{t^2}{2}(1+\lambda) + \frac{t^3}{2}(1+\lambda)\left(\frac{\lambda^{3\{-\log_\lambda t\}}}{1+\lambda+\lambda^2} - \frac{2\lambda^{2\{-\log_\lambda t\}}}{1+\lambda} + \lambda^{\{-\log_\lambda t\}}\right) \tag{6.2.23}$$

Remark 6.2.1. The expression in the large parentheses in Formula 6.2.23 is multiplicatively periodic: it takes the same value at t and $\frac{t}{\lambda}$. This illustrates the oscillatory behavior within the tubular neighborhood. Compare this result with the result of the Cantor string CS given in Section 2.2 and Equation 2.2.5 in Chapter 2. Note that, since the limiting behavior we are interested occurs as $t \to 0$, the oscillations are occurring in the *lower order* terms so we have *subcritical oscillations*; here, t^1 is the highest order term. For clarity, consider again the example of the Hilbert curve RFD. Figure 6.2.4 is a plot of Formula 6.2.23 for $\lambda = 2$. Notice that $V_{H,\Omega}(t)$ steadily increases almost linearly as t increases precisely because the dominating term is of order 1. It also stops increasing once $t = \frac{1}{2}$ because this is the point after which the entire Hilbert curve RFD is contained in the tubular neighborhood, giving total volume $|\Omega|_3 = \frac{3}{14}$ as deduced in Equation 5.1.2 in Chapter 5. Figure 6.2.5 is a plot of

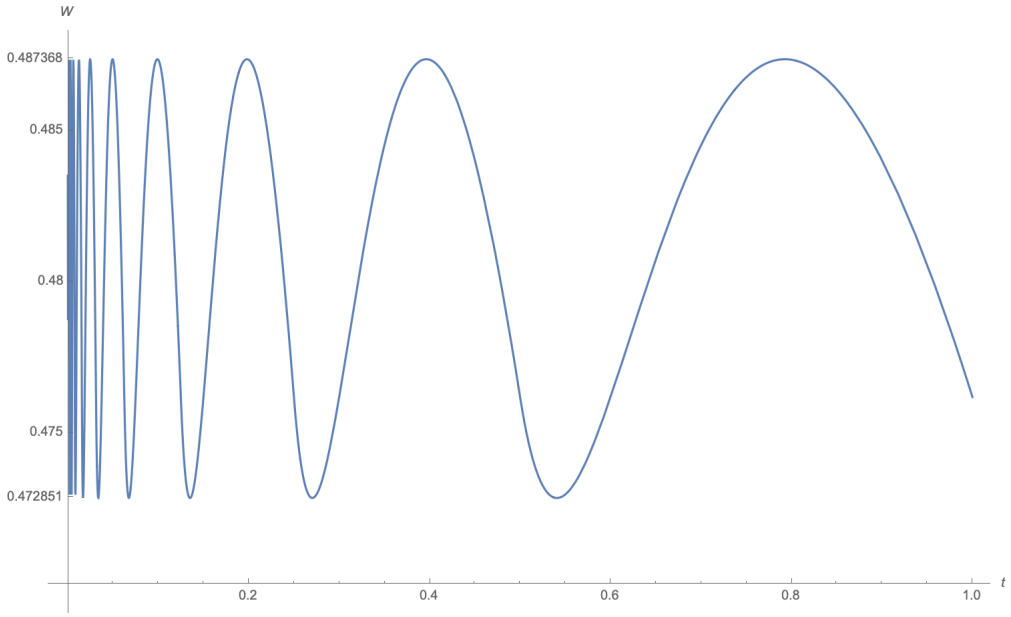

Figure 6.2.5: A Linear-Linear plot of $W_{H,\Omega}(t)$, the oscillatory term in $V_{H,\Omega}(t)$.

the oscillatory term, call it $W_{\Lambda,\Omega}(t)$, found in Formula 6.2.23 for $\lambda = 2$. More specifically,

$$W_{\Lambda,\Omega}(t) = \frac{\lambda^{3\{-\log_\lambda t\}}}{1+\lambda+\lambda^2} - \frac{2\lambda^{2\{-\log_\lambda t\}}}{1+\lambda} + \lambda^{\{-\log_\lambda t\}}, \tag{6.2.24}$$

so for $\lambda = 2$ we have

$$W_{H,\Omega}(t) = \frac{8^{\{-\log_2 t\}}}{7} - \frac{2\cdot 4^{\{-\log_2 t\}}}{3} + 2^{\{-\log_2 t\}} \tag{6.2.25}$$

Figure 6.2.6 is a Log-Linear plot of $W_{H,\Omega}(t)$ that normalizes the period.

As in Section 2.2 we can also express this oscillatory behavior more explicitly using the Fourier series of the map $u \mapsto b^{-\{u\}}$ given in Equation 2.2.6 in Chapter 2, and repeated here for convenience:

$$b^{-\{u\}} = \frac{b-1}{b} \sum_{n\in\mathbb{Z}} \frac{e^{2\pi i n u}}{\log b + 2\pi i n} \tag{2.2.6}$$

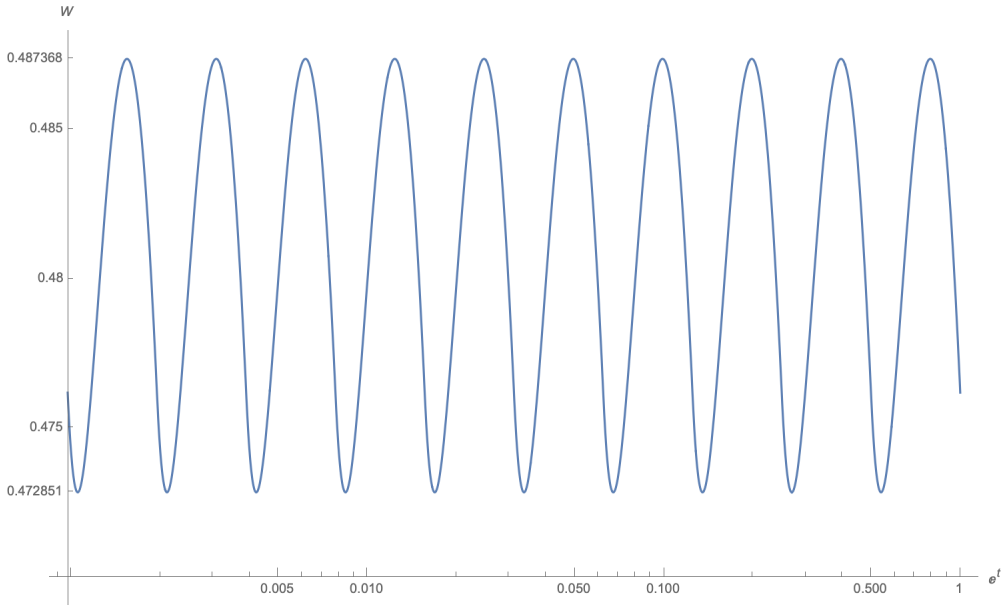

Figure 6.2.6: A Log-Linear plot of $W_{H,\Omega}(t)$, the oscillatory term in $V_{H,\Omega}(t)$.

Using Equation 2.2.6 and writing $\mathbf{p} = \frac{2\pi}{\log \lambda}$, we have

$$\begin{aligned}
\lambda^{\{-\log_\lambda t\}} = (\lambda^{-1})^{-\{-\log_\lambda t\}} &= \frac{\lambda^{-1}-1}{\lambda^{-1}} \sum_{n\in\mathbb{Z}} \frac{e^{2\pi i n(-\log_\lambda t)}}{\log \lambda^{-1} + 2\pi i n} \\
&= (1-\lambda) \sum_{n\in\mathbb{Z}} \frac{e^{-2\pi i n\left(\frac{\log t}{\log \lambda}\right)}}{-\log\lambda + 2\pi i n} = (1-\lambda) \sum_{n\in\mathbb{Z}} \frac{t^{-\frac{2\pi}{\log\lambda} i n}}{-\log\lambda\left(1 - \frac{2\pi}{\log\lambda} i n\right)} \qquad (6.2.26) \\
&= \frac{\lambda-1}{\log\lambda} \sum_{n\in\mathbb{Z}} \frac{t^{-in\mathbf{p}}}{1-in\mathbf{p}}.
\end{aligned}$$

Collecting all of these, we have

$$\lambda^{\{-\log_\lambda t\}} = \frac{\lambda-1}{\log\lambda} \sum_{n\in\mathbb{Z}} \frac{t^{-in\mathbf{p}}}{1-in\mathbf{p}}, \qquad (6.2.27)$$

$$\lambda^{2\{-\log_\lambda t\}} = \frac{\lambda^2-1}{\log\lambda} \sum_{n\in\mathbb{Z}} \frac{t^{-in\mathbf{p}}}{2-in\mathbf{p}}, \text{ and} \qquad (6.2.28)$$

$$\lambda^{3\{-\log_\lambda t\}} = \frac{\lambda^3-1}{\log\lambda} \sum_{n\in\mathbb{Z}} \frac{t^{-in\mathbf{p}}}{3-in\mathbf{p}}. \qquad (6.2.29)$$

We can use Equations 6.2.27, 6.2.28, and 6.2.29 to rewrite $W_{\Lambda,\Omega}(t)$ as

$$\begin{aligned} W_{\Lambda,\Omega}(t) &= \frac{\lambda^{3\{-\log_\lambda t\}}}{1+\lambda+\lambda^2} - \frac{2\lambda^{2\{-\log_\lambda t\}}}{1+\lambda} + \lambda^{\{-\log_\lambda t\}} \\ &= \frac{1}{1+\lambda+\lambda^2}\cdot\frac{\lambda^3-1}{\log\lambda}\sum_{n\in\mathbb{Z}}\frac{t^{-in\mathbf{p}}}{3-in\mathbf{p}} - \frac{2}{1+\lambda}\cdot\frac{\lambda^2-1}{\log\lambda}\sum_{n\in\mathbb{Z}}\frac{t^{-in\mathbf{p}}}{2-in\mathbf{p}} + \frac{\lambda-1}{\log\lambda}\sum_{n\in\mathbb{Z}}\frac{t^{-in\mathbf{p}}}{1-in\mathbf{p}} \\ &= \frac{\lambda-1}{\log\lambda}\left(\sum_{n\in\mathbb{Z}}\frac{t^{-in\mathbf{p}}}{1-in\mathbf{p}} - 2\sum_{n\in\mathbb{Z}}\frac{t^{-in\mathbf{p}}}{2-in\mathbf{p}} + \sum_{n\in\mathbb{Z}}\frac{t^{-in\mathbf{p}}}{3-in\mathbf{p}}\right). \end{aligned} \tag{6.2.30}$$

Thus, the volume of the tubular neighborhood of Λ with respect to Ω is,

$$V_{\Lambda,\Omega}(t) = t - \frac{t^2}{2}(1+\lambda) + \frac{t^3}{2}\cdot\frac{\lambda^2-1}{\log\lambda}\left(\sum_{n\in\mathbb{Z}}\frac{t^{-in\mathbf{p}}}{1-in\mathbf{p}} - 2\sum_{n\in\mathbb{Z}}\frac{t^{-in\mathbf{p}}}{2-in\mathbf{p}} + \sum_{n\in\mathbb{Z}}\frac{t^{-in\mathbf{p}}}{3-in\mathbf{p}}\right) \tag{6.2.31}$$

which we can write in terms of the complex dimensions of Λ:

$$\begin{aligned} V_{\Lambda,\Omega}(t) = t &- \frac{t^2}{2}(1+\lambda) \\ &+ \frac{t^3}{2}\cdot\frac{\lambda^2-1}{\log\lambda}\left(\sum_{\omega\in\mathcal{D}(\zeta_{\Lambda,\Omega},\mathbb{C})\setminus\{1,2\}}\frac{t^{-\omega}}{1-\omega} - 2\sum_{\omega\in\mathcal{D}(\zeta_{\Lambda,\Omega},\mathbb{C})\setminus\{1,2\}}\frac{t^{-\omega}}{2-\omega}\right. \\ &\left. + \sum_{\omega\in\mathcal{D}(\zeta_{\Lambda,\Omega},\mathbb{C})\setminus\{1,2\}}\frac{t^{-\omega}}{3-\omega}\right) \end{aligned} \tag{6.2.32}$$

This formula also allows us to establish the following important proposition about the Minkowski measurability of these relative fractal drums, one which again asserts that this class of RFDs is the correct one with which to study the complex dimensions of space-filling curves.

Proposition 6.2.1. The RFD (Λ,Ω) is Minkowski measurable (see Definition 3.3.6) for any $\lambda \geq 2$, the relative Minkowski dimension (see Definition 3.3.4) of $\Lambda = I^2$ with respect to Ω is $D = 2$, and the 2-dimensional relative Minkowski content is 1.

Proof. By Formula 6.2.31, we have

$$\frac{|\Lambda_t \cap \Omega|_3}{t^{3-2}} = 1 - \frac{t}{2}(1+\lambda) + \frac{t^2}{2} \cdot \frac{\lambda^2 - 1}{\log \lambda} \left(\sum_{n \in \mathbb{Z}} \frac{t^{-in\mathbf{p}}}{1 - in\mathbf{p}} - 2 \sum_{n \in \mathbb{Z}} \frac{t^{-in\mathbf{p}}}{2 - in\mathbf{p}} + \sum_{n \in \mathbb{Z}} \frac{t^{-in\mathbf{p}}}{3 - in\mathbf{p}} \right). \tag{6.2.33}$$

Taking the limit as $t \to 0^+$, the last two terms go to 0, and all that remains is the constant term, 1. Thus, by Definition 3.3.3,

$$\mathcal{M}^{*2}(\Lambda, \Omega) = \mathcal{M}^2_*(\Lambda, \Omega) = \mathcal{M}^2(\Lambda, \Omega) = \lim_{t \to 0^+} \frac{|\Lambda_t \cap \Omega|_3}{t^{3-2}} = 1. \tag{6.2.34}$$

Therefore, (Λ, Ω) is Minkowski measurable, the relative Minkowski dimension is $D = 2$, and the relative 2-dimensional Minkowski content of (Λ, Ω) is 1 as expected for the unit square. □

Next, we use the result of Proposition 6.1.1, i.e. that the relative fractal drum (Λ, Ω) is strongly d-languid for any $\Lambda \in \mathfrak{R}_2$, and recover the tubular volume formula, Formula 6.2.31, from a more general formula.

Definition 6.2.1. For consistency with [LRŽ17], given $s \in \mathbb{C}$ and a nonnegative integer k, the *rising factorial* (or *Pocchammer function*) is defined as

$$(s)_0 \coloneqq 1, \qquad \text{and} \qquad (s)_k \coloneqq s(s+1)(s+2)\cdots(s+k-1). \tag{6.2.35}$$

More generally, we have

$$(s)_k \coloneqq \frac{\Gamma(s+k)}{\Gamma(s)} \tag{6.2.36}$$

where Γ is the standard gamma function that extends the factorial function $n!$ for nonnegative integers n.

Theorem 6.2.1 ([LRŽ17] Theorem 5.3.13; Exact pointwise fractal tube formula via $\zeta_{A,\Omega}$)**.** Let (A, Ω) be a relative fractal drum in $\mathbb{R}^N$ which is strongly d-languid for some $\delta > 0$ and with d-languidity exponent $\kappa_d \in \mathbb{R}$. Furthermore, let $k > \kappa_d - 1$ be a nonnegative integer

and assume that $\overline{\dim}_B(A,\Omega) < N$. Then the following exact pointwise fractal tube formula, expressed in terms of the relative distance zeta function $\zeta_{A,\Omega} \coloneqq \zeta_{A,\Omega}(\cdot;\delta)$, holds for every $t \in (0, \min\{1, \delta, B^{-1}\})$:

$$V_{A,\Omega}^{[k]}(t) = \sum_{\omega \in \mathcal{D}(\zeta_{A,\Omega},\mathbb{C})} \operatorname{res}\left(\frac{t^{N-s+k}}{(N-s)_{k+1}}\zeta_{A,\Omega}(s), \omega\right) \tag{6.2.37}$$

Here, B is the constant appearing in **L2'**, κ_d is the d-languidity exponent occurring in the statement of hypotheses **L1** and **L2**, and $V_{A,\Omega}^{[k]}(t)$ is the kth primitive (antiderivative) of $V_{A,\Omega}(t)$.

Proposition 6.1.1 yields that our RFDs are strongly d-languid with languidity exponent $\kappa_d = -2$. Recall from the proof of Proposition 6.1.1 that $B = 1$ (see Equation 6.1.16). To recover our volume formula, we choose $\delta \geq \frac{1}{2}$ and $k = 0 > \kappa_d - 1 = -3$ so that $V_{\Lambda,\Omega}^{[k]}(t) = V_{\Lambda,\Omega}^{[0]}(t) = V_{\Lambda,\Omega}(t)$. Then Formula 6.2.37 yields

$$V_{\Lambda,\Omega}(t) = \sum_{\omega \in \mathcal{D}(\zeta_{\Lambda,\Omega},\mathbb{C})} \operatorname{res}\left(\frac{t^{3-s}}{3-s}\zeta_{\Lambda,\Omega}(s), \omega\right). \tag{6.2.38}$$

Recall from Theorem 5.2.1 that the set of complex dimensions of any curve $\Lambda \in \mathfrak{R}_2$ is

$$\mathcal{D}(\zeta_{\Lambda,\Omega}) = \left\{0 + \frac{2\pi}{\log\lambda} i\mathbb{Z}\right\} \cup \{1, 2\}. \tag{6.2.39}$$

When $\omega = 2$, we have

$$\begin{aligned} \operatorname{res}\left(\frac{t^{3-s}}{3-s}\zeta_{\Lambda,\Omega}(s), 2\right) &= \lim_{s\to 2} \frac{\lambda^2 - 1}{(s-1)(\lambda^s - 1)} \cdot \frac{t^{3-s}}{3-s} \\ &= \frac{(\lambda^2-1)t}{(1)(\lambda^2-1)(1)} = t, \end{aligned} \tag{6.2.40}$$

which is the first term in our volume formula, Formula 6.2.31. When $\omega = 1$, we have

$$\begin{aligned}\operatorname{res}\left(\frac{t^{3-s}}{3-s}\zeta_{\Lambda,\Omega}(s), 1\right) &= \lim_{s\to 1}\frac{\lambda^2-1}{(s-2)(\lambda^s-1)}\cdot\frac{t^{3-s}}{3-s}\\ &= \frac{(\lambda^2-1)t^2}{(-1)(\lambda-1)(2)}\\ &= \frac{(\lambda+1)\cancel{(\lambda-1)}t^2}{(-1)\cancel{(\lambda-1)}(2)} = -\frac{t^2}{2}(1+\lambda),\end{aligned} \tag{6.2.41}$$

which is the second term in Formula 6.2.31. When $\omega = 0 + in\mathbf{p}$, for each $n \in \mathbb{Z}$ we have

$$\begin{aligned}\operatorname{res}\left(\frac{t^{3-s}}{3-s}\zeta_{\Lambda,\Omega}(s), 0+in\mathbf{p}\right) &= \lim_{s\to in\mathbf{p}}\frac{(s-in\mathbf{p})(\lambda^2-1)t^{3-s}}{(s-2)(s-1)(3-s)(\lambda^s-1)}\\ &= \lim_{s\to in\mathbf{p}}\frac{t^3(\lambda^2-1)t^{-s}}{(1-s)(2-s)(3-s)}\cdot\lim_{s\to in\mathbf{p}}\frac{s-in\mathbf{p}}{\lambda^s-1}\\ &= \frac{t^3(\lambda^2-1)t^{-in\mathbf{p}}}{(1-in\mathbf{p})(2-in\mathbf{p})(3-in\mathbf{p})}\cdot\lim_{s\to in\mathbf{p}}\frac{1}{(\log\lambda)\lambda^s}\\ &= \frac{t^3(\lambda^2-1)}{\log\lambda}\cdot\frac{t^{-in\mathbf{p}}}{(1-in\mathbf{p})(2-in\mathbf{p})(3-in\mathbf{p})}.\end{aligned} \tag{6.2.42}$$

Using partial fraction decomposition on the second factor in the final expression in Equation 6.2.42, we get

$$\operatorname{res}\left(\frac{t^{3-s}}{3-s}\zeta_{\Lambda,\Omega}(s), 0+in\mathbf{p}\right) = \frac{t^3}{2}\cdot\frac{(\lambda^2-1)}{\log\lambda}\left(\frac{t^{-in\mathbf{p}}}{1-in\mathbf{p}} - 2\cdot\frac{t^{-in\mathbf{p}}}{2-in\mathbf{p}} + \frac{t^{-in\mathbf{p}}}{3-in\mathbf{p}}\right), \tag{6.2.43}$$

whence

$$\begin{aligned}&\sum_{n\in\mathbb{Z}}\operatorname{res}\left(\frac{t^{3-s}}{3-s}\zeta_{\Lambda,\Omega}(s), 0+in\mathbf{p}\right)\\ &\quad= \frac{t^3}{2}\cdot\frac{(\lambda^2-1)}{\log\lambda}\left(\sum_{n\in\mathbb{Z}}\frac{t^{-in\mathbf{p}}}{1-in\mathbf{p}} - 2\sum_{n\in\mathbb{Z}}\frac{t^{-in\mathbf{p}}}{2-in\mathbf{p}} + \sum_{n\in\mathbb{Z}}\frac{t^{-in\mathbf{p}}}{3-in\mathbf{p}}\right),\end{aligned} \tag{6.2.44}$$

which is the third, oscillatory term in our tubular volume formula, Formula 6.2.31. Consequently, we recover Formula 6.2.31 from the general formula for the volume of the tubular neighborhood of a strongly d-languid relative fractal drum:

$$\begin{aligned} V_{\Lambda,\Omega}(t) &= \sum_{\omega \in \mathcal{D}(\zeta_{\Lambda,\Omega},\mathbb{C})} \operatorname{res}\left(\frac{t^{3-s}}{3-s}\zeta_{\Lambda,\Omega}(s), \omega\right) \\ &= t - \frac{t^2}{2}(1+\lambda) + \frac{t^3}{2} \cdot \frac{\lambda^2 - 1}{\log \lambda} \left(\sum_{n \in \mathbb{Z}} \frac{t^{-in\mathbf{p}}}{1 - in\mathbf{p}} - 2 \sum_{n \in \mathbb{Z}} \frac{t^{-in\mathbf{p}}}{2 - in\mathbf{p}} + \sum_{n \in \mathbb{Z}} \frac{t^{-in\mathbf{p}}}{3 - in\mathbf{p}} \right) \end{aligned} \tag{6.2.45}$$

Oscillation of Points

For clarity and explicitness, we will turn again to the Hilbert curve. As mentioned in Remark 4.2.9 in Chapter 4, the following iterated function system (IFS) (see Definition 4.1.5 in Chapter 4) is derived in [Sag94] for the Hilbert curve.

$$\begin{aligned} H_0(z) &= \frac{1}{2}\bar{z}i \qquad & H_2(z) &= \frac{1}{2}(z+1+i) \\ H_1(z) &= \frac{1}{2}(z+i) & H_3(z) &= \frac{1}{2}(-\bar{z}i+i)+1 \end{aligned} \tag{4.2.16}$$

This IFS acts on the unit square, I^2, and if we choose the *initial set* (or *leitmotif*) for the IFS to be any curve connecting the points $(0,0)$ and $(1,0)$, then repeated application of 4.2.16 will produce approximating curves that converge to the Hilbert curve $f_{H*}(I) = H = I^2$, albeit different from the approximating polygons in the minimal construction. From this IFS, Sagan produced the first arithmetization of the Hilbert curve in 1991, i.e. a formula for the location of the image points $f_H(t) \in I^2$ given any $t \in I$. Let $t \in I$ be represented in quaternary form:

$$t = \sum_{n=1}^{\infty} \frac{q_i}{4^n} = 0.q_1q_2q_3\ldots \qquad \text{where } q_i \in \{0,1,2,3\}. \tag{4.2.3}$$

Then the image of t under the Hilbert mapping f_H (see Proposition 4.2.4 in Chapter 4) is

$$f_H(0.q_1q_2q_3\ldots) = \sum_{n=1}^{\infty} \left(\frac{1}{2}\right)^n (-1)^{e_{0_n}} \operatorname{sgn}(q_n) \begin{bmatrix} (1-d_n)q_n - 1 \\ 1 - d_n q_n \end{bmatrix} \tag{6.2.46}$$

where

$$\operatorname{sgn}(x) = \begin{cases} 0 & \text{if } x = 0 \\ 1 & \text{if } x > 0, \end{cases} \tag{6.2.47}$$

$$e_{0_n} = \#\left(\{q_k : q_k = 0 \text{ and } k < n\}\right) \mod 2 \tag{6.2.48}$$

$$e_{3_n} = \#\left(\{q_k : q_k = 3 \text{ and } k < n\}\right) \mod 2, \tag{6.2.49}$$

and

$$d_n = (e_{0_n} + e_{3_n}) \mod 2. \tag{6.2.50}$$

Note that f_H above is a vector-valued function and the expression in brackets in Formula 6.2.46 is a vector in $\mathbb{R}^2$.

Remark 6.2.2. The values e_{0_n} and e_{3_n} arise from cancellations that occur from successive applications of the same contraction mapping H_i in System 4.2.16. For a detailed derivation and explanation see [Sag94] Section 2.3, but for our discussions, it suffices to note that e_{0_n} controls whether or not the factor -1 is applied at any digit q_n. Since these are quaternary digits, they correspond to a quartic interval of the nth generation, and the quaternary representation of t corresponds to a quartic chain (see Definition 4.2.2 and Proposition 4.2.1 in Chapter 4). The application of a factor of -1 at generation n corresponds to the direction the traverse Φ_H requires when passing from a quartic interval of generation n to a quartic interval of generation $n+1$. This is what induces the oscillatory behavior of the points, as this factor of -1 is passed to the image vector accordingly.

Remark 6.2.3. Formula 6.2.46 is exact for any finite dyadic rational number in $I = [0, 1]$. Consequently, it can be used to approximate the image point $f_H(t)$ of any $t \in I$. The present author translated this formula into a Mathematica code that will not only provide the coordinates of any finite quaternary number, but also the intermediate image points under this mapping. The code is Code A.1.2 in Appendix A, Section A.1.

This concludes the main body of work presented in this dissertation, but in the remaining chapter, we have a few conjectures that will be addressed in later work.

Chapter 7

Future Results

The classes of curves (and associated relative fractal drums) studied herein are only a small collection of the space-filling curves that exist. There are many space-filling curves that are generated by other means, and over the course of this research, a point of focus has always been generalizing the constructions and theory to other space-filling curves. In this chapter we restrict ourselves, still, to space-filling curves induced by tessellations, and present two conjectures for two different classes of space-filling curves.

7.1 Extension to Regular Rectilinear Tessellations of I^N

The first class of interest is $\mathfrak{R}_N$, the class of space-filling curves induced by regular rectilinear tessellations of the unit N-cube, I^N. Recall that $\mathfrak{R}_2$ is the class of all plane-filling curves induced by regular rectilinear tessellations of I^2, so a natural question to ask is whether or not the construction of the relative fractal drum (Λ, Ω) detailed in Chapter 5 can be extended to $N \geq 3$. The present author has made recent advancements in this area, and has nearly found the correct generalization to higher dimensions. In light of these advancements, we present the following conjecture.

Conjecture 7.1.1 (A.D. Richardson, 2022)**.** Let $\lambda \in \{2, 3, 4, \ldots\}$ and let $\Lambda \in \mathcal{S}_N(\lambda) \subset \mathfrak{R}_N$ be a space-filling curve. Let (Λ, Ω) be the associated RFD, constructed "similarly" to the

RFDs constructed above in Chapter 5. Then a relative distance zeta function for (Λ, Ω) is

$$\zeta_{\Lambda,\Omega}(s) = \frac{(\lambda^N - 1)(N-1)!}{(s-N)(s-(N-1))\cdots(s-2)(s-1)(\lambda^s - 1)}. \tag{7.1.1}$$

Consequently, the set of relative complex dimensions of Λ is

$$\mathcal{D}(\zeta_{\Lambda,\Omega}) = \left\{0 + \frac{2\pi}{\log\lambda} i\mathbb{Z}\right\} \cup \{1, 2, \ldots, N\}, \tag{7.1.2}$$

and therefore Λ is a fractal by Definition 3.3.9. Since this is true for any $\lambda \in \{2, 3, 4, \ldots\}$, it follows that every space-filling curve in $\mathfrak{R}_N$ is a fractal by Definition 3.3.9.

Remark 7.1.1. The first thing to note about this relative distance zeta function is that it picks up a simple pole at each subdimension M where $0 \leq M \leq N$, and, as in Theorem 5.2.1, the poles with nonzero imaginary part all have real part equal to 0, i.e. the oscillations still only occur with respect to dimension 0. It is expected that there is a pole for each topological dimension based on the general theory of complex dimensions, but what is not immediately apparent is why there are no oscillations associated with dimensions other than 0. As mentioned in Remark 5.2.3, the lack of oscillation is easier to make sense of in higher dimensions. Recalling Remark 4.2.3, the oscillations above 0 are an artifact of the pointwise-defined nature of the λ-adic mapping Φ_λ which defines the traverse of the λ-adic subsqaures in $\mathbb{R}^N$. If there were oscillations associated with some other subdimension M for $0 < M < N$, then this ordering would require consecutive generations of point images to remain "close" in M-dimensional space since these M-dimensional objects can be written as unions of the point images as shown, for example, in Equation 4.2.6 in Remark 4.2.3. However, if this requirement is fulfilled, then points within some M-dimensional slice of $\mathbb{R}^N$ must be held "apart" from points in another M-dimensional slice as the generations increase, but this will break the inequality needed for uniform convergence of the approximating polygons (see, in particular, Inequality 4.2.12 in the proof of Proposition 4.2.4), and we have a contradiction.

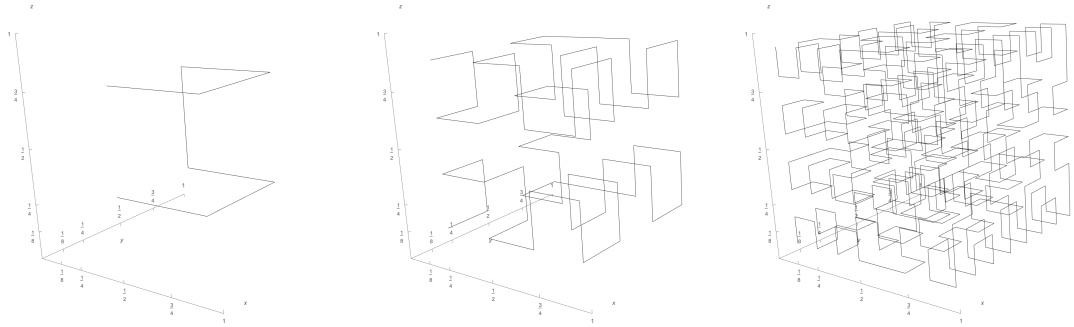

Figure 7.1.1: The first three approximations to the 3-dimensional Hilbert curve.

As is common, a clear example is given by the Hilbert curve, this time in $\mathbb{R}^3$, i.e. $f_H(t) : I \to I^3$. Figure 7.1.1 shows approximations to this curve. If oscillations occurred which are associated with dimension 2, then, given any planar slice of I^3, we would expect the 2-dimensional slices in consecutive generations to be mapped to each other. But this keeps some images of distinct planar slices separate from each other in $\mathbb{R}^3$ through some number of generations, a contradiction.

Once it is established that oscillations occur only above dimension 0, and that we must still pick up a singularity at every subdimension M for $0 \leq M \leq N$, the denominator of Equation 7.1.1 becomes clear. Next we must account for the volume factors these additional poles will introduce when we calculate the N-dimensional Minkowski content using this relative distance zeta function. In this case, there will appear a factor of $(N-1)!$ in the denominator when the residue at N is computed, and by extension in the calculation of the N-dimensional Minkowski content. Thus, we need an additional factor of $(N-1)!$ in the numerator, yielding Equation 7.1.1.

At the time of submission of this dissertation, the present author had already devised an N-dimensional fundamental cell for $(N-1)$-dimensional space-filling curves that results in this zeta function, but it does not scale down to $N = 2$, so we must leave Conjecture 7.1.1 as a conjecture for now.

7.2 Extension to Irregular Rectilinear Tessellations of I^N

Irregular rectilinear tessellations are like regular ones except the cells of the tessellation can be rectangles with differing side lengths. These tessellations can still result in space-filling curves much the same way regular rectilinear tessellations do. For now we can denote the class of N-dimensional space-filling curves generated by irregular rectilinear tessellations by $\mathfrak{I}_N$ The present author has a conjecture for the structure of the zeta functions and the RFDs associated with curves constructed in this way, but there are many details to include and another paper will be necessary to elucidate all of them. In some sense, this generalization is analogous to generalizing λ to noninteger values, but more explicitly it involves arbitrary finite sequences of dissection scalars that determine the cells of the decomposition of I^N to be applied in each generation. These dissection scalars may or may not be rationally related, and so two cases must be explored. The present author has an intuition that the results will have a structure and "flavor" similar to what one sees in Chapter 2 of [LvF13] where the geometric zeta functions of *lattice* and *nonlattice* fractal strings are explored and classified.

7.3 Extension to Regular Nonrectilinear Tessellations of $\mathbb{R}^N$

The next natural question is how to extend the RFD construction to space-filling curves that are induced by regular *non*rectilinear tessellations, i.e. tessellations by cells that are still congruent, but are not cubes. One class of examples in $\mathbb{R}^2$ can be illustrated by looking at a self-similar trapezoidal tessellation of a trapezoid, as pictured in Figure 7.3.1. The fact that such a tessellation results in a plane-filling curve is actually an exercise in [Sag94] (Exercise 12, Chapter 2) which is attributed to J. Mioduszewski. This tessellation has 4^n sub-trapezoids in each generation, and induces a variant of the Hilbert curve which instead fills the trapezoid so it makes sense that the complex dimensions of such a plane-filling curve will be the same as those of the Hilbert curve. Figure 7.3.2 shows the first approximating polygon for such a curve. However, the 2-dimensional Minkowski content will not (necessarily) be 1 as with the unit square, it will be the area of the planar figure, in this case the area of the trapezoid.

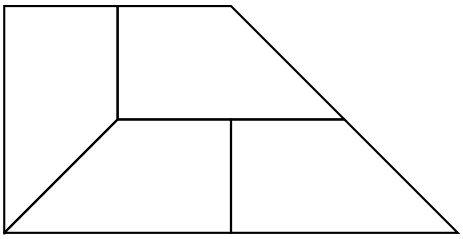

Figure 7.3.1: A trapezoid partitioned into four congruent similar trapezoids.

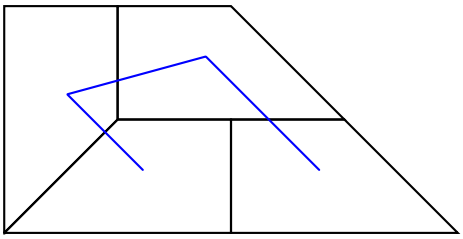

Figure 7.3.2: The first approximation to a "trapezoidal Hilbert curve".

Let $\mathfrak{N}_N$ represent the class of all N-dimensional space-filling curves induced by regular nonrectilinear λ-adic tessellations of $\mathbb{R}^N$ such that there are λ^{Nn} subcells in each generation. Since the cells of these tessellations are homeomorphic to regular cells of a rectilinear tessellation, we have the following conjecture.

Conjecture 7.3.1 (A.D. Richardson, 2022)**.** Let $\Gamma \in \mathfrak{N}_N$ be a space-filling curve and let $\lambda \in \{2, 3, 4, \ldots\}$. Let L be a projective transformation between the cells of the tessellation associated with Γ to the regular rectilinear cells associated with a curve $\Lambda \in \mathcal{S}_N(\lambda) \subset \mathfrak{R}_N$. Let (Γ, Ω) be the RFD associated with Γ, constructed "similarly" to the RFDs in Chapter 5. Then a relative distance zeta function for (Γ, Ω) is

$$\zeta_{\Gamma,\Omega}(s) = \frac{|\det L| \cdot (\lambda^N - 1)(N-1)!}{(s-N)(s-(N-1))\cdots(s-2)(s-1)(\lambda^s - 1)} \tag{7.3.1}$$

where $\det L$ is the determinant of L. Consequently, the set of relative complex dimensions of Γ is

$$\mathcal{D}(\zeta_{\Gamma,\Omega}) = \left\{0 + \frac{2\pi}{\log \lambda} i\mathbb{Z}\right\} \cup \{1, 2, \ldots, N\}, \tag{7.3.2}$$

and therefore Γ is a fractal by Definition 3.3.9. It follows that every space-filling curve in $\mathfrak{N}_N$ is a fractal by Definition 3.3.9.

Admittedly, the argument above is only a heuristic one, and there is much to verify and prove in this conjecture, but if this conjecture is not correct, a similar, more refined conjecture should be correct.

References

[Edg90] Gerald A. Edgar, *Measure, Topology, and Fractal Geometry*, Springer-Verlag, New York, 1990.

[Fal90] Kenneth Falconer, *Fractal Geometry: Mathematical Foundations and Applications*, 1st, Wiley, 1990.

[PR86] Heinz-Otto Peitgen and Peter Richter, *The Beauty of Fractals*, Springer-Verlag, Heidelberg, 1986.

[Man82] Benoit Mandelbröt, *The Fractal Geometry of Nature*, W. H. Freeman and Co., 1982.

[Sag94] Hans Sagan, *Space-Filling Curves*, 1st, Springer-Verlag, 1994.

[SS05] Elias M. Stein and Rami Shakarchi, *Real Analysis*, 1st ed., Princeton Lectures in Analysis, vol. III, Princeton University Press, 2005.

[LRŽ17] Michel L. Lapidus, Goran Radunović, and Darko Žubrinić, *Fractal Zeta Functions and Fractal Drums*, 1st ed., Springer International, 2017.

[LvF13] Michel L. Lapidus and Machiel van Frankenhuijsen, *Fractal Geometry, Complex Dimensions and Zeta Functions*, 2nd ed., Springer Science+Business Media, 2013.

[Lap91] Michel L. Lapidus, *Fractal Drums, Inverse Spectral Problems for Elliptic Operators and a Partial Resolution of the Weyl-Berry Conjecture*, Transactions of the American Math Society **325** (1991), 465–529.

[Fol99] Gerald B. Folland, *Real Analysis: Modern Techniques and Their Applications*, 2nd ed., Wiley-Interscience, 1999.

[Con78] John B. Conway, *Functions of One Complex Variable I*, 2nd ed., Springer, 1978.

[Pea90] Giuseppe Peano, *Sur une courbe, qui remplit toute une aire plane*, Mathematische Annalen **36** (1890), 157–160.

[Can78] Georg Cantor, *Ein Beitrag zur Mannigfaltigkeitslehre*, Crelle Journal **84** (1878), 242–258.

[Net79] Eugen Netto, *Beitrag zur Mannigfaltigkeitslehre*, Crelle Journal **86** (1879), 263–268.

[Hil91] David Hilbert, *Über die steatite Abbildung einer Linie auf ein Flächestück*, Mathematische Annalen **38** (1891), 459–460.

[Moo00] E.H. Moore, *On Certain Crinkly Curves*, Transactions of the American Math Society **1** (1900), 72–90.

[Wun73] Walter Wunderlich, *Über Peano-Kurven*, Elemente Der Mathematik **28** (1973), 1–10.

[Bou91] Paul Bourke, *L-System User Notes*, 1991 [Online]. http://paulbourke.net/fractals/lsys/.

Appendix A

Codes and Images

This appendix contains many of the codes used to produce the images in this dissertation, and there are some codes for interactive models related to the Hilbert curve and the RFD. In the last section, Section A.3, there are some more images of the different Hilbert curve relative fractal drums (RFDs). The present author invites the interested reader to copy and paste these codes into their own Mathematica notebook and explore the insightful interactive models.

A.1 Mathematica Codes

Code A.1.1 (Hilbert Curve Generations and a Node-Traversing Point)**.** The following code produces a nice interactive visualization of the first 9 approximations to the Hilbert curve, correctly scaled to lie within the unit square, I^2. The dyadic squares of each generation are shown as a grid. The red dot follows the traverse of the ordering given by Φ_H (see Proposition 4.2.3 in Chapter 4). The traverse is given by the built-in Mathematica command `HilbertCurve[n]` which returns a `Line` object determined by a list of points `{x,y}`. One notable issue with the built-in command (as mentioned in the documentation of the command) is that the step size between nodes (points) has length 1 for any generation n, so as n increases, the boundary of the approximations increases. In this code, and the other

Mathematica codes below, the node data is scaled down appropriately within the function gen[n] to fit within the unit square.

```
(*Point extraction function*)
extractPoints = Extract[#, {1, ## & @@ #} & /@ #2] &;

(*Rescale HilbertCurve[n] to fit generation n inside unit square*)
gen[n_] :=
  extractPoints[HilbertCurve[n, DataRange -> {{0, 1}, {0, 1}}],
     Range[4^n]]*(2^n - 1)/(2^n) + 1/(2^(n + 1));

(*Graph generations and point*)
Manipulate[
 Graphics[
  {Line[gen[n]],
   Red, PointSize[0.03], Point[gen[n][[i]]]},
  ImageSize -> Medium,
  Axes -> True,
  AxesOrigin -> {0, 0},
  AxesLabel -> {x, y},
  AspectRatio -> 1,
  PlotRange -> {{0, 1}, {0, 1}},
  Ticks -> {Range[2^n]*2^-n, Range[2^n]*2^-n},
  GridLines -> {Range[2^n]*2^-n, Range[2^n]*2^-n}
 ],
 {n, 1, 9, 1}, {i, 1, 4^n, 1}
 ]
```

Code A.1.2 (Hilbert Curve Arithmetization: Trajectory of Image Points)**.** The following code produces an interactive visualization of the image points of finite quaternaries in $[0,1]$ under the Hilbert mapping f_H. This code is a Mathematica translation of the Hilbert curve arithmetization computed in [Sag94] Sections 2.3 and 2.4, which is given by Formula 6.2.46 in Chapter 6 and repeated here for convenience.

Let $t \in I$ be represented in quaternary form:

$$t = \sum_{n=1}^{\infty} \frac{q_i}{4^n} = 0.q_1q_2q_3\ldots \qquad \text{where } q_i \in \{0,1,2,3\}. \tag{4.2.3}$$

Then the image of t under the Hilbert mapping f_H (see Proposition 4.2.4 in Chapter 4) is

$$f_H(0.q_1q_2q_3\ldots) = \sum_{n=1}^{\infty} \left(\frac{1}{2}\right)^n (-1)^{e_{0_n}} \operatorname{sgn}(q_n) \begin{bmatrix} (1-d_n)q_n - 1 \\ 1 - d_nq_n \end{bmatrix} \tag{6.2.46}$$

where

$$\operatorname{sgn}(x) = \begin{cases} 0 & \text{if } x = 0 \\ 1 & \text{if } x > 0, \end{cases} \tag{6.2.47}$$

$$e_{0_n} = \#\left(\{q_k : q_k = 0 \text{ and } k < n\}\right) \mod 2 \tag{6.2.48}$$

$$e_{3_n} = \#\left(\{q_k : q_k = 3 \text{ and } k < n\}\right) \mod 2, \tag{6.2.49}$$

and

$$d_n = (e_{0_n} + e_{3_n}) \mod 2. \tag{6.2.50}$$

Given any $t \in [0,1]$, writing it in quaternary form yields the generational addresses of the quartic intervals that comprise the chain which converges to t. As the number of digits increases, the more accurate the approximation to t becomes. Correspondingly, Formula 6.2.46 and this code produce increasingly accurate approximations to the image point $f_H(t)$ as the generation (number of digits) n increases. From this we can see the potential oscillation

of the image points as they converge to their attractor. In general, the approximation will be within an error of $\sqrt{2} \cdot 2^{-n}$, and the pattern of oscillation is dependent on the quaternary representation of t. This code has $t = \frac{1}{\pi}$ as a placeholder value for convenience.

```
(*Enter t in [0,1]*)
t = 1/Pi;

(*Produces list of first 10 quaternary digits of t*)
list = IntegerDigits[IntegerPart[N[t*4^10]], 4]

(*Gives Number of 0's or 3's preceding digit list[[j]], mod 2*)
e0[j_] := Mod[Count[Drop[list, -Length[list] + j - 1], 0], 2];
e3[j_] := Mod[Count[Drop[list, -Length[list] + j - 1], 3], 2];

(*Gives d_j factor in arithmetization*)
d[j_] := Mod[e0[j] + e3[j], 2];

(*Arithmetization of curve [Sagan, H. 1991]*)

hilbert[q_] := {Sum[(1/2^j)*(-1)^(e0[j])*
     Sign[q[[j]]]*((1 - d[j])*q[[j]] - 1), {j, Length[q]}],
   Sum[(1/2^j) (-1)^(e0[j])*Sign[q[[j]]]*(1 - d[j]*q[[j]]), {j,
     Length[q]}]};

(*Gives entry point into nth generation dyadic square point in I^2*)
hilbert[list]

(*Generates interactive point trajectory*)
Manipulate[
```

```
Column[{
  Graphics[
   {Red, PointSize[0.02],
    Point[hilbert[Drop[list, -Length[list] + n]]]},
   ImageSize -> Large,
   Axes -> True,
   AxesOrigin -> {0, 0},
   (*AxesLabel\[Rule]{x,y},*)
   AspectRatio -> 1,
   PlotRange -> {{0, 1}, {0, 1}},
   Ticks -> {Range[2^n]*2^-n, Range[2^n]*2^-n},
   GridLines -> {Range[2^n]*2^-n, Range[2^n]*2^-n}
   ], Grid[{{"Decimal", t, "\[TildeTilde]", N[t, 10]}, {"Generation",
      n}, {"Quaternary Truncation",
     Drop[list, -Length[list] + n]}, {"Entry Point of dyadic square",
      hilbert[Drop[list, -Length[list] + n]]}}]},
 Alignment -> Center],
{n, 1, Length[list], 1}
]
```

Code A.1.3 (Hilbert Curve RFD, scaled by $\frac{1}{2}$)**.** This code produces a 3-dimensional interactive model of the scaled down version of the Hilbert curve RFD detailed in Chapter 5 and pictured in Figures 5.1.2 and 5.1.3. This version is scaled down by a factor of $\frac{1}{2}$, and it shows how the prisms can be attached to the polygonal approximations directly, without translation. See Section A.3 below for more images. `M` is the highest generation of prisms to include. This code has `M=4` as a placeholder, but `M=7` or `M=8` provides a more detailed and striking model, albeit slower to compute and more difficult to manipulate.

```
(*Point extraction function*)
extractPoints = Extract[#, {1, ## & @@ #} & /@ #2] &;

(*Set max generation M*)
M = 4;

(*Compute coordinates of nodal points for all generations up to M*)
Do[
 (*Rescale HilbertCurve[n] to fit generation n inside unit square*)
 gen[n] = extractPoints[
      HilbertCurve[n, DataRange -> {{0, 1}, {0, 1}}],
      Range[4^n]]*(2^n - 1)/(2^n) + 1/(2^(n + 1));
 , {n, M}]

(*Creates list of vertex coordinates for all prisms up to generation M*)
prisGen = Reap[
    Do[
     prisCoord = Sow[Reap[
         Do[
          (*Creates list of vertex coordinates for prisms in generation n*)
          If[gen[n][[i, 1]] == gen[n][[i + 1, 1]],

           P11 = Append[gen[n][[i]], 0];
           P12 = Append[gen[n][[i]], 1/(2^(n + 1))];

           P13 = Append[
             ReplacePart[gen[n][[i]],
              1 -> gen[n][[i, 1]] + 1/(2^(n + 2))], 1/(2^(n + 2))];
```

```
    P21 = Append[gen[n][[i + 1]], 0];
    P22 = Append[gen[n][[i + 1]], 1/(2^(n + 1))];

    P23 = Append[
      ReplacePart[gen[n][[i + 1]],
       1 -> gen[n][[i, 1]] + 1/(2^(n + 2))], 1/(2^(n + 2))];
    ,

    P11 = Append[gen[n][[i]], 0];
    P12 = Append[gen[n][[i]], -1/(2^(n + 1))];

    P13 = Append[
      ReplacePart[gen[n][[i]],
       2 -> gen[n][[i, 2]] + 1/(2^(n + 2))], -1/(2^(n + 2))];

    P21 = Append[gen[n][[i + 1]], 0];
    P22 = Append[gen[n][[i + 1]], -1/(2^(n + 1))];

    P23 = Append[
      ReplacePart[gen[n][[i + 1]],
       2 -> gen[n][[i, 2]] + 1/(2^(n + 2))], -1/(2^(n + 2))];
    ];
   Sow[{P11, P12, P13, P21, P22, P23}]
   ,
   {i, 4^n - 1}]
  ][[2, 1]]]
,
```

```
    {n, M}]][[2, 1]];


(*Generates the model*)
Graphics3D[
 Table[Prism[prisGen[[n]]], {n, M}],
 Boxed -> False,
 Axes -> True,
 AxesOrigin -> {0, 0, 0},
 AxesLabel -> {x, y, z},
 Ticks -> {{1/8, 1/4, 1/2, 3/4, 1}, {1/8, 1/4, 1/2, 3/4,
    1}, {-1, -1/2, -1/4, -1/8, 0, 1/8, 1/4, 1/2, 1}}]
```

Code A.1.4 (Hilbert Curve RFD, unscaled)**.** This code is virtually identical to that of Code A.1.3, but the prisms are actual size. The model produced by this code allows us to visualize the nontrivial overlap of the subdrums that necessitates they be translated from the original positions of the approximating polygons. `M` is the highest generation of prisms to include. This code has `M=4` as a placeholder, but `M=7` or `M=8` provides a more detailed and striking model, albeit slower to compute and more difficult to manipulate.

```
(*Point extraction function*)
extractPoints = Extract[#, {1, ## & @@ #} & /@ #2] &;


(*Set max generation M*)
M = 4;


(*Compute coordinates of nodal points for all generations up to M*)
Do[
 (*Rescale HilbertCurve[n] to fit generation n inside unit square*)
 gen[n] = extractPoints[
```

```
      HilbertCurve[n, DataRange -> {{0, 1}, {0, 1}}],
      Range[4^n]]*(2^n - 1)/(2^n) + 1/(2^(n + 1));
 , {n, M}]

(*Creates list of vertex coordinates for all prisms up to generation M*)
prisGen = Reap[
    Do[
     prisCoord = Sow[Reap[
         Do[
          (*Creates list of vertex coordinates for prisms in generation n*)
          If[gen[n][[i, 1]] == gen[n][[i + 1, 1]],

           P11 = Append[gen[n][[i]], 0];
           P12 = Append[gen[n][[i]], 1/(2^(n))];

           P13 = Append[
             ReplacePart[gen[n][[i]],
              1 -> gen[n][[i, 1]] + 1/(2^(n + 1))], 1/(2^(n + 1))];

           P21 = Append[gen[n][[i + 1]], 0];
           P22 = Append[gen[n][[i + 1]], 1/(2^(n))];

           P23 = Append[
             ReplacePart[gen[n][[i + 1]],
              1 -> gen[n][[i, 1]] + 1/(2^(n + 1))], 1/(2^(n + 1))];
           ,

           P11 = Append[gen[n][[i]], 0];
```

```
            P12 = Append[gen[n][[i]], -1/(2^(n))];


            P13 = Append[
              ReplacePart[gen[n][[i]],
               2 -> gen[n][[i, 2]] + 1/(2^(n + 1))], -1/(2^(n + 1))];


            P21 = Append[gen[n][[i + 1]], 0];
            P22 = Append[gen[n][[i + 1]], -1/(2^(n))];


            P23 = Append[
              ReplacePart[gen[n][[i + 1]],
               2 -> gen[n][[i, 2]] + 1/(2^(n + 1))], -1/(2^(n + 1))];
            ];
           Sow[{P11, P12, P13, P21, P22, P23}]
           ,
           {i, 4^n - 1}]
          ][[2, 1]]]
      ,
      {n, M}]][[2, 1]];


(*Generates the model*)
Graphics3D[
 Table[Prism[prisGen[[n]]], {n, M}],
 Boxed -> False,
 Axes -> True,
 AxesOrigin -> {0, 0, 0},
 AxesLabel -> {x, y, z},
 Ticks -> {{1/8, 1/4, 1/2, 3/4, 1}, {1/8, 1/4, 1/2, 3/4,
```

```
    1}, {-1, -1/2, -1/4, -1/8, 0, 1/8, 1/4, 1/2, 1}}]
```

Code A.1.5 (Hilbert Curve RFD, using rectangular prisms)**.** This code is very similar to that of Code A.1.3, but it contains a duplicate command to repeat the prisms in each generation, producing the RFD (H, Θ) which uses rectangular prisms instead of triangular prisms. (See Remark 5.3.1 of Section 5.3 in Chapter 5.) `M` is the highest generation of prisms to include. This code has `M=4` as a placeholder, but `M=7` or `M=8` provides a more detailed and striking model, albeit slower to compute and more difficult to manipulate.

```
(*Point extraction function*)
extractPoints = Extract[#, {1, ## & @@ #} & /@ #2] &;


(*Set max generation M*)
M = 4;


(*Compute coordinates of nodal points for all generations up to M*)
Do[
 (*Rescale HilbertCurve[n] to fit generation n inside unit square*)
 gen[n] = extractPoints[
      HilbertCurve[n, DataRange -> {{0, 1}, {0, 1}}],
      Range[4^n]]*(2^n - 1)/(2^n) + 1/(2^(n + 1));
 , {n, M}]


(*Creates list of vertex coordinates for all prisms up to generation M
for one half*)
prisGen1 = Reap[
    Do[
     prisCoord1 = Sow[Reap[
         Do[
```

```
(*Creates list of vertex coordinates for prisms in
generation n*)
If[gen[n][[i, 1]] == gen[n][[i + 1, 1]],

 P11 = Append[gen[n][[i]], 0];
 P12 = Append[gen[n][[i]], 1/(2^(n + 1))];

 P13 = Append[
   ReplacePart[gen[n][[i]],
    1 -> gen[n][[i, 1]] + 1/(2^(n + 2))], 1/(2^(n + 2))];

 P21 = Append[gen[n][[i + 1]], 0];
 P22 = Append[gen[n][[i + 1]], 1/(2^(n + 1))];

 P23 = Append[
   ReplacePart[gen[n][[i + 1]],
    1 -> gen[n][[i, 1]] + 1/(2^(n + 2))], 1/(2^(n + 2))];
 ,

 P11 = Append[gen[n][[i]], 0];
 P12 = Append[gen[n][[i]], -1/(2^(n + 1))];

 P13 = Append[
   ReplacePart[gen[n][[i]],
    2 -> gen[n][[i, 2]] + 1/(2^(n + 2))], -1/(2^(n + 2))];

 P21 = Append[gen[n][[i + 1]], 0];
 P22 = Append[gen[n][[i + 1]], -1/(2^(n + 1))];
```

```
            P23 = Append[
              ReplacePart[gen[n][[i + 1]],
               2 -> gen[n][[i, 2]] + 1/(2^(n + 2))], -1/(2^(n + 2))];
            ];
           Sow[{P11, P12, P13, P21, P22, P23}]
           ,
           {i, 4^n - 1}]
          ][[2, 1]]]
     ,
     {n, M}]][[2, 1]];

(*Creates list of vertex coordinates for all prisms up to generation M
for the other half*)
prisGen2 = Reap[
    Do[
     prisCoord2 = Sow[Reap[
         (*Creates list of vertex coordinates for prisms in
         generation n*)
         Do[
          If[gen[n][[i, 1]] == gen[n][[i + 1, 1]],

           P11 = Append[gen[n][[i]], 0];
           P12 = Append[gen[n][[i]], 1/(2^(n + 1))];

           P13 = Append[
             ReplacePart[gen[n][[i]],
              1 -> gen[n][[i, 1]] - 1/(2^(n + 2))], 1/(2^(n + 2))];
```

```
    P21 = Append[gen[n][[i + 1]], 0];
    P22 = Append[gen[n][[i + 1]], 1/(2^(n + 1))];

    P23 = Append[
      ReplacePart[gen[n][[i + 1]],
       1 -> gen[n][[i, 1]] - 1/(2^(n + 2))], 1/(2^(n + 2))];
    ,

    P11 = Append[gen[n][[i]], 0];
    P12 = Append[gen[n][[i]], -1/(2^(n + 1))];

    P13 = Append[
      ReplacePart[gen[n][[i]],
       2 -> gen[n][[i, 2]] - 1/(2^(n + 2))], -1/(2^(n + 2))];

    P21 = Append[gen[n][[i + 1]], 0];
    P22 = Append[gen[n][[i + 1]], -1/(2^(n + 1))];

    P23 = Append[
      ReplacePart[gen[n][[i + 1]],
       2 -> gen[n][[i, 2]] - 1/(2^(n + 2))], -1/(2^(n + 2))];
    ];
   Sow[{P11, P12, P13, P21, P22, P23}]
   ,
   {i, 4^n - 1}]
  ][[2, 1]]]
,
```

```
     {n, M}]][[2, 1]];


(*Generates the model*)
Graphics3D[
 {Table[Prism[prisGen1[[n]]], {n, M}],
  Table[Prism[prisGen2[[n]]], {n, M}]},
 Boxed -> False,
 Axes -> True,
 AxesOrigin -> {0, 0, 0},
 AxesLabel -> {x, y, z},
 Ticks -> {{1/8, 1/4, 1/2, 1}, {1/8, 1/4, 1/2, 1}, {1/8, 1/4, 1/2,
    1}}]
```

A.2 Lindenmayer Systems

All of the figures in this dissertation which depict approximations to plane-filling curves were produced using an appropriate *Lindenmeyer system* (or *L-system*). Some of them are readily available online and some were developed by the present author after studying examples found online. They are given here for the interested reader. A very nice collection of L-systems for fractal-like constructions can be found on Paul Bourke's website, [Bou91].

Code A.2.1 (Sierpiński Gasket, Figure 3.4.1)**.**

```
Axiom: X
Rules:
    X -> X-Y+X+Y-X
    Y -> YY
Angle: -120
```

Code A.2.2 (Hilbert curve, Figure 4.2.1)**.**

```
Axiom: L

Rules:

    L -> +RF-LFL-FR+

    R -> -LF+RFR+FL-

Angle: 90
```

Code A.2.3 (Moore curve, Figure 4.2.2)**.**

```
Axiom: LFL+F+LFL

Rules:

    L -> -RF+LFL+FR-

    R -> +LF-RFR-FL+

Angle: 90
```

Code A.2.4 (Peano curve of the switchback type, Figure 4.3.1)**.**

```
Axiom: R

Rules:

    L -> LFRFL-F-RFLFR+F+LFRFL

    R -> RFLFR+F+LFRFL-F-RFLFR

Angle: 90
```

Code A.2.5 (Peano curve of the meandering type, Figure 4.3.2)**.**

```
Axiom: L

Rules:

    L -> LF+RFR+FL-F-LFLFL-FRFR+

    R -> RF-LFL-FR+F+RFRFR+FLFL-

Angle: 90
```

Code A.2.6 (Accordion curve, Figure 5.2.5)**.**

This is not an efficient L-system to generate an accordion curve, but it is the code used in this dissertation.

```
Axiom: A
Rules:
    A -> FB+F+FC+
    B -> FFBB
    C -> FFBB-F-BBFFF+F+BBFFF-D-E
    D -> F
    E -> FFFFFFFBBBB+F+FFFFFFFBBBB-F-FFFFFFFBBBB+F+FFFFFFFBBBB-H-J
    H -> F
    J -> FFFFFFFFFFFFFFFBBBB+F+FFFFFFFFFFFFFFFBBBB-F-
         FFFFFFFFFFFFFFFBBBB+F+FFFFFFFFFFFFFFFBBBB-F-
         FFFFFFFFFFFFFFFBBBB+F+FFFFFFFFFFFFFFFBBBB-F-
         FFFFFFFFFFFFFFFBBBB+F+FFFFFFFFFFFFFFFBBBB
Angle: 90
```

A.3 More Images of the Hilbert Curve Relative Fractal Drum

Below are some more images of the scaled version of the Hilbert curve relative fractal drum (RFD) and some more images of the RFD using rectangular prisms. The Mathematica codes for these images are given in Code A.1.3 and Code A.1.5, respectively, in Section A.1. Using those codes, the images below are produced by orienting the model to be viewed from above and below.

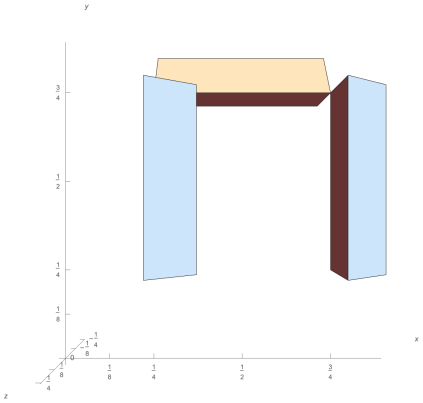

Figure A.3.1: Hilbert curve RFD top view, generation 1.

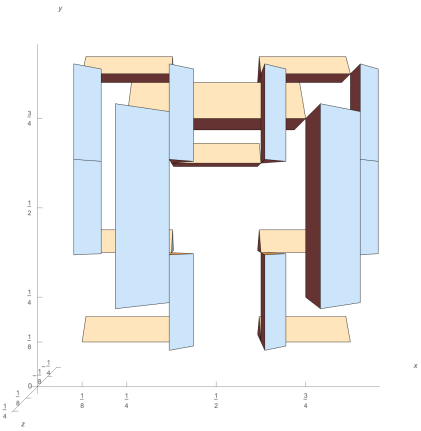

Figure A.3.2: Hilbert curve RFD top view, generations 1 and 2.

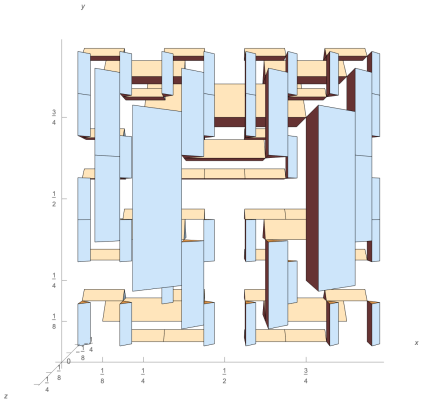

Figure A.3.3: Hilbert curve RFD top view, generations 1–3.

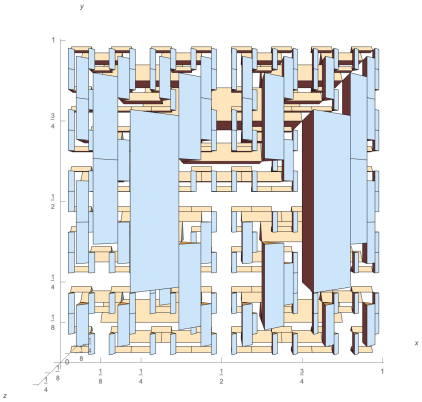

Figure A.3.4: Hilbert curve RFD top view, generations 1–4.

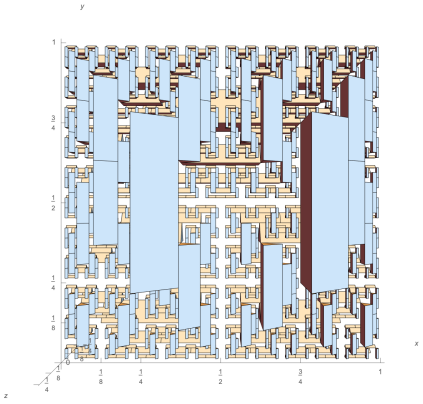

Figure A.3.5: Hilbert curve RFD top view, generations 1–5.

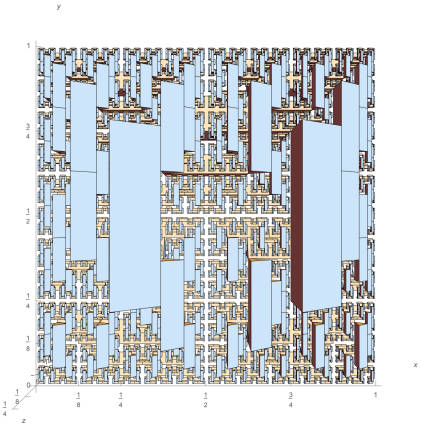

Figure A.3.6: Hilbert curve RFD top view, generations 1–6.

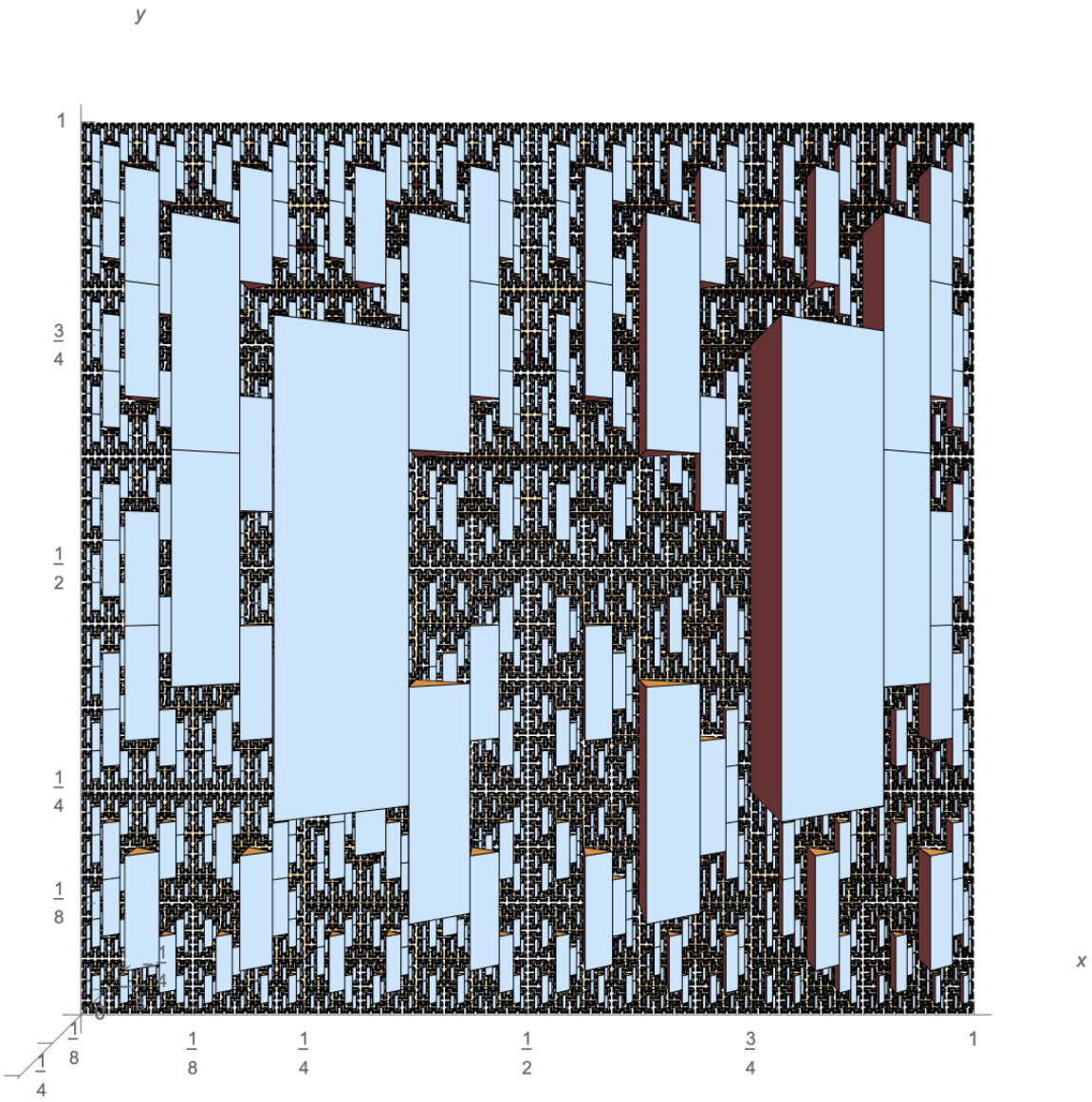

Figure A.3.7: Hilbert curve RFD top view, generations 1–8.

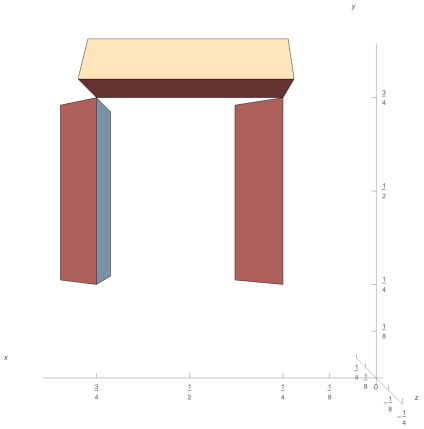

Figure A.3.8: Hilbert curve RFD bottom view, generation 1.

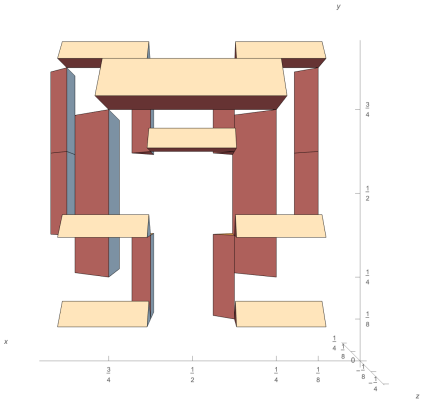

Figure A.3.9: Hilbert curve RFD bottom view, generations 1 and 2.

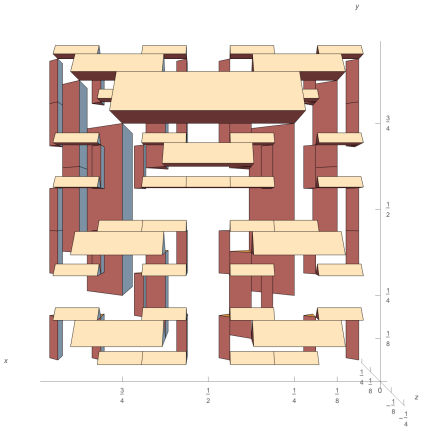

Figure A.3.10: Hilbert curve RFD bottom view, generations 1–3.

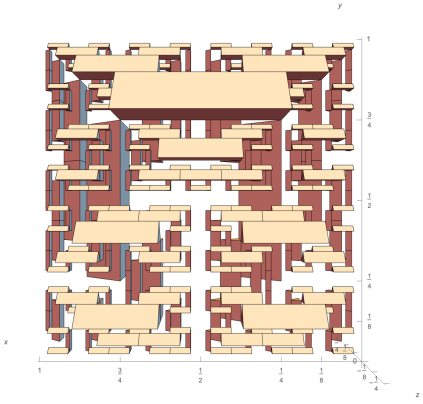

Figure A.3.11: Hilbert curve RFD bottom view, generations 1–4.

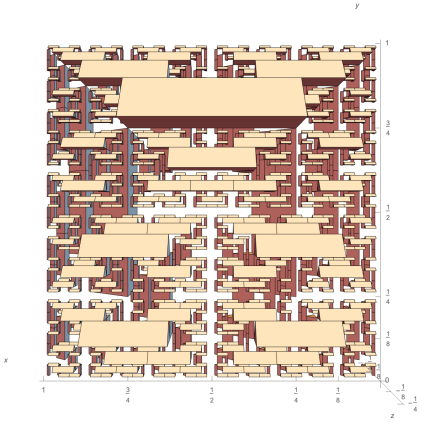

Figure A.3.12: Hilbert curve RFD bottom view, generations 1–5.

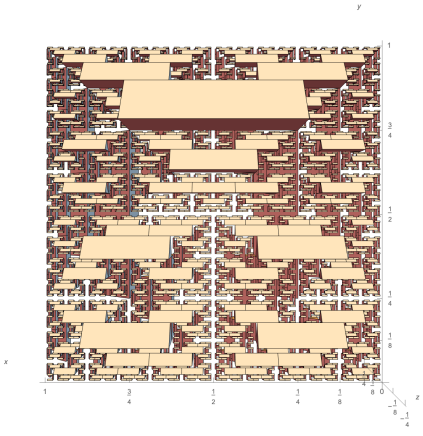

Figure A.3.13: Hilbert curve RFD bottom view, generations 1–6.

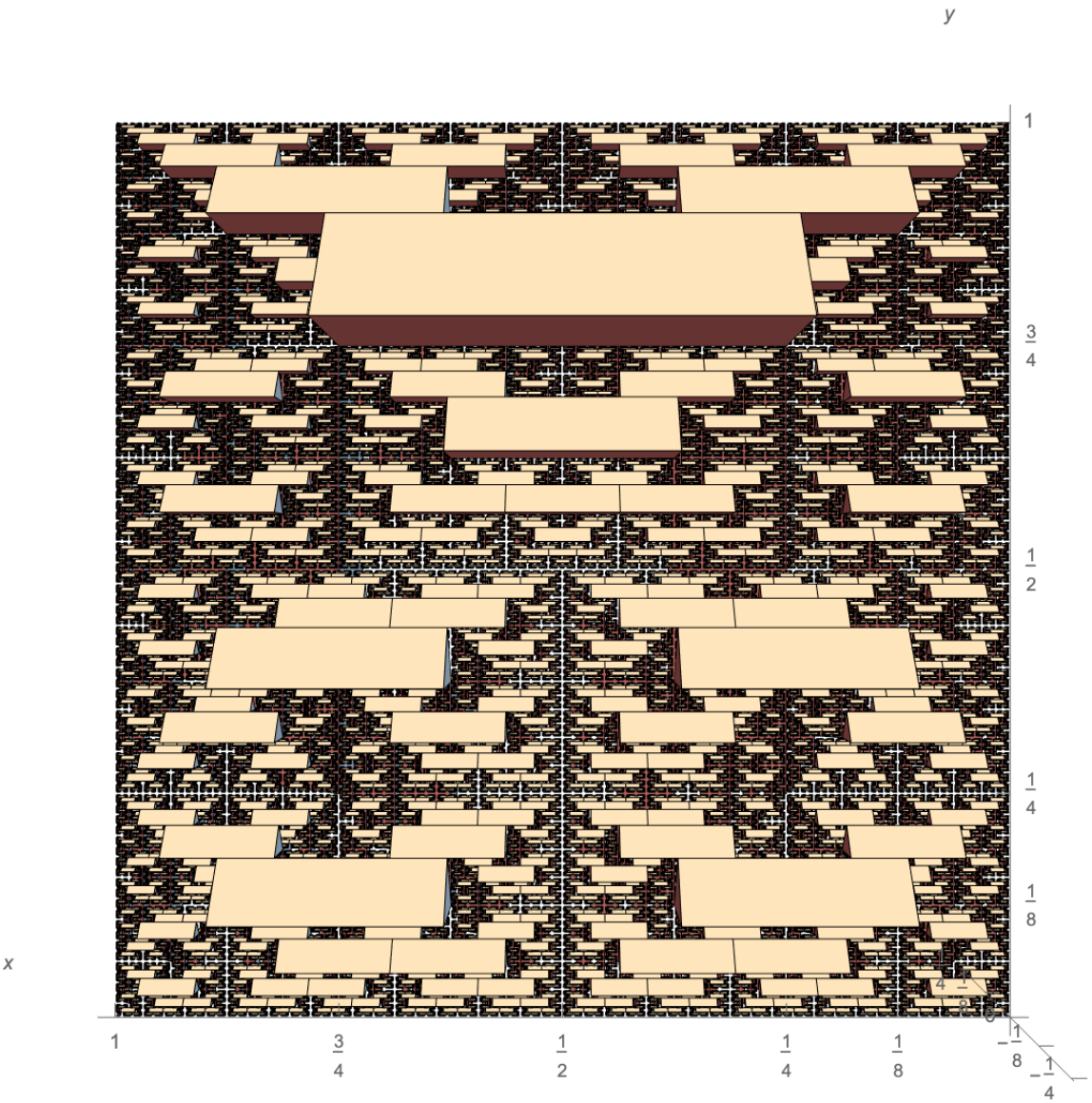

Figure A.3.14: Hilbert curve RFD bottom view, generations 1–8.

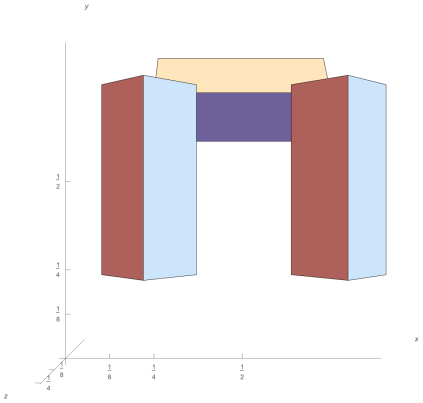

Figure A.3.15: Hilbert curve rectangular RFD top view, generation 1.

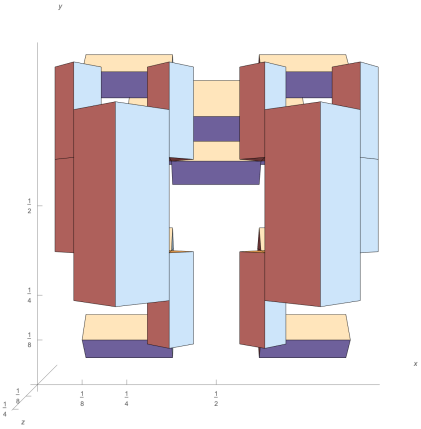

Figure A.3.16: Hilbert curve rectangular RFD top view, generations 1 and 2.

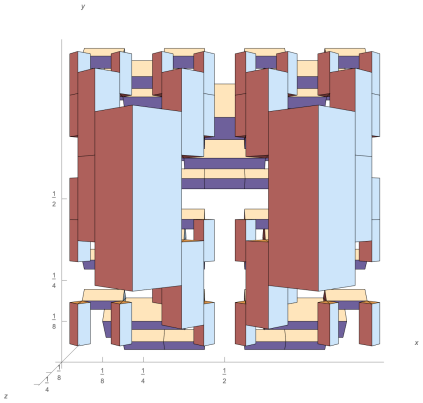

Figure A.3.17: Hilbert curve rectangular RFD top view, generations 1–3.

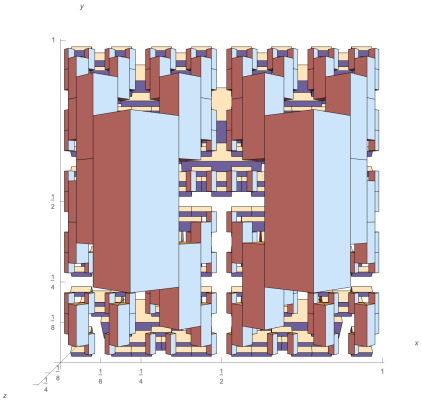

Figure A.3.18: Hilbert curve rectangular RFD top view, generations 1–4.

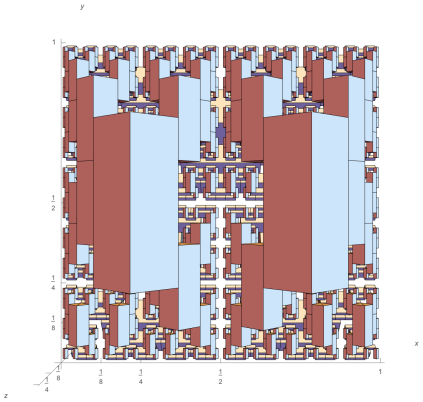

Figure A.3.19: Hilbert curve rectangular RFD top view, generations 1–5.

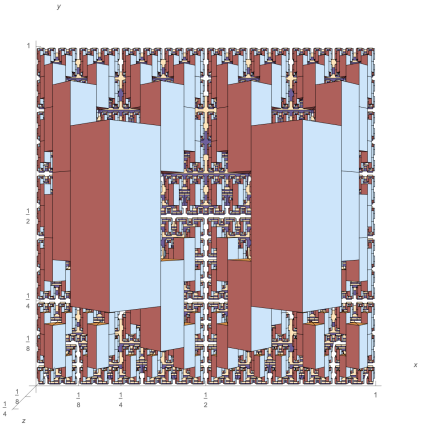

Figure A.3.20: Hilbert curve rectangular RFD top view, generations 1–6.

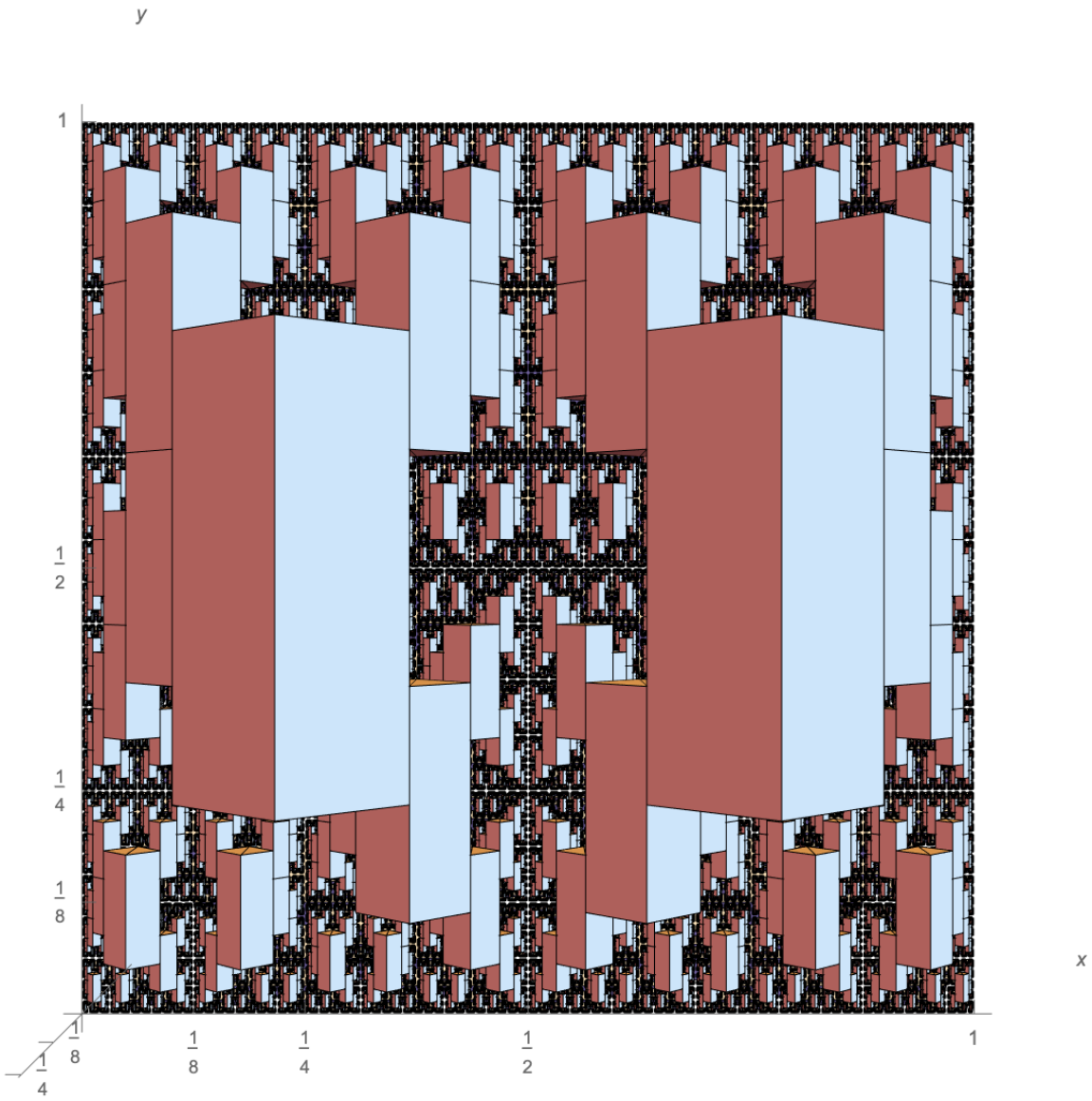

Figure A.3.21: Hilbert curve rectangular RFD top view, generations 1–8.

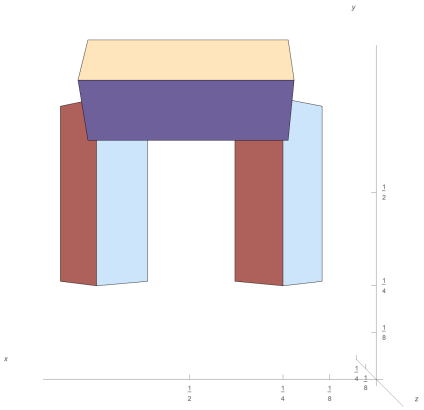

Figure A.3.22: Hilbert curve rectangular RFD bottom view, generation 1.

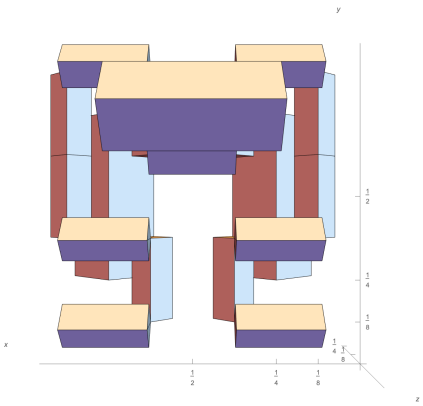

Figure A.3.23: Hilbert curve rectangular RFD bottom view, generations 1 and 2.

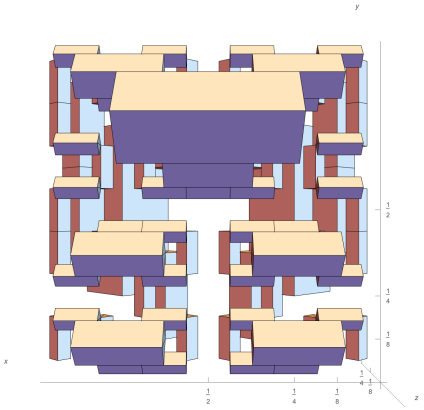

Figure A.3.24: Hilbert curve rectangular RFD bottom view, generations 1–3.

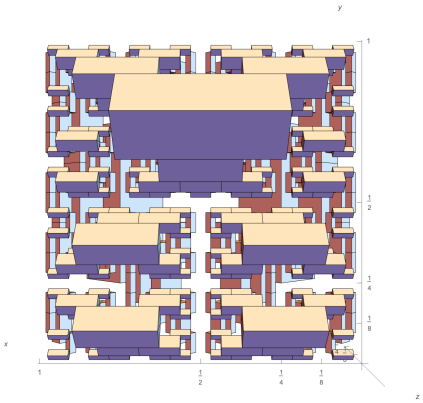

Figure A.3.25: Hilbert curve rectangular RFD bottom view, generations 1–4.

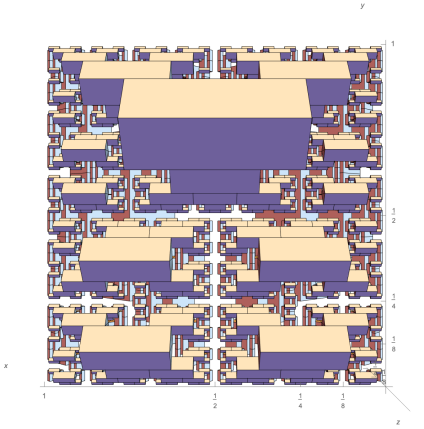

Figure A.3.26: Hilbert curve rectangular RFD bottom view, generations 1–5.

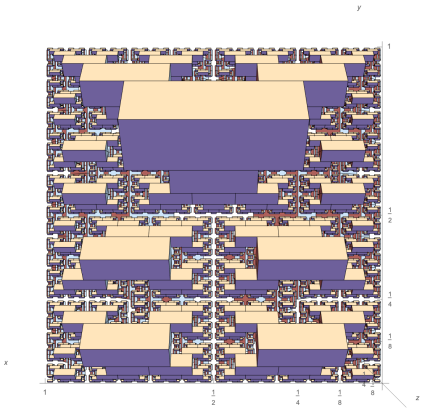

Figure A.3.27: Hilbert curve rectangular RFD bottom view, generations 1–6.

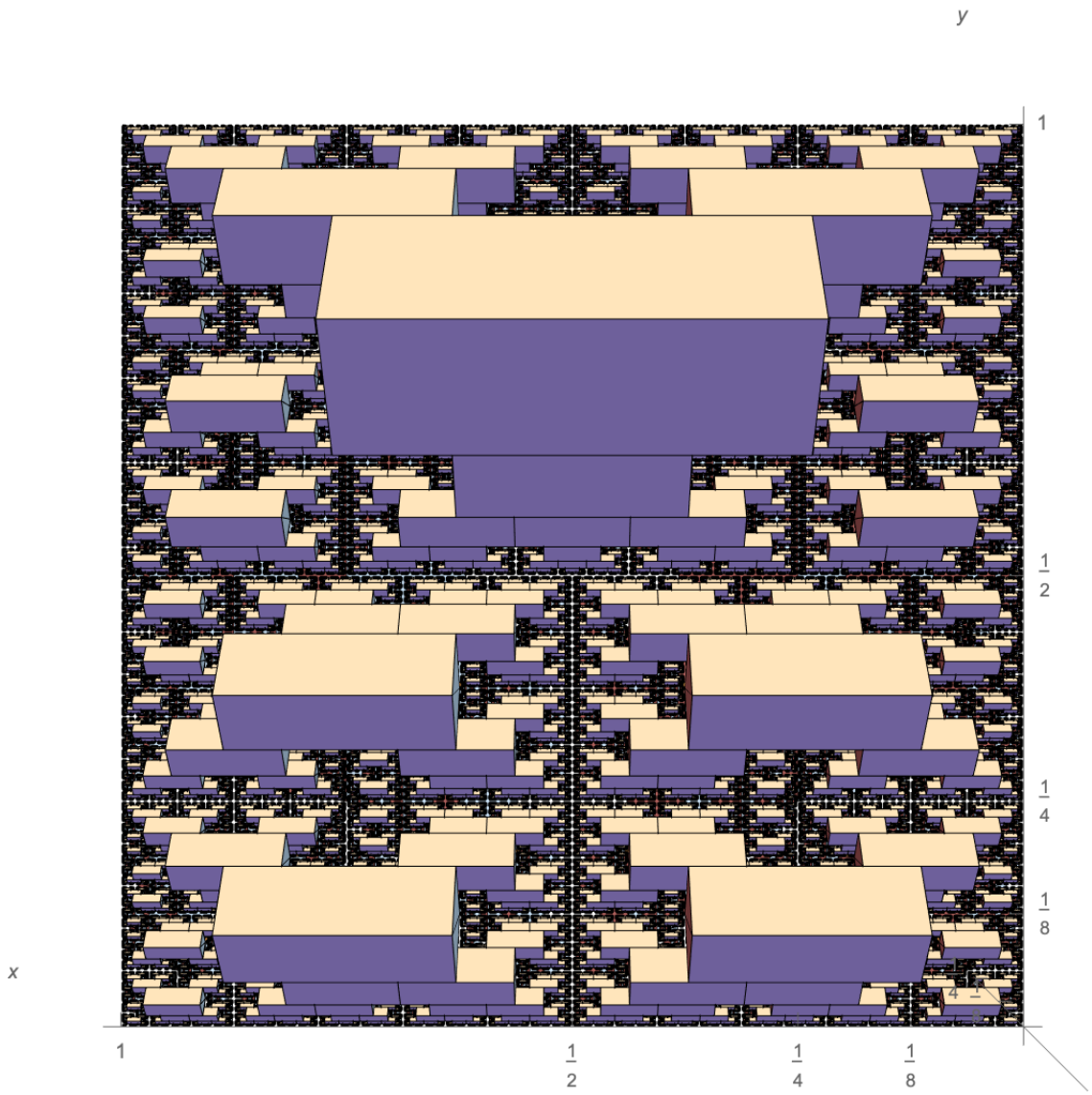

Figure A.3.28: Hilbert curve rectangular RFD bottom view, generations 1–8.

Index